
Somatic Mutations Drive Vascular Malformation Initiation, Progression, and Predisposition

by

Daniel Aaron Snellings

Department of Molecular Genetics and Microbiology
Duke University

Date: _____

Approved:

Douglas Marchuk, Supervisor

Beth Sullivan

Michael Hauser

Timothy Reddy

Craig Lowe

Dissertation submitted in partial fulfillment of the requirements for the degree of
Doctor of Philosophy in the Department of Molecular Genetics and Microbiology
in the Graduate School of Duke University
2022

ABSTRACT

Somatic Mutations Drive Vascular Malformation Initiation, Progression, and Predisposition

by

Daniel Aaron Snellings

Department of Molecular Genetics and Microbiology
Duke University

Date: _____

Approved:

Douglas Marchuk, Supervisor

Beth Sullivan

Michael Hauser

Timothy Reddy

Craig Lowe

An abstract of a dissertation submitted in partial fulfillment of the requirements for
the degree of Doctor of Philosophy in the Department of Molecular Genetics and
Microbiology
in the Graduate School of Duke University
2022

Copyright © 2022 by Daniel Aaron Snellings
All rights reserved except the rights granted by the
Creative Commons Attribution-Noncommercial Licence

Abstract

Vascular malformations are a diverse class of focal lesions that may occur throughout the body and affect different vascular beds. Since the advent of next-generation sequencing it has become clear that virtually all vascular malformations are caused by postzygotic genetic changes occurring in a single cell: somatic mutations.

Somatic mutations are widely accepted to be the initial, catalyzing event for vascular malformation. These mutations are a mix of gain-of-function and loss-of-function and occur in canonical vascular genes, or known oncogenes. From the past two decades of research, we have identified numerous genes which contribute to vascular malformation; yet, despite this genetic diversity, the mutations identified in individual malformations has thus far been—without exception—monogenic.

In this document I present the first type of vascular malformation where digenic somatic mutations are a common and critical component of lesion pathogenesis. Furthermore, I propose that somatic mutations cause not only lesion initiation, but may drive the initiation, progression, and predisposition to vascular malformation.

In support of this hypothesis, I first identify that vascular malformations in hereditary hemorrhagic telangiectasia are initiated by somatic mutations via a two-hit mechanism. Second, I determine that cerebral cavernous malformations harbor up to 3 distinct somatic mutations that synergize to fuel lesion progression. Finally, I show that developmental venous anomalies harbor a somatic mutation which creates a mosaic field of mutant cells that predisposes to cerebral cavernous malformations.

for my friend
LUCA FRANZINI

Contents

| | |
|---|-------------|
| Abstract | iv |
| List of Tables | x |
| List of Figures | xi |
| List of Abbreviations and Symbols | xii |
| Acknowledgements | xiii |
| 1 Introduction | 1 |
| 1.1 Vascular Malformations | 2 |
| 1.2 Genetic Mechanisms of Vascular Malformation | 2 |
| 2 Two-Hit Mechanism of Hereditary Hemorrhagic Telangiectasia | 4 |
| 2.1 Premise | 5 |
| 2.2 Results | 6 |
| 2.2.1 Telangiectasia Harms from a Somatic Mutation in <i>ENG</i> or <i>ACVRL1</i> | 7 |
| 2.2.2 Somatic and Germline Mutations are Biallelic | 11 |
| 2.2.3 Mutations are Consistent with Homozygous Loss of Function . | 13 |
| 2.2.4 Telangiectasia from the Same Individual Harbor Unique Somatic Mutations | 18 |
| 2.3 Discussion | 18 |
| 2.3.1 Evidence for a Genetic Two-Hit Mechanism | 18 |
| 2.3.2 Necessary, but Not Sufficient | 21 |

| | | |
|----------|--|-----------|
| 2.3.3 | Sensitivity for Detecting Somatic Mutations | 22 |
| 2.3.4 | Mutant Cell Metastasis | 23 |
| 2.3.5 | Probability of Multiple Somatic Mutations | 23 |
| 2.3.6 | Two-Hit Mechanism for <i>SMAD4</i> & JP-HHT | 24 |
| 2.3.7 | Compound Heterozygosity | 25 |
| 2.3.8 | Therapeutic Potential | 25 |
| 2.4 | Methods | 26 |
| 2.5 | Contributions and Acknowledgements | 32 |
| 3 | <i>PIK3CA</i> Mutations Fuel Cerebral Cavernous Malformations | 33 |
| 3.1 | Premise | 34 |
| 3.2 | Results | 36 |
| 3.2.1 | <i>PIK3CA</i> Mutations Occur in Familial and Sporadic CCMs . . | 36 |
| 3.2.2 | CCMs Harbor Multiple Somatic Mutations in Different Genes | 37 |
| 3.2.3 | <i>PIK3CA</i> and CCM/ <i>MAP3K3</i> Mutations in the Same Cell . . | 40 |
| 3.3 | Discussion | 41 |
| 3.3.1 | Three-Hit Model of CCM Pathogenesis | 43 |
| 3.3.2 | Role of Clonal Expansion in Mutagenesis | 44 |
| 3.3.3 | Therapeutic Implications | 44 |
| 3.3.4 | DVA Predispose to CCM and Other PI3K-Related Diseases . . | 45 |
| 3.4 | Methods | 46 |
| 3.5 | Contributions and Acknowledgements | 52 |
| 4 | Developmental Venous Anomalies Predispose to Malformation | 54 |
| 4.1 | Premise | 55 |
| 4.2 | Results | 56 |
| 4.2.1 | Mutations in <i>MAP3K3</i> and CCM Genes are Mutually Exclusive | 56 |

| | | |
|----------|---|-----------|
| 4.2.2 | Cellular Phase of Somatic <i>MAP3K3</i> and <i>PIK3CA</i> Mutations | 58 |
| 4.2.3 | CCMs and DVA Harbor a Shared Mutation in <i>PIK3CA</i> | 60 |
| 4.2.4 | Plasma miRNAs Reflect PI3K Activation in DVA Patients | 60 |
| 4.2.5 | Relative Probability of Multiple Somatic Mutations | 62 |
| 4.3 | Discussion | 64 |
| 4.3.1 | <i>MAP3K3</i> GOF and CCM LOF Have Similar Molecular Effects | 64 |
| 4.3.2 | DVA Clonal Expansion Promotes Additional Mutations | 65 |
| 4.3.3 | DVA May Contribute to Additional Phenotypes | 67 |
| 4.4 | Methods | 67 |
| 4.5 | Contributions and Acknowledgements | 72 |
| 5 | Conclusions & Musings | 73 |
| 5.1 | HHT Pathogenesis | 73 |
| 5.2 | CCM Pathogenesis | 73 |
| 5.2.1 | Regrowth after Surgical Resection | 73 |
| 5.2.2 | CCM & Meningioma | 73 |
| 5.3 | Developmental Venous Anomalies as a Primer for Disease | 77 |
| 5.3.1 | Association with Sporadic CCM | 77 |
| 5.3.2 | Association with Other Diseases | 77 |
| 5.3.3 | Cowden Syndrome | 77 |
| 5.3.4 | Implications | 77 |
| 5.4 | Other Vascular Malformations | 77 |
| 5.4.1 | Classification of Vascular Malformations and Vascular Tumors | 77 |
| 5.4.2 | Sturge-Weber Syndrome and Somatic Mutations in <i>GNAQ</i> . . | 77 |
| 5.4.3 | The Curious Case of Infantile Hemangioma | 77 |
| 5.5 | The Molecular Basis of Genetic Dominance | 80 |

| | | |
|---------------------|---|------------|
| 5.5.1 | Phenotypic Dominance \neq Genetic Dominance | 80 |
| 5.5.2 | Knudsons Fingerprint | 80 |
| 5.5.3 | The Diverse Functional Effects of Genetic Mutations | 80 |
| 5.6 | The Intersection of Somatic Mutagenesis and Evolution | 80 |
| 5.6.1 | The Creation of New Alleles | 80 |
| 5.6.2 | The Relationship Between Mutability and Fitness Landscape . | 80 |
| 5.6.3 | Recurring Mutations & Convergent Evolution | 80 |
| 5.6.4 | Clonal Evolution of Somatic Mutants | 80 |
| 5.6.5 | Cancer | 80 |
| 5.7 | Somatic Mutations | 80 |
| 5.7.1 | The Role of Somatic Mutations in Aging | 80 |
| 5.7.2 | Constitutional Intolerance & Somatic Permissiveness | 80 |
| 5.7.3 | Somatic Reversion of Pathogenic Mutations | 80 |
| 5.7.4 | What is the Consequence of RNA Mutations? | 80 |
| 5.8 | Innovation in the Sequencing Era | 80 |
| 5.8.1 | Detection of Somatic Mutations | 80 |
| 5.8.2 | Single Cell Sequencing | 80 |
| 5.8.3 | Utility of Rare Disease Research in Mechanistic Discovery . | 80 |
| 5.8.4 | Data Democratization & Individual Privacy | 80 |
| 5.8.5 | Growing Importance of Informatics in Biology | 80 |
| A | Probability of Multiple Somatic Mutations | 81 |
| Bibliography | | 82 |
| Biography | | 102 |

List of Tables

| | | |
|-----|---|----|
| 2.1 | Mutations Identified in HHT Telangiectasia | 9 |
| 2.2 | Phase of Somatic and Germline Mutation Pairs. | 13 |
| 2.3 | Predicted Consequences of Germline and Somatic Mutations. | 17 |

List of Figures

| | | |
|-----|---|----|
| 2.1 | Low Frequency Somatic Mutations Detected in Telangiectasia. | 10 |
| 2.2 | Establishing Phase of Germline and Somatic Mutations. | 12 |
| 2.3 | Mutations in <i>ACVRL1</i> Disrupt Splicing. | 15 |
| 2.4 | Each Telangiectasia is Seeded by a Unique Somatic Mutation. | 19 |
| 3.1 | Familial and Sporadic CCM Harbor Somatic Mutations in <i>PIK3CA</i> . . | 38 |
| 3.2 | Single-Nucleus Sequencing of CCMs with Three Pathogenic Mutations. | 42 |
| 3.3 | Correspondence of Bulk and Single-Nucleus Sequencing. | 51 |
| 4.1 | <i>MAP3K3</i> Somatic Mutations and Cellular Phase in CCM | 57 |
| 4.2 | CCM and Adjacent DVA Harbor Identical <i>PIK3CA</i> Mutations | 59 |
| 4.3 | Differentially Expressed micro-RNAs in CCM and DVA | 62 |
| 4.4 | Genetic Model of CCM Pathogenesis | 63 |
| 5.1 | <i>KLF4</i> Mutations in COSMIC. | 75 |

List of Abbreviations and Symbols

Abbreviations

| | |
|--------|--|
| VM | Vascular Malformation |
| CCM | Cerebral Cavernous Malformation |
| HHT | Hereditary Hemorrhagic Telangiectasia |
| AVM | Arteriovenous Malformation |
| DVA | Developmental Venous Anomaly |
| SWS | Sturge-Weber Syndrome |
| PWS | Port-Wine Stain |
| FFPE | Formalin-Fixed Paraffin-Embedded |
| COSMIC | Catalog Of Somatic Mutations In Cancer |
| LOH | Loss Of Heterozygosity |

Acknowledgements

First, I would like to acknowledge everyone that donated tissue and participated in these studies. This is ultimately for them, and without them, would not be possible.

I would like to thank my advisor, Douglas Marchuk, for his mentorship and guidance throughout my research and for his boundless enthusiasm for science. I am fortunate to have an amazing role model as a mentor. I am also thankful for the support of the current and former members of the Marchuk Lab: Han Kyu Lee, Sarah Wetzel-Strong, Leandro Barbosa Do Prado, Matthew Detter, Francesca Galeffi, Carol Gallione, Christian Benavides, Catherine Neilson, and Erin Griffin. I would also like to thank Craig Lowe for his mentorship and for always welcoming me into his lab. I also thank the members of the Lowe Lab for always being open to talk science and for their friendship. I would also like to acknowledge the members of my thesis advisor committee for their advice throughout these studies: Beth Sullivan, Michael Hauser, Timothy Reddy, and Craig Lowe.

I could not have completed any of this work without the support of our many collaborators. In particular I would like to acknowledge the contributions of Aileen Ren, Mark Kahn, Issam Awad, Mark Ginsberg, Paul Oh, Michael Lawton, Marie Faughnan, Romuald Girard, Amy Akers, the Angioma Alliance Foundation, and the Cure HHT Foundation. I would also like to acknowledge funding from the National Heart Lung and Blood Institute and the American Society for Human Genetics.

I would like to acknowledge multiple core research facilities at Duke University that were critical for the completion of this work: Sequencing and Genomic Technologies Core (Nicolas Devos, Holly Dressman, Laura-Leigh Rowlette, Fangfei Ye), Duke Human Vaccine Institute Flow Cytometry Core (Derek Cain, Evan Trudeau, Steven Slater), and the Duke Center for Genomic and Computational Biology High-throughput Applied Research Data Analysis Cluster (Hilmar Lapp, Gregory Steffen, Dan Somers).

Lastly, I thank my family and friends for their loving support throughout this journey.

1

Introduction

1.1 Vascular Malformations

Vascular malformations (VMs) are a class of lesion that consist of malformed—but functional—blood vessels. VMs may occur throughout the body and may affect various vascular beds (i.e. capillaries, veins, and arteries). While VMs may be restricted to a single type of vessel, they are often observed as mixed vascular malformations (e.g. arterio-venous malformation) and mixed vascular-lymphatic malformations (e.g. capillary-lymphatic-venous malformation). In the past VMs were considered to be congenital lesions; while many VMs are present at birth, there are numerous examples of spontaneous *de novo* VM formation in adulthood.

VMs virtually always occur as focal lesions, affecting one region of the vasculature, rather than presenting as a systemic vascular defect. This observation likely reflects the fact that a systemic defect in vascular development is likely incompatible with life, therefore individuals with such severe vascular defects do not survive to birth. Even though VMs are focally restricted, they are a source of significant morbidity and mortality in affected individuals. The clinical phenotypes produced by VMs vary depending on size and location, though they are often prone to rupture (due to increased flow through a fragile vascular bed) or hemorrhage (due to leaky endothelial junctions). The VMs that I will discuss in the following chapters commonly form in the brain and may cause a range of neurological phenotypes including: stroke, epilepsy, seizures, and neurological deficit.

1.2 Genetic Mechanisms of Vascular Malformation

There is strong genetic component to VMs and many inherited VM disorders that initially appear to contradict the focal nature of VMs. In people with an inherited VM disorder, the pathogenic mutation is present in every cell in their body. Why then, do such individuals develop a VM in their left hand and not their right hand?

The answer is that additional local events occur after birth that seed the formation of a VM in a particular location; many such events in VMs take the form of somatic mutations.

VMs may occur sporadically in otherwise healthy individuals, however there are also several familial mendelian disorders characterized by the development of VMs. Many of the familial VM disorders are inherited via an autosomal dominant allele. Despite the systemic presence of the causal mutation in these disorders, the resulting VMs are strictly focal lesions

2

Two-Hit Mechanism of Hereditary Hemorrhagic Telangiectasia

This chapter is adapted from a study published in *AJHG* (Snellings et al., 2019)

2.1 Premise

Hereditary Hemorrhagic Telangiectasia (HHT) is a Mendelian disease characterized by the development of multiple focal vascular malformations consisting of arteriovenous malformations in visceral organs and telangiectasia in mucosal and cutaneous tissue. The genetic etiology of HHT has been established and is caused by mutations in *ENG* (McAllister et al., 1994), *ACVRL1* (Johnson et al., 1996), and rarely *SMAD4* (Gallione et al., 2004); all of which follow an autosomal dominant inheritance pattern. Despite our understanding of the genetics of and downstream pathways involved in HHT, the molecular mechanisms that initiate HHT-related vascular malformation are poorly understood. Early studies of the functional consequences of HHT causal mutations established that these result in the loss of function of the gene product. These findings, in combination with autosomal dominant inheritance, led to the presumption that vascular malformations result from haploinsufficiency of the mutated gene product (Pece et al., 1997; Abdalla et al., 2000; Ola et al., 2018). However, haploinsufficiency does not account for why HHT-related vascular malformations occur as strictly focal lesions, despite the systemic presence of the causal germline mutation. This disconnect between genotype and phenotype led to an alternative long-standing hypothesis that HHT-related vascular malformations result from a Knudsonian two-hit mechanism, where a local somatic mutation in the wild type allele of the affected gene seeds the formation of focal lesions.

The only published study which directly addresses the two-hit hypothesis attempted to determine whether Endoglin was present on the endothelial lining of arteriovenous malformations from an individual with HHT with a causal mutation in the corresponding gene *ENG* (Pece-Barbara et al., 1999). Endoglin immunostaining was visible in the vessel lining, albeit at low levels. The presence of Endoglin in HHT-associated vascular malformations would contradict a two-hit mechanism,

however complete loss of staining might not be predicted to occur, especially with the heterogeneous—and potentially mosaic—tissue of an arteriovenous malformation that may only contain a minority of cells that harbor the somatic mutation. Previous attempts to address this hypothesis at the DNA level have been hampered by the limitations of past sequencing technology. The advent of next-generation sequencing has drastically increased our sensitivity for detecting low-frequency somatic mutations. Somatic mutations have been identified in a diverse array of vascular malformations (Al-Olabi et al., 2018; Soblet et al., 2017; Limaye et al., 2015, 2009; Shirley et al., 2013; Couto et al., 2015; Luks et al., 2015) including recent evidence that sporadic arteriovenous malformations, not associated with HHT, harbor somatic activating mutations in *KRAS* or *MAP2K1* (Nikolaev et al., 2018; Couto et al., 2017). Notably, a genetic two-hit mechanism is known to contribute to Cerebral Cavernous Malformations (CCM) (Akers et al., 2009; McDonald et al., 2014; Gault et al., 2009) and Capillary Malformation-Arteriovenous Malformation Syndrome (CM-AVM) (Macmurdo et al., 2016); like HHT, both diseases are caused by autosomal dominant loss of function mutations. Here we demonstrate that HHT-related telangiectasia contain biallelic mutations in *ENG* or *ACVRL1*, resulting in homozygous loss of function; evidence in support of the long-standing hypothesis that telangiectasia pathogenesis follows a genetic two-hit mechanism.

2.2 Results

To determine whether a genetic two-hit mechanism underlies HHT pathogenesis, we tested three underlying expectations of the two-hit mechanism: 1) telangiectasia contain a somatic mutation in the same gene as a germline mutation which causes HHT, 2) the somatic and germline mutations are biallelic, and 3) both mutations result in loss-of-function.

2.2.1 Telangiectasia Harmor a Somatic Mutation in ENG or ACVRL1

We used capture-based library preparations to sequence 19 telangiectasia for the three genes mutated in HHT (*ENG*, *ACVRL1*, and *SMAD4*) and 13 other vascular malformation-related genes (see Methods for identity of genes). The 13 non-HHT vascular malformation genes were chosen with the possibility that they also might harbor somatic mutations, but primarily to serve as control genes, since the two-hit mechanism requires a mutation in the corresponding HHT gene harboring the causal germline mutation. Somatic mutations in these other genes may or may not contribute to HHT pathogenesis, but absence of a somatic mutation in the casual HHT gene would violate the first expectation of the genetic two-hit mechanism.

In each telangiectasia we identified a pathogenic germline mutation in either *ENG* or *ACVRL1*. Although in most cases the individuals' germline mutation was already known from clinical diagnostic sequencing, we intentionally remained blinded to this information until after our own sequence analysis of the tissue samples. In 6003-1, the individual harbors a silent germline mutation which was found by the clinical lab and noted as a variant of unknown significance. Below we show that this variant is indeed the pathogenic germline variant in this individual.

We used the MuTect2 variant caller to detect variants present in the sequence data. To identify candidate somatic mutations, we removed variants based on several stringent filtering criteria including briefly; intronic or intergenic variants, population frequency $>0.01\%$, $<0.1\%$ or <5 total supporting reads, low coverage, strand specificity, and low base quality scores. To validate or refute the authenticity of each candidate somatic mutation we performed an independent round of amplification using primers flanking each putative variant position for each sample, and sequenced to $>10000x$ coverage. In each tissue sample, the identical somatic variant was re-identified. Thus, these variants were bona fide somatic mutations

existing in the telangiectatic tissue. In total, we identified somatic variants in 9 of 19 telangiectasia; 5 in *ENG*(NM_001114753.1 (*ENG_v001*)) 4 in *ACVRL1*(NM_000020.2 (*ACVRL1_v001*)) (Table 2.1) (Figure 2.1) (See Methods). In each case, the somatic mutation was found in the same gene as the pathogenic germline mutation. Somatic mutations were not found in any of the other 15 genes sequenced, not even in one of the other HHT casual genes. Importantly, no telangiectasia harbored more than a single somatic mutation. The lack of mutational noise suggests these mutations are pathobiologically significant. Importantly, all are consistent with strong mutations; five of the variants are small indels resulting in a frameshift, three are in-frame indels, and one is a point mutation 4 bases after an exon-intron boundary that is predicted to impact RNA splicing.

Although these variants fall well below the 50% allele frequency expected for germline variants, it is formally possible that these variants exist constitutionally as very rare, somatic mosaic variation in the individual. We next investigated whether these somatic mutations were present in constitutional DNA from the individual. A source of constitutional DNA (saliva) was available for three of the nine mutation-positive samples, and in each we find that the somatic mutation was completely absent or present at a level no higher than technical sequencing noise in that sample (see Methods). Saliva was not available for 6001, but we obtained and sequenced DNA from multiple telangiectasia collected from this same individual. This enabled us to determine whether any of the five somatic mutations that we identified in individual samples was present in tissue of near identical pathobiology from the same individual; compared with saliva as a control, this is a more powerful test for somatic mosaicism. We found that the somatic mutations identified in five of the telangiectasia for which we identified a mutation were entirely absent in all other telangiectasia from this same individual. Finally, Sample 6005-1 is a single archived FFPE telangiectasia and no source of constitutional DNA is available. In total, we

Table 2.1: Mutations Identified in HHT Telangiectasia.

| Sample | Germline Mutation | Somatic Mutation | Discovery Reads ^a | Validation Reads ^a | Constitutional Reads ^a |
|---------|------------------------------------|---|------------------------------|-------------------------------|-----------------------------------|
| 6001-1 | <i>ENG</i> c.1080_1083del | <i>ENG</i> c.293_304del | 33/1318 (2.5%) | 1067/100268 (1.1%) | 0/26462 (0%) |
| 6001-3 | same as above | <i>ENG</i> c.1195_1196delAGfsX2 | 5/1080 (0.46%) | 723/115963 (0.62%) | 0/24357 (0%) |
| 6001-7 | same as above | <i>ENG</i> c.1237_1238insCAfsX7 | 27/5127 (0.53%) | 341/115570 (0.30%) | 0/23066 (0%) |
| 6001-8 | same as above | <i>ENG</i> c.578delCinsT GCG p.T193MR | 111/4845 (2.3%) | 1142/142572 (0.80%) | 0/21315 (0%) |
| 6001-10 | same as above | <i>ENG</i> c.205delGfsX6 | 33/3389 (1.0%) | 3575/326894 (1.1%) | 0/22098 (0%) ^b |
| 6001-* | same as above | NF | | | |
| 6002-1 | <i>ACVRL1</i> c.1451G>A p.R484Q | <i>ACVRL1</i> c.349delGinsTTfsX52 | 20/2217 (0.90%) | 309/24018 (1.3%) | 0/65818 (0%) |
| 6002-2 | same as above | <i>ACVRL1</i> c.1378_3_1402del19ins9 | 26/1649 (1.6%) | 3189/202550 (1.6%) | 6/155855 (0.0038%) |
| 6003-1 | <i>ACVRL1</i> c.474A>T p.G158G | <i>ACVRL1</i> c.625+4A>T | 101/3392 (3.0%) | 372/16303 (2.3%) | 2/38924 (0.0051%) |
| 6004-1 | <i>ACVRL1</i> c.1232G>A p.R411Q | NF | | | |
| 6004-2 | same as above | NF | | | |
| 6005-1 | <i>ACVRL1</i> c.1232G>A p.R411Q | <i>ACVRL1</i> c.1206delCfsX12 | 133/1664 (8.0%) | 2671/189690 (1.4%) | N/A |

*Eight additional telangiectasia from patient 6001 with no identified somatic mutation
 For multiple telangiectasia collected from one individual the sample ID is listed as (Patient#)-(Telangiectasia#), NF = None Found

^aAllele frequency in other telangiectasia from 6001

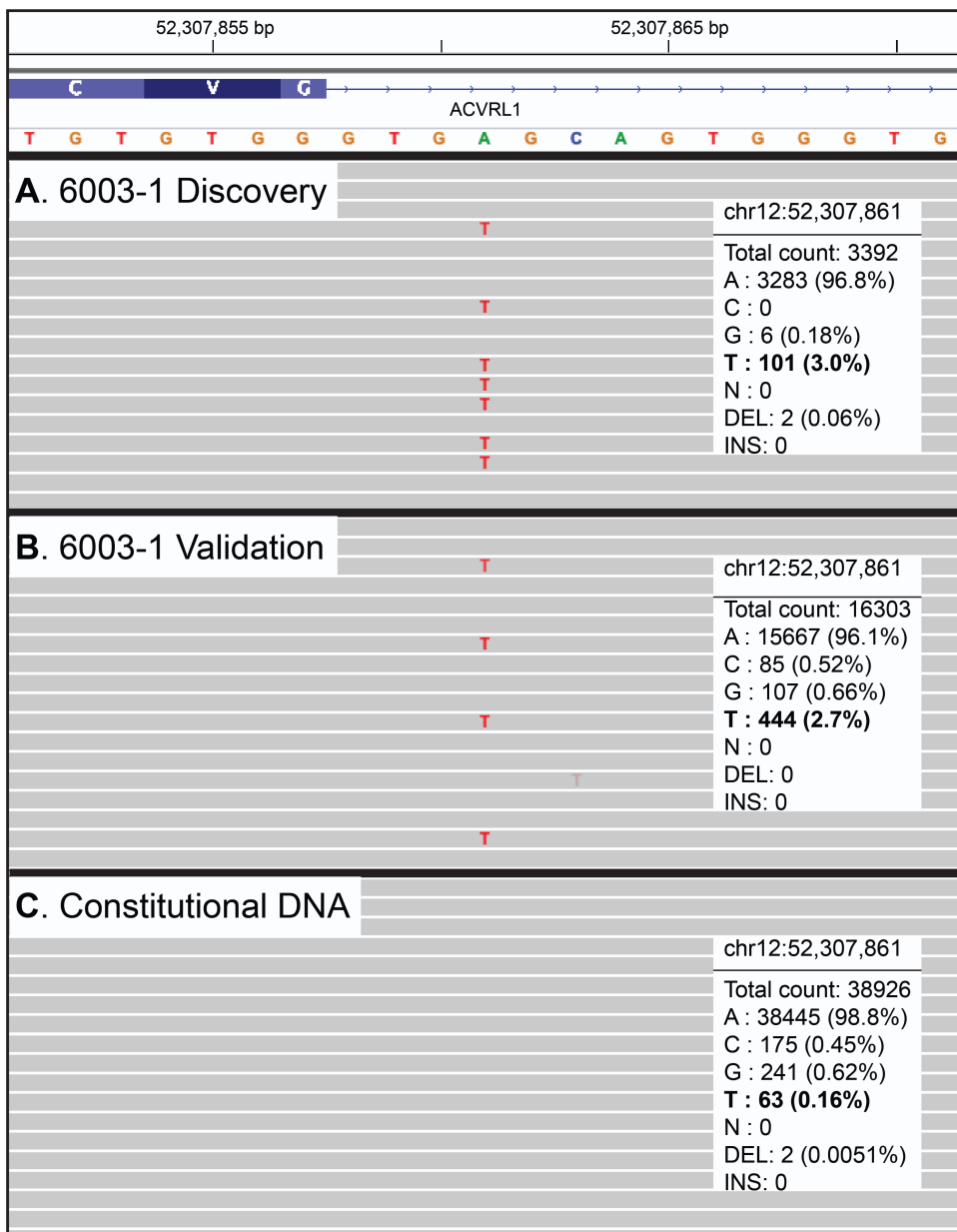


FIGURE 2.1: Low Frequency Somatic Mutations Detected in Telangiectasia. Visualization with IGV of next-generation sequencing data for one representative sample with a somatic mutation in *ACVRL1*. The somatic mutation in 6003-1, an A>T point mutation, is present at low frequency in DNA from telangiectatic tissue used for (A) discovery (capture-based sequencing) and (B) validation (amplicon-based sequencing). The mutation is below the level of sequencing noise in (C) constitutional DNA (amplicon-based sequencing) confirming the mutation is somatic.

found that 9 of 19 telangiectasia harbor a somatic mutation specifically in the same gene as a pathogenic germline mutation and that these mutations are not present constitutionally. The presence of somatic mutations in telangiectasia fulfills the 1st expectation of the genetic two-hit mechanism.

2.2.2 Somatic and Germline Mutations are Biallelic

The 2nd expectation of the genetic two-hit mechanism is that the somatic and germline mutations are biallelic; such that the somatic mutation occurs on the wild-type allele of the affected gene, in trans with the germline mutation. To determine if the mutations are biallelic we examined whether they were arranged in a cis or trans configuration by sequencing amplicons that cover the nucleotide positions of both somatic and germline mutations in a single molecule. The amplicons were sequenced with either short-read (Illumina) or long-read (PacBio) chemistry, depending on the amplicon size, in order to generate reads that would span the two mutations. In contrast to traditional Sanger sequencing which measures the population average at each position, both Illumina and PacBio chemistries output sequences of single DNA molecules. In total we generated mutation-spanning reads for 7 telangiectasia, each with more than 100 reads that contained the somatic mutation. From these mutation-spanning reads we established that >95% of reads with the somatic mutation possessed the wild type allele at the position of the germline mutation, showing that all 7 mutation pairs are in trans configuration (Table 2.2) (Figure 2.2A-B). Any two variants in a chromosome must be arranged in cis or trans with an equal probability of either arrangement. Considering this, our observation that 7/7 mutation pairs are arranged in trans corresponds to a p-value of 0.008 demonstrating significant bias towards a trans configuration. These data show that the somatic and germline mutations are biallelic, fulfilling the 2nd expectation of the genetic two-hit mechanism.

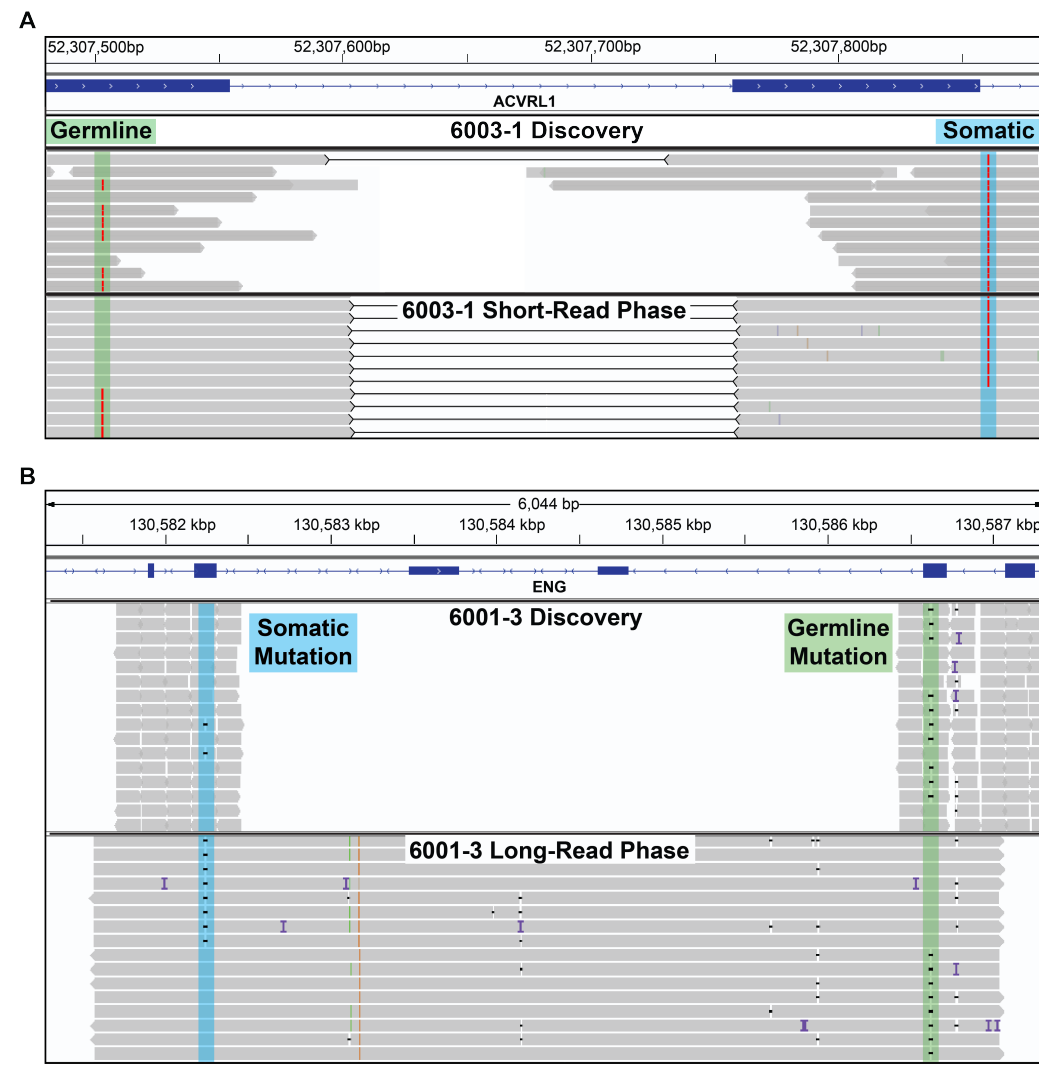


FIGURE 2.2: Establishing Phase of Germline and Somatic Mutations.
 IGV visualization of two samples showing both methods of establishing phase. Each panel shows reads from the initial discovery sequencing and the reads used to establish phase. (A) Somatic and germline mutations in 6003-1 are both A>T point mutations and highlighted by the blue and green regions respectively. Since the distance between these mutations is relatively small (357bp) phase was established using Illumina short-reads (also used for validation). Black lines between reads denote read pairs, showing that both reads originate from a single molecule of DNA. Each molecule with the somatic mutation contains the wild-type allele at the germline mutation position proving the mutations are biallelic. (B) Somatic and germline mutations in 6001-3, both small deletions. The genomic distance between these mutations is 4377bp. In long reads that span the two mutations, each read with the somatic mutation contains the wild-type allele at the position of the germline mutation.

Table 2.2: Phase of Somatic and Germline Mutation Pairs.

| Sample | Total Reads | Trans Reads | Cis Reads | P-value |
|---------|-------------|----------------------------|-----------|------------------------|
| 6001-1 | N/A | N/A | N/A | N/A |
| 6001-3 | 112 | 112 (100%) ^a | 0 (0%) | 1.9×10^{-34} |
| 6001-7 | 155 | 153 (98.7%) ^a | 2 (1.3%) | 2.6×10^{-43} |
| 6001-8 | 593 | 590 (99.5%) ^a | 3 (0.5%) | 1.0×10^{-171} |
| 6001-10 | N/A | N/A | N/A | N/A |
| 6002-1 | 125 | 120 (96.0%) ^a | 5 (4.0%) | 5.5×10^{-30} |
| 6002-2 | 3189 | 3160 (99.0%) ^{bc} | 29 (1.0%) | 4.2×10^{-890} |
| 6003-1 | 372 | 364 (97.8%) ^{bc} | 6 (1.4%) | 1.4×10^{-99} |
| 6005-1 | 2671 | 2653 (99.3%) ^{bc} | 18 (0.7%) | 6.3×10^{-759} |

^aReads generated with PacBio long-read chemistry)

^bReads generated with Illumina short-read chemistry

^cThese reads were also used for validation shown in Table 2.1

2.2.3 Mutations are Consistent with Homozygous Loss of Function

The 3rd expectation of the genetic two-hit mechanism is that the biallelic somatic and germline variants both result in loss of function. Due to the functional studies and extensive allelic series of mutations in each of the HHT genes, HHT is known to be caused by loss of function mutations. The germline mutation in 4 of the 5 individuals in this study has been identified previously in an individual with HHT and are reported in ClinVar (6001:VCV000213214.2, 6002:VCV000212796.2, 6004/6005:VCV000008243.2). There are also several publications supporting the pathogenicity of these mutations (Johnson et al., 1995; Bossler et al., 2006; Gallione et al., 1998; Ricard et al., 2010; Olivieri et al., 2007). These are all therefore bona fide loss of function mutations. The germline mutation in 6003-1, a silent mutation in *ACVRL1* exon 4, has been identified before in an individual with HHT, however it was classified as a variant of unknown significance (VUS). We used the in silico tool

Human Splicing Finder 3.1 (Desmet et al., 2009) to analyze this variant and found that it was predicted to both disrupt an exonic splice enhancer and create an internal splice donor site, potentially activating a cryptic splice site. Based on this prediction, we extracted RNA from peripheral blood leukocytes of 6003 and a control individual and performed RT-PCR to examine the splicing of *ACVRL1* transcripts. RNA from 6003 shows a new splice variant that is not present in control wild-type RNA (Figure 2.3B). As predicted by the Splice Finder program, the aberrant transcript is spliced precisely at the internal splice donor created by the mutation. The resulting transcript is missing the portion of exon 4 downstream of the germline mutation and skips exon 5 resulting in the in-frame deletion of 52 amino acids (Figure 2.3D-E). This deleted region contains several codons with known pathogenic missense mutations, suggesting that the 52 amino acid deletion would likely also result in loss of function. It is possible that the skipping of exon 5 is due to alternative splicing observed only in peripheral blood leukocytes, rather than a result of the mutation. If exon 5 is retained, the mutation would then generate a protein lacking 17 amino acid residues from exon 4 but then be frameshifted for the remainder of the transcript. With this evidence, all of the identified germline mutations meet the American College of Medical Genetics (ACMG) criteria for pathogenic mutations (Richards et al., 2015), fulfilling the first half of the 3rd expectation of the genetic two-hit mechanism.

In contrast to the germline mutation, many of which have been previously identified, the somatic mutations we identified are all novel. The ACMG guidelines for establishing pathogenicity are not applicable to somatic variants, however several lines of evidence support that all of the somatic mutations result in loss of function. Five of the nine somatic mutations result in a frameshift; all resulting in premature termination codons which would generate transcripts susceptible to nonsense-mediated decay. Frameshift mutations in *ENG* or *ACVRL1* are the most common mechanism for loss of function leading to HHT. Based on this, the 5

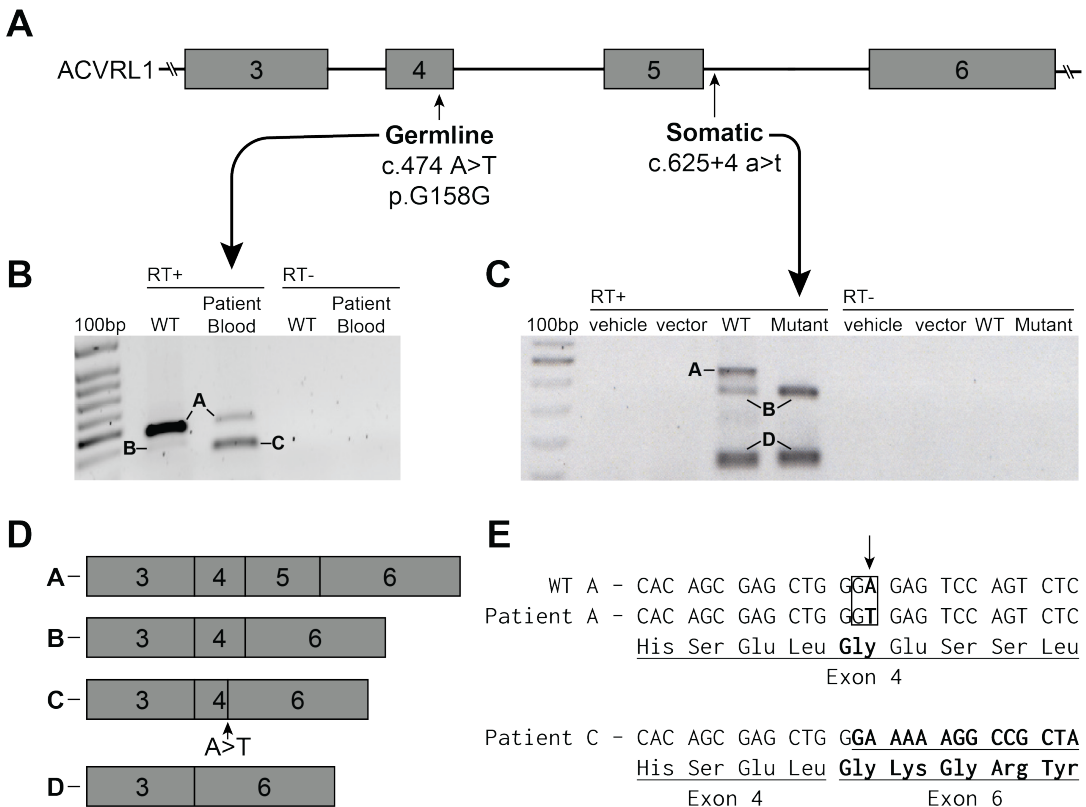


FIGURE 2.3: Mutations in *ACVRL1* Disrupt Splicing.

(A) The gene structure of *ACVRL1* exons 3–6 marked with the location of the germline and somatic mutations found in 6003-1. (B) RT-PCR showing *ACVRL1* transcripts from peripheral blood leukocytes taken from wild-type (WT) and peripheral blood leukocytes containing the germline mutation. The labeled bands were excised and sequenced. Full length transcript (Band A) is present in both the control and leukocytes from 6003 although the level in leukocytes from 6003 is greatly reduced. Band B in the control contains complete exons 3, 4 and 6. This splice variant has been seen previously and differs from band C which splices from the newly created splice donor site within exon 4 directly to exon 6. (C) As the somatic mutation is only present in 3.0% of reads it would be challenging to detect misspliced RNA from the biopsied tissue. Therefore, we inserted wild-type and mutant sequence of *ACVRL1* into an in vitro splicing vector, pSPL3-*ACVRL1*, and used RT-PCR to visualize the impact of the mutation on splicing. Only WT band A shows the full-length transcript containing exon 5; there is no corresponding full-length transcript from the plasmid containing the somatic mutation. (D) Exon structure of *ACVRL1* transcripts determined by sequencing the excised bands. (E) Sequence of DNA showing the nature of the germline mutation. In *ACVRL1* transcripts containing the germline mutation, exon 4 is shortened due to the activation of a cryptic splice site.

somatic frameshift mutations likely result in loss of function. Other than frameshift mutations, the other 4 somatic mutations we identified consisted of 3 in-frame deletions and 1 intronic mutation predicted to impact splicing. These 4 mutations are not present in the genome aggregation database (gnomAD) showing that the population allele frequency of these variants is extremely low or zero. For the somatic in-frame deletion mutation found in 6001-8, there are two reports of different in-frame deletions with overlap at this position which are known to cause HHT, suggesting that the somatic deletion in 6001-8 is likely to result in loss of function. The somatic mutations in 6001-1 and 6002-2 also result in in-frame deletions, which delete 4 and 7 amino acids respectively. Comparing the crystal structures of *ENG* and *ACVRL1* we determined that the somatic mutations in 6001-1 and 6002-2 delete portions of a beta strand and helix respectively, potentially impacting protein folding (Table 2.3). The in silico tool PROVEAN was used to predict how the protein would tolerate these deletions. The threshold of -2.5 or lower (more negative) is considered a deleterious change. The scores for 6001-8, 6001-1, and 6002-2 were -6.106, -14.903, and -25.903 respectively, strongly suggesting that all three are deleterious. The remaining somatic mutation is intronic, and occurs 4 nucleotides from the exon-intron boundary. We used Human Splicing Finder 3.1 to predict the effect of this variant on splicing, and found that it is likely to disrupt the donor site. This prediction was confirmed by RT-PCR using an in vitro splicing construct which revealed that the somatic mutation prevents the formation of full-length *ACVRL1* transcripts (Figure 2.3C). In summary we present evidence supporting that the biallelic germline and somatic mutations all likely result in loss of function, fulfilling the 3rd expectation of the genetic two-hit mechanism.

Table 2.3: Predicted Consequences of Germline and Somatic Mutations.

| Sample | Germline Mutation | Somatic Mutation |
|---------|---|---|
| 6001-1 | Frameshift: PVS1 6 supporting publications | In-Frame Deletion (-4 residues) PROVEAN: Deleterious (-14.903) deletes region in β -sheet gnomAD AF: 0 |
| 6001-3 | same as above | Frameshift common ENG LOF mechanism, expect NMD |
| 6001-7 | same as above | Frameshift common ENG LOF mechanism, expect NMD |
| 6001-8 | same as above | In-Frame Delins (-1 +2 residues) 2 pathogenic in-frame indels overlapping this codon (Shovlin et al., 1997; Argyriou et al., 2006) PROVEAN: Deleterious (-6.106) gnomAD AF: 0 |
| 6001-10 | same as above | Frameshift common ENG LOF mechanism, expect NMD |
| 6002-2 | same as above | In-Frame Delins (-7 +1 residues) PROVEAN: Deleterious (-25.903) deletes region in α -helix gnomAD AF: 0 |
| 6003-1 | Cryptic Splice Site: PS3 in silico predicted to activate cryptic site in vitro evidence (Figure 2.3) | Splice Site in silico predicted to disrupt donor site gnomAD AF: 0 |
| 6005-1 | Missense: PS1 16 supporting publications | Frameshift common <i>ACVRL1</i> LOF mechanism, expect NMD |

AF = Allele Frequency; NMD = Nonsense Mediated Decay

Germline variant classification according to ACMG guidelines (Richards et al., 2015)

PVS1 = Very strong evidence for pathogenicity; PS1-4 = Strong evidence

PROVEAN scores below -2.5 are predicted deleterious

2.2.4 Telangiectasia from the Same Individual Harbor Unique Somatic Mutations

We next sought to determine whether mutant cells in different telangiectasia derive from a somatic mutation in a common ancestor cell, or whether the mutant cell population in each telangiectasia derives from an independent somatic mutation event. To test this, we examined the somatic mutations present in multiple telangiectasia from single individuals. In 6001, for which we had obtained 13 different telangiectasia, we identified a somatic mutation in 5 telangiectasia tissue samples. In each case the somatic mutation in each telangiectasia was unique. Likewise, for 6002, for which we had two telangiectasia, we identified a unique somatic mutation in each (Figure 2.4). These results are consistent with independent mutation events rather than the somatic mutation occurring in a progenitor cell or clonality due to a metastasis from a single initial lesion.

2.3 Discussion

2.3.1 Evidence for a Genetic Two-Hit Mechanism

In this study we present strong evidence that vascular malformations associated with HHT, specifically, cutaneous telangiectasia, follow a genetic two-hit mechanism of pathogenesis. HHT is also associated with arteriovenous malformations in lung, liver, brain and the gastrointestinal tract, but these tissues are not available for prospective collection. We postulate that the visceral, deeper vascular malformations that occur in HHT also follow this two-hit mechanism.

The two-hit hypothesis for HHT pathogenesis has persisted for decades without evidence, but these low frequency somatic mutations are challenging to identify using traditional sequencing methods. The only published study to address this topic employed immunohistochemical staining in an attempt to identify endothelial cells lacking staining in the lining of HHT-related arteriovenous malformations (Bourdeau

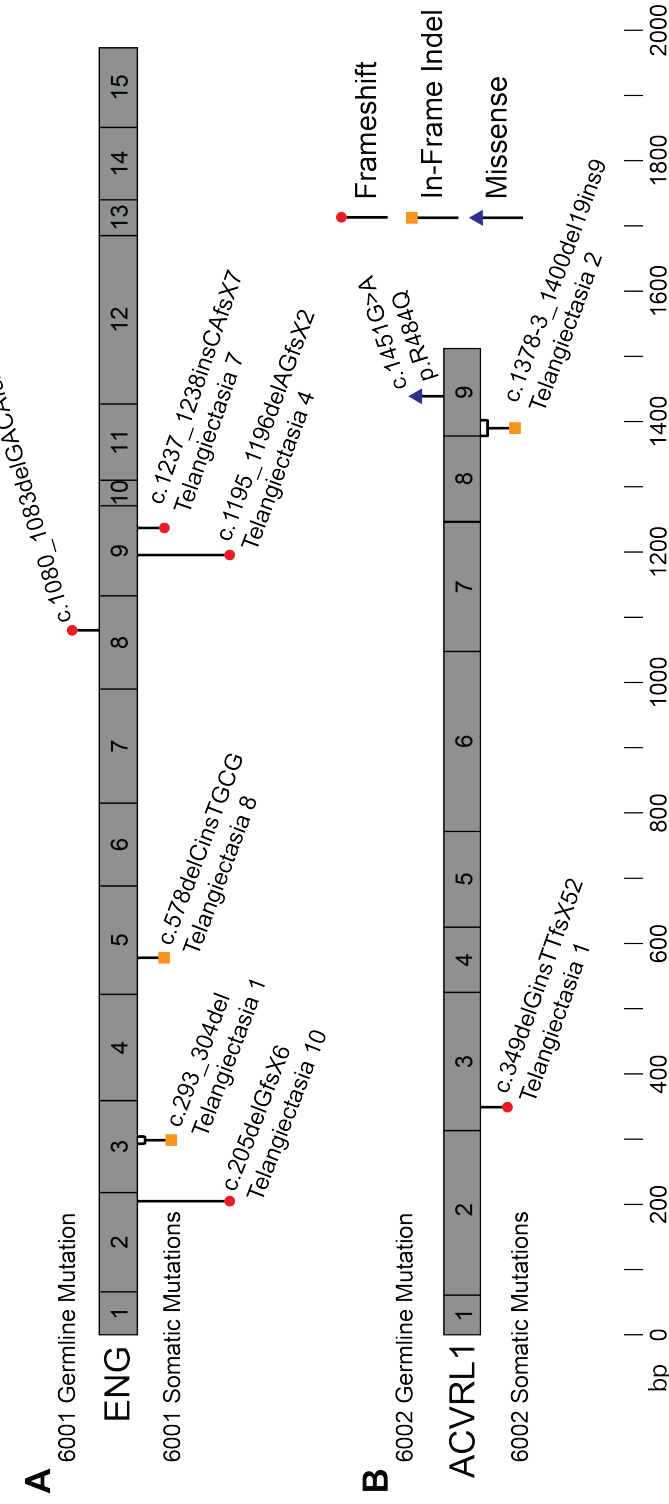


FIGURE 2.4: Each Telangiectasia is Seeded by a Unique Somatic Mutation.

Schematic representation of exons in *ENG* and *ACVR1L* with germline and somatic mutations identified in (A) 5 telangiectasia collected from 6001 and (B) 2 telangiectasia collected from 6002. In each panel the common germline mutation is listed above the gene and somatic mutations in each telangiectasia below the gene. Gene structure and mutation position are drawn to scale.

et al., 2000). However, the absence of staining as a proxy for the gain of a mutation could be difficult to discover, especially if only a fraction of a cells would exhibit this lack of signal.

Using next-generation sequencing with unique molecular identifiers we successfully identified somatic mutations in multiple telangiectasia from different individuals with HHT. The somatic mutations we identified were present at frequencies ranging between 0.46% and 8.0% in the tissue, with an average of 2.3%. The low allele frequency is likely a result of two main contributing factors; the presence of normal tissue in the skin biopsy, and somatic mosaicism within the telangiectasia. The telangiectasias in this study were sampled as skin punch biopsies and although some of the surrounding skin tissue was removed before DNA extraction, an undetermined amount of normal tissue invariably remained. However, after removing the surrounding tissue, the enrichment for the vascular component of the tissue was subjectively greater than the often low somatic mutation allele frequency might suggest. We posit that a second explanation for the low mutant allele frequency is that telangiectasia are mosaic for the somatic mutation. This agrees with existing data from mouse models of HHT showing that induced retinal AVMs are mosaic: consisting of both heterozygous and homozygous null cells (Jin et al., 2017). It is also consistent with the heterogeneity seen in Cerebral Cavernous Malformations (Detter et al., 2018; Malinverno et al., 2019) and the low mutant allele frequency in somatic mutations of other vascular malformation disorders (Al-Olabi et al., 2018; Soblet et al., 2017; Limaye et al., 2015, 2009; Shirley et al., 2013; Couto et al., 2015; Luks et al., 2015; Nikolaev et al., 2018; Couto et al., 2017; Akers et al., 2009; McDonald et al., 2014). Vascular malformations, similar to tumors in cancer, appear to be seeded by somatic mutations; however unlike tumors, vascular malformations do not appear to consist of pure populations of clonally expanded mutant cells, but contain a substantial percentage of unmutated cells.

In addition to the data presented here, the two-hit hypothesis of HHT-related vascular malformations is consistent with observations from mouse models of the disease. Whereas constitutional loss of both copies of *Eng* or *Acvrl1* in mice is embryonic lethal, mice heterozygous for constitutional deletion of either gene show extremely mild phenotypes with relatively few, if any, detectable vascular malformations(Bourdeau et al., 1999; Srinivasan et al., 2003). Robust mouse models of HHT that recapitulate vascular malformation phenotypes require the use of Cre-Lox technology to delete both copies of *ENG* in a temporally controlled (postnatal), cell-type specific (endothelial cells) manner.

In these mouse models of HHT it is also required that biallelic KO of the HHT gene occur in endothelial cells. Several groups have experimented with expressing Cre recombinase in different vascular-related cell types including pericytes (*NG2*-Cre), vascular smooth muscle cells (*Myh11*-Cre), and endothelial cells (*Scl*-Cre & *Pdgfb*-Cre); however, mice only develop vascular malformations when Cre is expressed in endothelial cells (Tual-Chalot et al., 2015; Choi et al., 2014; Garrido-Martin et al., 2014; Mahmoud et al., 2010). We have attempted to confirm that the somatic mutations we identified in human lesions occur in the endothelium by using laser capture microdissection, however these efforts have been hampered by the small quantity of tissue in telangiectasia biopsies and the difficulty of isolating a single layer of cells by microdissection. This question may be more easily addressed in larger arteriovenous malformations; however, these samples have been thus far inaccessible due to the rarity of their removal in individuals with HHT.

2.3.2 *Necessary, but Not Sufficient*

Interestingly, in addition to the local requirement for loss of both alleles, vascular malformations in this model only develop after injury such as an ear punch, or by VEGF injection (Choi et al., 2012). This requirement of an angiogenic stimulus is

consistent in mouse models for all HHT genotypes: *Eng*, *Acvrl1*, and *Smad4* (Kim et al., 2018). The requirement for knockout of both copies of the gene supports the genetic two-hit mechanism we describe here. In addition, the necessity for an angiogenic stimulus suggests that loss of both copies of the relevant HHT gene is necessary, but not sufficient, for the development of the vascular malformation.

2.3.3 Sensitivity for Detecting Somatic Mutations

We might have expected to find somatic mutations in every telangiectasia, however we only found somatic mutations in 9 of the 19 we sequenced. The next-generation sequencing strategy we employ for discovering somatic mutations is extremely sensitive for the detection of point mutations and small indels. However, there are several other types of genetic alterations that would result in biallelic loss of function due to loss of heterozygosity (LOH). LOH is a common occurrence in many tumors in cancer, and is a predominant mechanism of somatic loss/mutation. LOH can occur due to a variety of genetic mechanisms: large deletions, chromosome loss, and mitotic recombination. Given the apparent capacity for even a low fraction of somatically mutant cells to initiate the vascular malformation, it follows that the same would be true for LOH-associated mutational events; therefore, these mutations would appear instead as allelic imbalance rather than outright LOH. But if the level of allelic imbalance is as low as the frequency of somatic mutations we have observed in this study, we might expect linked marker haplotype ratios in the range of 48% to 52% at nearby markers; this slight and even trivial imbalance would be difficult if not impossible to detect and validate. It is also possible that non-genetic mechanisms such as loss of expression due to epigenetic silencing account for biallelic loss of function. This process, like the LOH associated events, would not be detected by our sequencing strategy; a problem that is only exacerbated by low allele frequency. Thus, it may not be surprising that we identified a somatic mutation in approximately

only 9 of the VMs that were sequenced. We postulate it is highly likely that all of the 10 telangiectasia with no identified somatic mutation have biallelic loss by one of these other mechanisms.

2.3.4 Mutant Cell Metastasis

One consequence of the genetic two-hit mechanism that might appear to be improbable is that, if true, a new somatic mutation must occur in every one of the numerous vascular malformations in HHT. For example, some affected individuals have dozens or more visible telangiectasia on the skin and mucocutaneous surfaces alone (Gonzalez et al., 2019; Letteboer et al., 2008; Plauchu et al., 1989). An attractive hypothesis to reconcile this conundrum would be if a somatic mutation first occurs in a circulating progenitor cell which then proliferates and seeds the formation of multiple telangiectasia. There is precedence for this mechanism in another vascular malformation syndrome, Blue Rubber Bleb Nevus syndrome. These individuals display multiple small vascular lesions which harbor an identical somatic double-mutation in the *TEK* gene. These vascular lesions appear to be anatomically-dispersed clones arising from an original, dominant, large lesion (Soblet et al., 2017). In HHT-related vascular malformations, we report evidence that contradicts this hypothesis: different telangiectasia collected from the same individual harbor different, unique somatic mutations. This observation does not exclude the possibility that circulating cells may in some cases spread telangiectasia, however the data thus far suggests that the primary mechanism is independent somatic mutation events.

2.3.5 Probability of Multiple Somatic Mutations

The dilemma of the requirement for numerous independent somatic mutation events in a single gene can be resolved with a probabilistic argument. Considering the size of the human genome (3.23×10^9 bp), the probability that a random somatic

mutation occurs in the coding sequence of *ENG* (3201 bp) in trans (50% likelihood) with a pathogenic *ENG* germline mutation is ~0.00005%. Compounding this value with empirical evidence that single cells have anywhere from 100 to 1500 somatic mutations per cell (Milholland et al., 2017; Lodato et al., 2015; Lo Sardo et al., 2017), and an estimate that 5.66% of exonic somatic mutations result in LOF (Milholland et al., 2017); we calculate a conservative estimate that 0.00028% of cell have biallelic LOF *ENG* mutations. An adult human has at least 6×10^{11} endothelial cells (Sender et al., 2016), therefore we estimate that an individual with HHT and a germline mutation in *ENG* has biallelic LOF *ENG* mutations in ~1.5 million endothelial cells. It is clear that each cell with *ENG* biallelic LOF does not result in vascular malformation as individuals with HHT have at most hundreds, not millions, of telangiectasia. This disparity is consistent with the idea that telangiectasia only develop under very specific conditions: likely that the somatic mutation must occur in a specific type of vascular bed, in an endothelial cell, and must be followed by local angiogenic stimulus.

2.3.6 Two-Hit Mechanism for *SMAD4* & JP-HHT

Our samples consisted of telangiectasia from individuals with HHT from a single HHT Centre of Excellence. This cohort had germline mutations in either *ENG* or *ACVRL1*, and somatic mutations were identified in telangiectasia from both genotypes. Mutations in *SMAD4* cause the combined syndrome HHT and Juvenile Polyposis (JP-HHT), however individuals with *SMAD4* mutations only account for ~2% of HHT cases (Gallione et al., 2004). Unfortunately, no individuals with JP-HHT were present in our cohort, but we believe it is likely that JP-HHT-related telangiectasia follow an identical genetic two-hit mechanism, resulting from somatic mutations in *SMAD4*.

2.3.7 Compound Heterozygosity

As HHT is caused by germline mutations in any one of 3 genes, an interesting question is whether the compound effect of a LOF mutation in two different HHT genes could drive pathogenesis (e.g. a germline mutation in *ENG* and a somatic mutation in *ACVRL1*). However, thus far all of the somatic mutations we identified in HHT-related telangiectasia occur in the same gene as that harboring the germline mutation. This human genetic data is consistent with the observation that mice with combined deficiency for one allele each of *Acvrl1* and *Eng* are fertile, viable and are not teeming with vascular malformations (Eleftheriou et al., 2016) (Srinivasan and Marchuk, unpublished), as might be expected if trans-heterozygosity of mutations in these two HHT-genes could initiate vascular malformation development.

2.3.8 Therapeutic Potential

A genetic two-hit mechanism for HHT pathogenesis has therapeutic implications. Certain efforts to develop therapies for HHT assume a model of haploinsufficiency of the relevant HHT gene. These strategies attempt to increase the amount of the affected gene product by increasing the level of transcript/protein arising from the wild-type allele (Ruiz-Llorente et al., 2017). We show here that some fraction of cells within the malformation do not possess a wild-type allele. Even if expression in surrounding heterozygous cells could be increased, the null cells would remain devoid of protein, suggesting that this avenue of therapy may be ineffective. By contrast, a more effective strategy may be gene replacement, reintroducing a fully wild-type allele into the mutated cells (Seki et al., 2003), as this would simultaneously provide an extra copy of the gene to both the heterozygous and null cells. This strategy is particularly attractive as it might inhibit new VM formation by adding back a second wild-type copy of the mutated gene.

2.4 Methods

Sample Collection

Individuals were enrolled in the study after giving informed consent (approved by either the St. Michael's Hospital IRB committee or the Duke University Health System IRB Committee). Diagnosis of HHT was based on identification of a pathogenic germline mutation, or by exhibiting at least three of the four symptoms as per the Curaçao criteria (Supp Table 1) (Shovlin et al., 2000). Telangiectasia were resected using a 3mm punch biopsy, after local anesthesia (1% xylocaine with epinephrine), with standard aseptic technique. Sample 6005-1 was immediately formalin fixed (10% formalin) and paraffin embedded (FFPE), and then shipped at room temperature. All other samples were immediately frozen at -80 Celsius, and then shipped on dry ice. Saliva samples were obtained using Oragene DNA saliva kits at the time of tissue collection. Blood from individual 6003 was obtained during a subsequent visit, shipped at room temperature, and immediately used for RNA extraction.

DNA and RNA Extraction

DNA from telangiectasia samples was extracted using the DNeasy Blood and Tissue Kit (Qiagen). DNA from FFPE sample 6005-1 was extracted using QIAamp DNA FFPE Tissue Kit (Qiagen). Genomic DNA and RNA were extracted from peripheral blood leukocytes from individual 6003 and from a non-HHT control individual using the Genta PureGene Blood Kit (Qiagen) and TRIzol Reagent (Invitrogen) extraction protocols, respectively, as per the manufacturers' directions.

Targeted Sequencing

To enable the detection of somatic mutations in telangiectasia we used a next generation sequencing strategy. Somatic mutations involved in the pathogenesis of other vascular malformation diseases such as cerebral cavernous malformations often have

a low allele frequency due to somatic mosaicism in the malformation. Somatic mosaicism is also present in retinal AVMs from mouse models of HHT suggesting that low allele frequency may be a confounder when identifying somatic variants in telangiectasia. In addition, the telangiectasia samples collected for this study consist of bulk biopsied tissue which have not been enriched for any particular cell type. Considering these potential sources of normal (non-mutant) cell contamination, we sequenced telangiectasia to >1000x coverage and incorporated a unique molecular identifier to enable the detection of variants as low as 0.1% allele frequency. Eighteen fresh-frozen samples and one FFPE sample were sequenced using a custom Agilent SureSelect panel covering 16 genes implicated in various vascular malformation disorders: *ENG*, *ACVRL1*, *SMAD4*, *BRAF*, *CCM2*, *FLT1*, *FLT4*, *GNAQ*, *KDR*, *KRAS*, *KRIT1*, *MAP2K1*, *NRAS*, *PDCD10*, *PIK3CA*, and *PTEN*. Though *GDF2* variants have been identified in an HHT-like phenotype, these cases are extremely rare. Moreover, mutations in *GDF2* have not been identified in any individual at the Toronto HHT Centre for Excellence therefore *GDF2* was not included in the panel. To ensure the generation of high-quality sequencing libraries, the Agilent NGS FFPE QC Kit was used to determine the extent of DNA degradation in the FFPE sample. Samples with ΔCq values >2 were excluded from the study as per manufacturer recommendation. Sequencing libraries were generated using the Agilent SureSelect XT HS Kit. Samples were then pooled and sequenced on an iSeq 100 (Illumina) with paired-end 150bp reads. Across all samples, target regions were sequenced to a mean depth of 2803x with 78% of the target region at >1000x and 96% of the target region at >100x.

Mutation Detection

Sequencing data was processed and analyzed using a custom pipeline based on the GATK best practices for somatic short variant discovery. Briefly, after analyzing

the raw data with fastQC to ensure high quality data, the adapter sequences were trimmed from reads using bbdduk, reads were aligned to the hg19 human reference genome using bowtie2, duplicates were removed based on UMI sequence using fgbio, variants were called using MuTect2 in tumor-only mode, and variants were annotated using snpSift. The resulting variant call file (VCF) was filtered through several steps to identify somatic mutations. To identify variants that may change the protein sequence or impact splicing, we selected for variants that occur within exons or within 10bp of an exon. From this set, we removed variants that are present in the population at >0.01% frequency by comparing to 3 databases (dbSNP, 1000 Genomes project, and the Exome Aggregation Consortium [ExAC]); as these variants are more common than the frequency of HHT (1–5 in 10000) (Grosse et al., 2014). We removed any variants present in <0.02% of sequence reads, as this is the reported technical limit of detection for the SureSelect XT technology. We also removed variants in regions with <100x coverage, variants with <5 supporting reads, variants that were strand specific, and variants where <50% of alternative bases had a quality score >30 (>Q30). Candidate somatic variants identified in the targeted sequencing data were then validated by sequencing amplicons generated during a second, independent round of PCR amplification. We designed primers for each sample to specifically amplify the position of the somatic mutation and 100–200bp of flanking sequence. When possible, the primers were designed such that they would capture the position of both the germline and somatic mutations within a single amplicon. Each primer was synthesized with the following Illumina flow cell adapter sequences such that the amplicons could be easily indexed and sequenced:

For: 5'-TCGTCGGCAGCGTCAGATGTGTATAAGAGACAG-[primer]-3'

Rev: 5'-GTCTCGTGGGCTCGGAGATGTGTATAAGAGACAG-[primer]-3'

Amplicons were prepared from telangiectasia DNA and constitutional DNA if available (Supp Table 1) using two rounds of PCR. The first round of PCR was 25 cycles and served to amplify the target region from genomic DNA. Amplicons from the first round were purified using AMPure XP beads (Beckman Coulter) and used for a second round of PCR using 8 cycles to attach a sample index using the Nextera XT Index Kit. Amplicons from the second round were purified, pooled, and sequenced on an iSeq 100 with 150bp paired-end reads to a depth of >10000x. The frequency of the somatic mutation in telangiectasia and constitutional DNA was determined using custom scripts, excluding bases <Q15. As these amplicons were sequenced in the same run, it is possible for a low level of index misassignment causing switching of reads between samples. This could cause some reads from telangiectasia to be assigned as constitutional reads and vice versa. To estimate the rate of index misassignment, we examined pairs of samples that target different genomic locations and quantified the proportion of misassigned reads between these samples. Based on this we estimate that the rate of misassignment is 0.2–0.8%, relative to the sample of origin. For example, if one sample has a somatic mutation with a frequency of 1% and was sequenced to 100000x coverage, then 2–8 reads containing the somatic mutation would be misassigned to each of the other samples in the pool.

Establishing Phase

To establish the phase of the somatic and germline mutations we used either short-read sequencing with Illumina chemistry, or long-read sequencing with PacBio chemistry depending on the distance between the two mutations. For mutations <500bp apart, we generated amplicons during the validation process that cover the positions of both the somatic and germline mutations. These amplicons were sequenced on an iSeq 100 as described above. For mutations >500bp we designed primers such that the resulting amplicon would cover the position of both the germline and somatic

mutations for each sample. Each primer was synthesized with the PacBio ‘universal tag’ as follows to enable indexing and sequencing:

For: 5’-/5AmMC6/GCAGTCGAACATGTAGCTGACTCAGGTCAC-[primer]-3’

Rev: 5’-/5AmMC6/TGGATCACTTGTGCAAGCATCACATCGTAG-[primer]-3’

We generated amplicons spanning the somatic and germline mutations using the LongAmp Taq DNA Polymerase Kit as per manufacturer instructions. These amplicons were purified with AMPure XP beads and used for a second round of PCR to attach the sample index. This process used no more than 30 cycles of PCR total. These amplicons were pooled and sequenced across one SMRT cell on a PacBio Sequel System. The sequence reads were aligned to the hg19 human genome using Minimap2 in ava-pb mode. The single molecule resolution of these technologies allowed us to determine how the mutant alleles are arranged; if the mutations are in trans then reads will have either the somatic mutant allele or the germline mutant allele, if the mutations are in cis then reads will have either no mutant alleles or both mutant alleles. In total we generated mutation-spanning reads for 7 telangiectasia, each with >100 reads which contained the somatic mutation. The p-values reported for phase status were calculated using a binomial distribution with the null hypothesis that a random mutation has an equal probability of cis or trans configuration with a nearby variant. The genomic distance between mutations varied greatly with the closest mutations in sample 6005-1 with 26 bases between mutations, and the most distant in 6001-10 with 18.7 kilobases between mutations. Of the 9 telangiectasia with identified somatic mutations, the distance between mutations in 6002-2, 6003-1, and 6005-1 was small enough to allow for mutation-spanning reads using illumina chemistry (Table. 2). Mutation-spanning reads were generated for 6001-3, 6001-7, 6001-8, and 6002-1 using PacBio chemistry. We were unable to generate amplicons

spanning the mutations for 6001-1 and 6001-10. The sequence downstream of the somatic mutation in these telangiectasia contains several repetitive regions which, combined with the genomic distance and limited quantity of input DNA may have contributed to PCR failure. One notable confounder in this analysis is the generation of chimeric reads resulting from template switching during PCR. The generation of chimeric reads is known to interfere with amplicon-based haplotype phasing by switching a variant from one strand to another, potentially generating new haplotypes not present in the original sample (Laver et al., 2016). In practice, chimeric reads randomize the arrangement of the somatic and germline mutations. The frequency of chimeric arrangements is highly dependent on the distance between mutations and the number of PCR cycles used to make the amplicons. To reduce the number of chimeric reads in our libraries we used no more than 30 cycles for amplification. A previous study reports a chimeric arrangement frequency of 6.5% for 29 cycles of amplification for mutations 9kbp apart (Laver et al., 2016). Chimeric reads may account for the very few discordant reads in some of our samples, as shown in Table 2.2. Nonetheless, these were so minor in comparison to the great majority of the reads that phase could be unequivocally determined.

in vitro Splicing

A 3.8kb fragment of *ACVRL1* genomic DNA spanning from 431 bases upstream of exon 3 to 215 bases downstream from exon 8 was amplified and this entire insert was ligated into the MCS of pSPL3, a splicing vector (Church et al., 1994). Clones were sequenced to ensure that no PCR-induced errors were present in the exons and adjacent intronic regions of the insert. The specific mutation, c.625+4A>T, was introduced using site directed mutagenesis and again, clones were sequenced to verify that the only sequence difference was at the intended site. Plasmid DNA from empty vector, wild type (control) vector and mutation-containing vector were transfected

into HEK293T cells using Lipofectamine 3000 (ThermoFisher Scientific), incubated for 24 hours, and then the RNA was extracted using TRIzol and Direct-zol RNA miniprep kit (Zymo Research).

Reverse-Transcription PCR

RNA extracted from peripheral blood leukocytes and from transfected cells was used as template for cDNA synthesis using the Maxima H Minus First Strand cDNA kit (ThermoFisher Scientific). An RT primer in *ACVRL1* exon 8 was used in the RNA from blood while a vector-specific RT primer was used for the RNA from transfected cells to ensure that only RNA from the transfected vectors was being used as template for cDNA synthesis. cDNA from peripheral blood leukocytes was PCR amplified using primers in exons 3 and 6 while cDNA from the transfected cells was PCR amplified using primers in exons 3 and 8. PCR reactions were run on 1% agarose gels, the bands excised and Sanger sequenced.

2.5 Contributions and Acknowledgements

This chapter is adapted from a study published in AJHG (Snellings et al., 2019) with the following authors: Daniel A. Snellings, Carol J. Gallione, Dewi S. Clark, Nicholas T. Vozoris, Marie E. Faughnan, and Douglas A. Marchuk. DAS performed all sequencing experiments. CJG performed in vitro splicing experiments. DSC, NTV, and MEF provided tissue samples. DAM and DAS designed experiments.

We thank all participants and their families who donated samples for this study. We thank Dr. Nicolas Devos and the Duke Sequencing and Genomic Technologies Core for assistance designing experiments and sequencing. This study was supported by U.S. Department of Defense grant (W81XWH-17-1-0429) and a Fondation Leducq Transatlantic Network of Excellence Grant in Neurovascular Disease (17 CVD 03). MEF also received financial support from the Nelson Arthur Hyland Foundation.

3

PIK3CA Mutations Fuel Cerebral Cavernous Malformations

This chapter is adapted from a study published in *Nature* (Ren & Snellings et al., 2021)

3.1 Premise

Vascular malformations such as cerebral cavernous malformations (CCMs) that arise in the central nervous system are an important cause of stroke and disability in younger individuals (Heiskanen, 1993; Fischer et al., 2013). Most CCMs arise sporadically as single lesions, but a minority present as part of a familial, autosomal dominant form of the disease that is associated with multiple lesions (Cavalcanti et al., 2012). Classic genetic studies have associated familial CCM disease with heterozygous germline loss of function mutations in three genes, *KRIT1*, *CCM2*, and *PDCD10*, that encode the components of a heterotrimeric protein complex (the “CCM complex”) (Fisher & Boggon, 2014; Plummer et al., 2005). Subsequent studies have demonstrated that CCM lesions harbor an additional somatic mutation in the same gene as the germline mutation, implicating biallelic loss of function of the affected CCM gene as the cause of the disease (Gault et al., 2005; Akers et al., 2009). Consistent with this monogenic loss of function mechanism, sporadic CCMs harbor biallelic somatic mutations in one of the CCM genes, resulting in homozygous loss of function (McDonald et al., 2014). Mouse models confirm that deletion of any of the CCM genes in the brain endothelial cells of neonatal mice confers CCM lesions, proving a causal role for loss of CCM complex function in this disease. These studies have generated the current genetic model of CCM pathogenesis in which biallelic loss of function mutations in a single CCM gene is sufficient for CCM lesion development.

Serial imaging studies to define the natural history of human CCMs has revealed that most are slow-growing and clinically silent (Akers et al., 2017; Al-Shahi Salman et al., 2012; Horne et al., 2016). In contrast, those that cause stroke and seizure are typically fast-growing and associated with repeated lesional hemorrhage (Awad & Polster, 2019; Porter et al., 1997). Such aggressive, symptomatic lesions are surgically resected if possible to prevent or treat associated neurologic complica-

tions, but surgery is associated with high morbidity and cost and is impractical for patients with multiple lesions or lesions in less reachable locations such as the spinal cord. Why a subset of CCM lesions exhibits rapid growth associated with clinical symptoms is unknown. Recent mouse and human studies suggest that a gut microbiome containing more invasive gram negative bacteria or an impairment of the gut barrier that blocks translocation of bacterial products such as lipopolysaccharide may modulate CCM growth through effects on TLR4-MEKK3-KLF2/4 signaling in brain endothelial cells (Tang et al., 2019, 2017; Polster et al., 2020). Plasma biomarkers of angiogenesis have also been correlated with lesional clinical activity (Girard et al., 2018; Lyne et al., 2019). However, individuals with familial CCM disease who harbor numerous silent lesions identified by MRI imaging also often manifest symptomatic hemorrhage and aggressive growth of a single lesion (Polster et al., 2019). Thus the current understanding of the environmental and genetic factors that contribute to CCM growth fails to explain important aspects of the disease natural history, especially the emergence of rapidly growing symptomatic lesions which account for the majority of clinically significant outcomes.

Recent studies of sporadic vascular malformations have identified acquired gain of function mutations in a number of central signaling pathways, including the RAS/MAPK/ERK pathway in congenital hemangiomas and capillary malformations and the PI3K/AKT/mTOR pathway in venous and lymphatic malformations (Ten Broek et al., 2019; Rodriguez-Laguna et al., 2019; Castillo et al., 2019; Wetzel-Strong et al., 2017; Luks et al., 2015; Limaye et al., 2015) (and reviewed in (Quiesser et al., 2018)). Many of these gain of function mutations, e.g. those in *PIK3CA*, the catalytic subunit of PI3K, are identical to those that have been identified in cancer cells (Castillo et al., 2016; Castel et al., 2016; Limaye et al., 2015; Koren et al., 2015; Samuels et al., 2005). However, unlike cancer, in which mutations in multiple driver genes such as tumor suppressor genes and oncogenes combine to

promote growth (Bailey et al., 2018; McGranahan et al., 2015), the pathogenesis of vascular malformations has been considered monogenic. The studies described below reveal that symptomatic CCM disease arises through a cancer-like paradigm in which the accumulation of multiple somatic mutations in the same cell results in both the loss of a vascular malformation suppressor gene (i.e. the CCM gene) and the gain of vascular malformation growth gene (i.e. *PIK3CA*). These studies reveal that clinically significant cavernous malformations arise through a compound genetic mechanism like that previously described for cancer, identify PI3K signaling as a major downstream effector pathway in CCM disease, and suggest that symptomatic CCMs may be effectively treated with the approved drug rapamycin (aka Sirolimus).

3.2 Results

3.2.1 *PIK3CA* Mutations Occur in Familial and Sporadic CCMs

To determine whether human CCM lesions harbor gain of function mutations in *PIK3CA* or other genes that have been associated with increased cell growth and proliferation, 79 surgically resected CCM lesions (a single lesions per individual) were sequenced with a targeted panel of 66 genes, including the three causal CCM genes, genes involved in PI3K signaling and associated pathways, other oncogenic pathway genes, and other genes found to be mutated in vascular malformations (full gene list in methods). The collected CCM lesions were classified as “familial”, “sporadic” or “unknown” based on genetic and clinical evaluations (described in the methods). To ensure that any sequence variants identified in the CCM lesions were specific to CCM disease, 68 distinct surgically resected human brain arteriovenous malformations (bAVMs) were collected and sequenced. Like CCM lesions, bAVMs are neurovascular malformations enriched in vascular endothelial cells; thus the cellular composition of bAVMs is similar to that of CCM lesions. Since bAVMs and CCMs share a similar biological organization but arise due to distinct pathogenic

mechanisms bAVMs provide a control with which to identify mutations in CCM lesions that are specific to CCM pathogenesis.

Variants called from the sequencing data were filtered to select for those with at least 5 supporting alternate reads, a variant allele frequency greater than 0.5%, predicted functional consequence, and several other filtering criteria. Remarkably, sequencing revealed that 56/79 (71%, $P=1.23 \times 10^{-12}$) resected human CCM lesions harbor a somatic mutation in *PIK3CA* (Figure 3.1A). By contrast, none of the 68 bAVM samples harbored a somatic mutation in *PIK3CA*. The variant allele frequency of the *PIK3CA* mutations in CCM lesions ranged between 0.7% and 17.5% with a mean of 4.7%, suggesting mosaicism within the CCM lesion. All of the *PIK3CA* mutations occurred at known hotspots in the catalogue of somatic mutations in cancer (COSMIC and Figure 3.1D). Significantly, analysis of 62 other genes with listings in the COSMIC database failed to identify mutations in any genes other than *PIK3CA* and the CCM genes. No mutations were found in other components of the PI3K pathway, including *PTEN* and *AKT1/2/3*, revealing strong specificity for *PIK3CA* mutations in CCM. The three most common *PIK3CA* mutations identified in CCM lesions (E542K, E545K, and H1047R) were validated with droplet digital PCR and SNaPshot (single nucleotide extension) assays. Mutations in *PIK3CA* were detected in 14/21 known familial lesions (9/15 *KRIT1*, 4/5 *CCM2*, 1/1 *PDCD10*), and 12/15 known sporadic lesions (Figure 3.1B). Each CCM lesion harbored no more than one somatic mutation in *PIK3CA*, and all of the *PIK3CA* mutations identified in CCM lesions have previously been determined to activate PI3K signaling (Dogrueluk et al., 2015).

3.2.2 CCMs Harbor Multiple Somatic Mutations in Different Genes

Previous studies have demonstrated that human CCM lesions harbor somatic mutations in one of the three causal CCM genes. In this cohort, somatic mutations

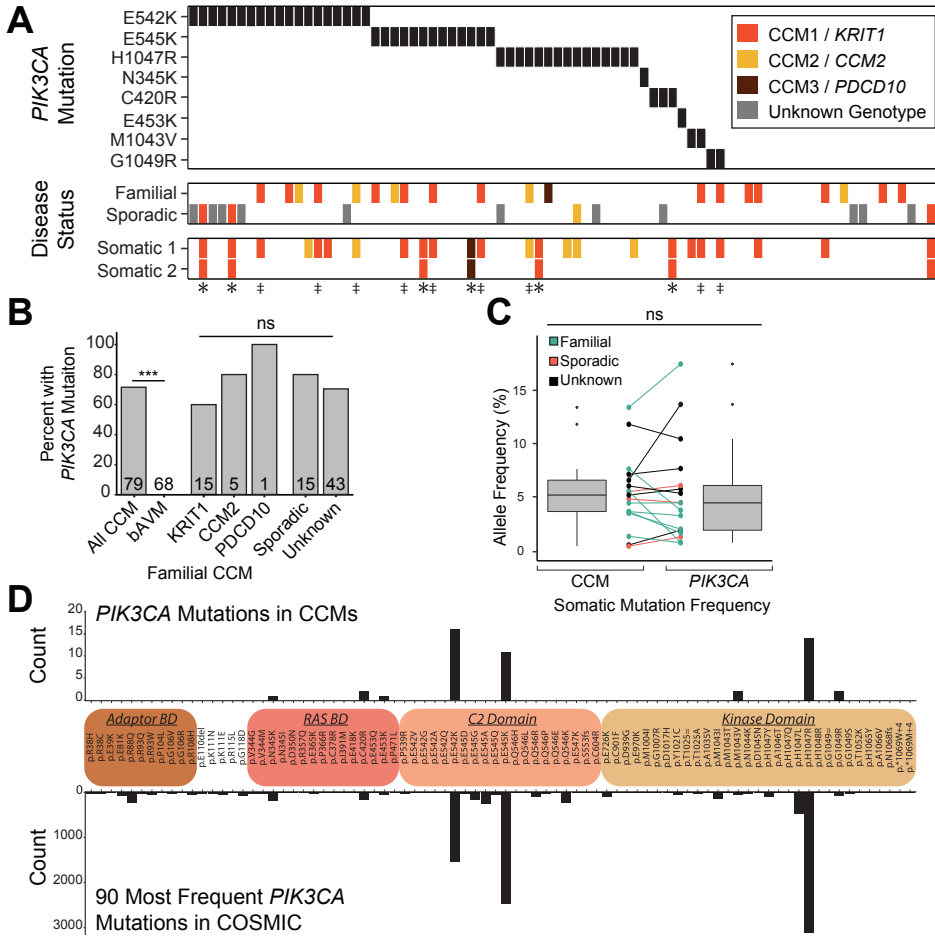


FIGURE 3.1: Somatic activating *PIK3CA* mutations are detected in CCMs.

A, A schematic summary of the germline and somatic mutations in *KRIT1*, *CCM2* and *PDCD10*, and the somatic mutations in *PIK3CA*. Color denotes the affected CCM gene. Samples listed as neither familial nor sporadic are deidentified banked CCMs lacking either clinical information or genetic evidence supporting either classification. * indicates familial CCMs with an activating mutation in *PIK3CA* and both germline and somatic mutations in a CCM gene. ‡ indicates known or presumed sporadic CCMs with an activating mutation in *PIK3CA* and two somatic mutations in a CCM gene. **B**, Distribution of activating mutations in *PIK3CA* present in sporadic CCMs, all three forms of familial CCMs, and control brain AVMs. **C**, The relationship between somatic *PIK3CA* and CCM mutations and *PIK3CA* activating mutations is graphed. Points indicate individual mutations in either a CCM gene or *PIK3CA*. Lines connect the CCM gene and *PIK3CA* gene mutations present in a single sample. **D**, The distributions of somatic *PIK3CA* mutations identified in human CCMs (top) and cancer (bottom) as reported in COSMIC. ns indicates P not significant; $P > 0.05$. *** indicates $P < 1^{-16}$.

in CCM genes were identified in 24/79 (30%) of CCM lesions. The relatively low discovery rate of somatic CCM mutations may reflect types of mutations that are not detectable with short-read sequencing, such as large indels or chromosomal rearrangements. Notably, in the CCM lesions in which we positively identified a somatic loss of function CCM mutation, 21/24 (88%) also harbored a somatic gain of function *PIK3CA* mutation. This apparent enrichment in the co-detection of CCM and *PIK3CA* somatic mutations is consistent with poor sample quality that reduced sensitivity and/or low variant allele frequency in many lesions. Thus the true frequency of *PIK3CA* mutations in CCM lesions is likely to be higher than the 71% reported above. The identification of multiple mutations in CCM genes is consistent with the previously described two-hit model of CCM pathogenesis with the addition of a third hit in *PIK3CA*. In 9 samples of familial CCM (‡ on Figure 3.1A), we detected distinct loss of function germline and somatic mutations in the same CCM gene in addition to a gain of function mutation in *PIK3CA* for a total of 3 genetic hits. In 6 samples of presumed sporadic CCM (* on Figure 3.1A), we detected two distinct loss of function somatic mutations in the same CCM gene in addition to a gain of function mutation in *PIK3CA* for a total of 3 genetic hits. These data indicate that no fewer than three independent somatic mutation events contributed to the pathogenesis of those lesions. A comparison of variant allele frequency between CCM and *PIK3CA* somatic mutations in lesions where both mutations were found revealed no significant correlation ($P > 0.15$) (Figure 3.1C). This balanced mutation frequency is consistent with a pathogenic mechanism in which both CCM and *PIK3CA* somatic mutations arise in a single cell during lesion formation, or one in which CCM mutant cells and *PIK3CA* mutant cells co-exist in similar numbers. Finally, the specific mutant *PIK3CA* alleles identified in resected human CCM lesions closely mirrored those identified in human cancers in the COSMIC database (Figure 3.1D), consistent with a shared molecular and cellular mechanism.

3.2.3 *PIK3CA* and CCM/MAP3K3 Mutations in the Same Cell

The identification of both *PIK3CA* and CCM gene somatic mutations in CCMs raises a critical question: Do these mutations occur in the same cell, or are these mutations in two distinct clonal populations that intermix to form a CCM. To address this question we performed single-nucleus DNA sequencing (snDNA-seq) on 3 sporadic and 2 familial CCMs using the Tapestri platform (Xu et al., 2019). Nuclei isolated from frozen tissue were stained with DAPI and subjected to fluorescence-activated nucleus sorting to isolate single nuclei for input into the Tapestri instrument, where the nuclei were partitioned into droplets and the exons of *KRIT1*, *CCM2*, *PDCD10*, and *PIK3CA* were amplified (Figure 3.2A). Bulk sequencing of sample 5003 identified one somatic mutation in *PIK3CA* and two somatic mutations in *KRIT1*. These same somatic mutations were identified in the snDNA-seq data which show that the majority of somatic mutant nuclei harbored all three mutations. In sporadic CCMs 5038 and 5079 only one somatic CCM gene mutation was called in addition to the *PIK3CA* somatic mutation. In sample 5079 the second somatic CCM gene mutation is clearly present in total reads, however due to poor efficiency of the amplicon there were insufficient reads per nuclei to reliably establish cellular phase with the other two mutations. Data from both 5038 and 5079 show that the majority of mutant cells harbor both the somatic *PIK3CA* and CCM gene mutations. Likewise snDNA-seq data for familial CCMs 5065 and 5073 show the majority of somatic mutant nuclei (excluding nuclei with only the germline CCM gene mutation) harbor the *PIK3CA* mutation and both CCM gene mutations (Figure 3.2B). While the majority of somatic mutant nuclei in all 5 samples harbor all of the identified somatic mutations, notably there is a smaller number of nuclei observed with each possible combination of genotypes. This observation is highly unlikely to reflect genuine biology as the creation of all genotypes would require identical somatic mutations.

to occur in multiple clonal populations within the CCM. Some of the observed genotype combinations may represent intermediate clonal populations that formed prior to acquiring the full set of mutations, however the majority of these genotype combinations are likely due to allelic dropout (ADO)—a common technical artifact in single-nucleus/cell DNA sequencing data and has been noted by many previous studies (Xu et al., 2019; Szulwach et al., 2015; Satas & Raphael, 2018). To estimate the rate of ADO for each sample we identified heterozygous SNPs called in the snDNA-seq data and evaluated the ratio of heterozygous to homozygous nuclei and determined the rate of ADO to be $8.4\% \pm 4.1\%$. We also observed dropout of the constitutional CCM pathogenic allele as evidenced by the presence of WT nuclei in familial CCM samples 5065 and 5073. As a result of ADO, the number of nuclei with all somatic mutations is likely underestimated in each sample. Despite the confounding effects of ADO, all 5 samples clearly indicate that the *PIK3CA* and CCM gene somatic mutations occur in the same cell.

3.3 Discussion

These studies demonstrate powerful synergy between mutations that confer loss of CCM function and gain of *PIK3CA* function in both mouse models of CCM disease and a majority of resected human CCMs. These findings provide new insight into the mechanisms underlying the puzzling natural history of this vascular disease, explain why the disease has not been successfully modeled in mature mice with CCM loss of function alone, and reveal a compound genetic disease mechanism for vascular malformation that is highly analogous to that elucidated for human cancer. Translationally, they also provide strong evidence that approved drugs capable of inhibiting the downstream PI3K effector mTOR, and perhaps the PI3K pathway generally, may be used to block the growth and neurologic complications of clinically symptomatic CCM lesions.

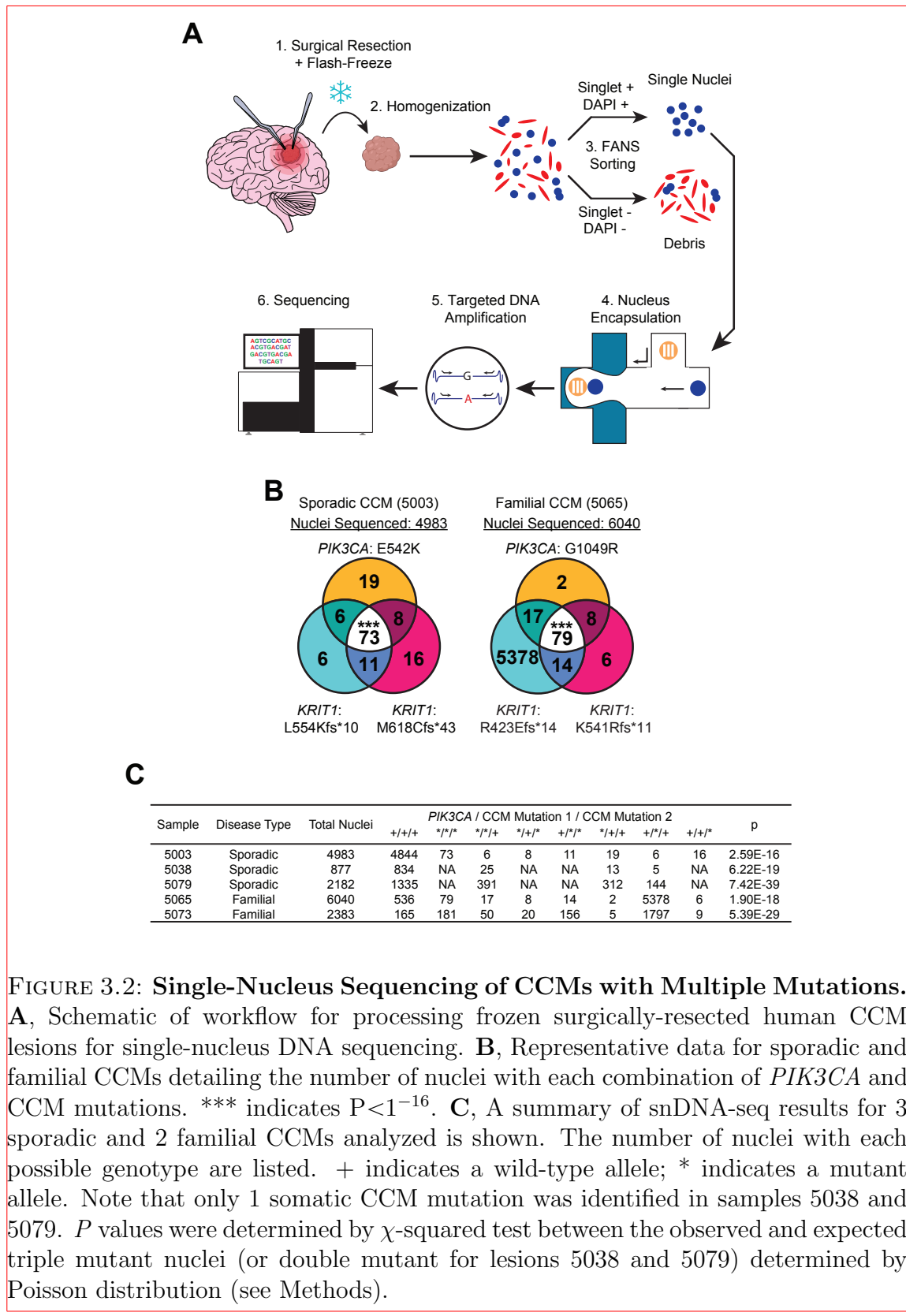


FIGURE 3.2: Single-Nucleus Sequencing of CCMs with Multiple Mutations.

A, Schematic of workflow for processing frozen surgically-resected human CCM lesions for single-nucleus DNA sequencing. **B**, Representative data for sporadic and familial CCMs detailing the number of nuclei with each combination of *PIK3CA* and CCM mutations. *** indicates $P < 1^{-16}$. **C**, A summary of snDNA-seq results for 3 sporadic and 2 familial CCMs analyzed is shown. The number of nuclei with each possible genotype are listed. + indicates a wild-type allele; * indicates a mutant allele. Note that only 1 somatic CCM mutation was identified in samples 5038 and 5079. P values were determined by χ^2 -squared test between the observed and expected triple mutant nuclei (or double mutant for lesions 5038 and 5079) determined by Poisson distribution (see Methods).

3.3.1 Three-Hit Model of CCM Pathogenesis

The most significant conceptual advance of this study is the discovery of a compound genetic mechanism of vascular malformation pathogenesis. To date, vascular malformations have been considered monogenic in origin, due either to bi-allelic loss of function mutations (e.g HHT (Snellings et al., 2019), CM-AVM (Lapinski et al., 2018), previously CCM (Akers et al., 2009; McDonald et al., 2014), or mono-allelic gain of function mutations (e.g. Sturge-Weber syndrome (Shirley et al., 2013), sporadic bAVM (Nikolaev et al., 2018), venous malformations (Limaye et al., 2015), lymphatic malformations (Luks et al., 2015), and blue rubber bleb nevus (Soblet et al., 2017; Tang et al., 2017; Goss et al., 2019; Davis et al., 2020; Francis et al., 2019; Couto et al., 2017, 2015)). Our studies identify a digenic, “triple-hit” mechanism involving the acquisition of as many as three distinct genetic mutations that culminate in loss of CCM gene function and gain of *PIK3CA* function as the basis for rapidly growing, clinically symptomatic CCMs. Thus, aggressive CCM lesions arise via the acquisition of multiple somatic mutations that synergize in a manner similar to that of established cancer drivers. By analogy to cancer, the CCM genes may be considered vascular “suppressor genes”, required to constrain vessel growth, while *PIK3CA* may be considered a vascular “oncogene”, capable of driving excess vascular growth. As in cancer, the combined loss of a vascular suppressor and gain of a vascular activator is a potent combination that culminates in aggressive, symptomatic disease. Significantly, the present study demonstrates that either CCM loss of function or *PIK3CA* gain of function alone are sufficient to confer a modest vascular phenotype. These less aggressive vascular lesions are analogous to benign tumors that become malignant after mutation of another driver gene, a scenario consistent with clinical reports of sudden aggressive growth in small, pre-existing CCM lesions. Whether distinct synergistic driver gene combinations underlie other

vascular malformations is an important future question that may be addressed by deeper genomic sequencing of human vascular malformations.

3.3.2 Role of Clonal Expansion in Mutagenesis

A key question raised by our studies is how CCM loss of function and *PIK3CA* gain of function interact at the cellular and molecular levels during lesion genesis. Insights gleaned from both genetic analysis of human CCM lesions and mouse genetic models are highly complementary and support an endothelial cell autonomous mechanism in which the two pathways are both directly and indirectly linked. Single cell genomic DNA sequencing of both sporadic and familial human CCM lesions reveals that a majority of mutant cells harbor acquired mutations in both a CCM gene and *PIK3CA*, strong evidence of interaction at the single cell level and that the majority of clonal expansion occurs after acquisition of all three mutations. Aileen Ren showed that sporadic lesions arise in *Slc11c1*(BAC)-CreERT2; *Krit1*^{fl/fl}; R26-LSL-*Pik3ca*^{H1047R} animals due to Cre leak that is exclusively endothelial, identifying the endothelial cell as the target cell type and, like the human genetic sequencing data, suggestive of a clonal mechanism in which emergence of a single compound mutant endothelial cell is sufficient for lesion formation.

3.3.3 Therapeutic Implications

Our identification of *PIK3CA* activation in CCM immediately suggests that PI3K inhibitors may be an effective therapeutic for CCM. *PIK3CA* mutations are extremely common in cancers. As a result, there is decades of extensive research on the mechanism of *PIK3CA* activation and many efforts to develop cancer therapies targeting this signaling axis. Among these therapeutics is rapamycin—an off-patent small-molecule drug targeting mTOR (a downstream effector of *PIK3CA*)—which may be made cheaply available to CCM patients. To test the efficacy of rapamycin for

preventing CCM, Aileen Ren developed a mouse model with both biallelic CCM loss of function, and *Pik3ca* gain of function. These mice develop aggressive lesions soon after induction. Aileen showed that rapamycin is extremely effective in preventing lesion formation in these mice (Ren et al., 2021). This preliminary data suggests that rapamycin may be a good candidate for pre-clinical trials, though the true test will be whether rapamycin is able to regress existing lesions. Lesion prevention is of course a step forward but given the non-trivial side effects of rapamycin, it is unlikely that long-term treatment will be a viable option. In contrast, if rapamycin is able to regress lesions, then a treatment program may consist of brief intermittent periods of dosing which would more amenable to the patient population.

3.3.4 DVA Predispose to CCM and Other PI3K-Related Diseases

A clinical clue to the pathogenesis of human CCM disease that may be explained by our findings is the observation that sporadic CCMs frequently arise at sites of pre-existing developmental venous anomalies (DVAs) (24–32% assessed by MRI, and up to 100% in one study that assessed this relationship at the time of surgical resection (Wurm et al., 2005; Porter et al., 1999; Abdulrauf et al., 1999)). Since DVAs are benign and do not undergo surgical resection, there are no data addressing their genetic basis. However, DVA is found in a majority of individuals with Cowden's syndrome, an inherited disease caused by germline heterozygous loss of function mutations in *PTEN* that is also the result of PI3K gain of function (Dhamija et al., 2018; Tan et al., 2007). A parsimonious explanation for these clinical observations is that endothelial cells with pre-existing *PIK3CA* mutations sufficient to confer DVA subsequently acquire CCM loss of function mutations and transform into more aggressive sporadic CCM lesions. While such a clinical pathogenesis remains entirely speculative until DVA genetic sequencing is performed, it would support a mechanism highly analogous to cancer in which accrued mutations convert a benign vascular

abnormality into a more malignant one.

3.4 Methods

CCM Collection

Human CCM tissue specimens were obtained from surgically resected specimens from three sources including the Barrow Neurological Institute, Angioma Alliance biobank, and University of Chicago. This study was approved by each institutions respective Institutional Review Board.

Brain AVM Collection

Brain AVM tissue specimens were obtained from the nodal tissue of surgically resected brain AVMs (M.T.L). For non-vascular lesion controls (NVLCs), temporal lobe specimens were similarly acquired from subjects undergoing anterior temporal lobectomies for medically refractory epilepsy. All tissues were frozen at -80°C and stored in a biobank. This study was approved by the University of California San Francisco Institutional Review Board and performed in compliance with the Health Insurance Portability and Accountability Act regulations.

DNA Extraction

DNA from human CCM samples was extracted using the DNeasy Blood and Tissue Kit (Qiagen). Extractions were done as per the manufacturers' directions excepting cases where less than 25mg of tissue was available. For samples <25mg the manufacturer recommended volumes were either halved or quartered—depending on the amount of tissue available—to optimize final DNA concentration and yield. Final DNA concentrations were quantified using Qubit dsDNA BR assay kit (Invitrogen cat. Q32850) according to manufacturer recommended protocol.

Droplet Digital PCR

Identification of somatic *PIK3CA* mutations was performed using droplet digital PCR (ddPCR) according to manufacturer protocol for mutation detection assays (BioRad 10047489 Ver B). For each sample with sufficient DNA yield, 30–100ng of DNA was incorporated into droplets using the QX200 AutoDG system (BioRad). After PCR, fluorescence from the resulting droplets was read using the QX200 droplet reader (BioRad). These steps were repeated for three assays testing the presence of the three most common *PIK3CA* mutations: E542K, E545K, and H1047 (ThermoFisher assay IDs: Hs000000085_rm, Hs000000086_rm, Hs000000088_rm, respectively). Each assay included a no-template control, a wild-type control, and a mutation-positive control for the mutation being assayed. The mutation-positive controls were DNA extracted from cell lines with known heterozygous mutation of E542K (T84), E545K (HCT15), or H1047R (HCT116). The output of the droplet reader was analyzed using the QuantaSoft software (BioRad). The gates for positive and negative mutation status were drawn with respect to the distribution of droplets in the mutation-positive controls and applied to all samples.

SNaPshot

Human CCM samples with an E542K, E545K, or H1047R *PIK3CA* mutation identified by sequencing or ddPCR underwent tertiary confirmation of mutation status using SNaPshot (Applied Biosystems), a single-base extension sanger sequencing assay. An initial round of PCR amplified exons 9 and 20. In a second round of PCR, primers directly adjacent to the assayed nucleotide was extended with ddNTPs and sequenced on a 3130 Genetic Analyzer (Applied Biosystems). Sequences were examined using GeneMapper software (Applied Biosystems). The allele frequency of the mutation by dividing the area under the peak of the mutant allele by the total area under both allele peaks. The primers used in this analysis were synthesized

according to designs in a previously published assay for *PIK3CA* mutations (Hurst et al., 2009).

Sequencing

Previous studies identifying somatic mutations in CCMs and bAVMs have reported alternate allele frequencies less than 1%. To enable the detection of variants at such low frequencies we aimed to sequence samples to an average of 1000x (actual mean coverage 1102x) coverage in addition to leveraging 10bp unique molecular identifiers (UMIs) to mitigate the impact of PCR duplication. These conditions allow us to theoretically detect variants as low as 0.5% allele frequency.

Sequencing libraries for the human CCMs and bAVMs were prepared using the SureSelect XT HS target enrichment workflow (Agilent). The targeting panel used for sequencing the CCMs covers the following genes: *KRIT1*, *CCM2*, *PDCD10*, *PIK3CA*, *PTEN*, *AKT1*, *KRAS*, *RAF*, *NRAS*, *MAP2K1*, *RASA1*, *TEK*, *GNAQ*, *GNA11*, *MAP2K2*, *PPP2R5D*, *ACVRL1*, *ENG*, *SMAD4*, *AKT2*, *AKT3*, *CCBE1*, *CDKN1C*, *FLT1*, *FLT4*, *FOXC2*, *GATA2*, *GDF2*, *GJC2*, *GLMN*, *KIF11*, *MTOR*, *PIK3R2*, *PTPN14*, *SOX18*, *STAMBP*, *VEGFC*, *MAP2K4*, *MAP3K1*, *MAPK1*, *JAK1*, *JAK2*, *JAK3*, *KDR*, *NOTCH1*, *PDGFRA*, *PDGFRB*, *RET*, *HRAS*, *TP53*, *MSH2*, *MYB*, *MYCN*, *MYC*, *ERBB2*, *EGFR*, *NTRK2*, *ODC1*, *SLC25A21*, *PTTG1*, *TSC1*, *TSC2*, *EPHB2*, *TGFBR1*, *TGFBR2*, *TGFBR3*.

The bAVM samples were sequenced using a customized Agilent Comprehensive Cancer panel which covers 175 genes including *PIK3CA*. After library preparation, CCM samples were pooled and sequenced across 1 lane of a HiSeq4000 (illumina) with paired-end 150bp reads. bAVM samples were pooled and sequenced across a NovaSeq6000 SP flow cell (illumina) with paired-end 150bp reads.

Sequence Analysis

Sequencing data was processed according to the GATK (Broad Institute) best practices for somatic short variant discovery with slight modifications for “tumor-only” sequencing data. As a secondary method for variant discovery we developed custom software designed specifically for the detection of somatic mutations in sequencing data from samples with no available normal tissue. This software was implemented as part of Gonomics, an ongoing effort to develop an open-source genomics platform in the Go programming language. Gonomics can be accessed at github.com/vertgenlab/gonomics.

After variant calling the resulting variants were functionally using snpEff. In this process each variant was annotated with: the protein-level consequence of coding mutations; the predicted impact of missense mutations according to SIFT, PolyPhen2, and PROVEAN; membership in several SNP databases including dbSNP, 1000 Genomes project, and ExAC; and membership in the Catalogue of Somatic Mutations in Cancer (COSMIC). We filtered the resulting list of variants using the following inclusion criteria: >100x total coverage; >5 supporting reads; <90% strand specificity; >0.5% alternate allele frequency; <1% population allele frequency according to the above mentioned SNP databases; and membership in the COSMIC database.

Single-Nucleus DNA Sequencing

Frozen human CCM lesion tissue obtained from medically-indicated, surgical resection were prepared for single-nucleus DNA sequencing (snDNA-seq) following a nuclei isolation protocol by Martelotto L. (dx.doi.org/10.17504/protocols.io.3fkgjkw). All steps prior to loading on the Tapestri platform were performed in <3 hours. Nuclei were maintained at 4°C throughout the protocol. Frozen tissue was homogenized by Dounce in Nuclei EZ Lysis Buffer (Sigma-Aldrich), briefly washed, filtered through

a 70 μ m mesh, stained with DAPI, and filtered through a 35 μ m mesh. The CCM homogenate was sorted using a FACS AriaII (BD) (70 μ m nozzle, 70psi, 4-Way Purity, chiller) gating to retain singlet DAPI-positive events (Figure 3.3). Up to 400,000 sorted nuclei were collected in 1ml of the following buffer prepared with ultrapure nuclease-free water: Na₂SO₄ 82mM, K₂SO₄ 30mM, glucose 10mM, HEPES 10mM, MgCl₂ · 6H₂O 5mM, BSA 2%. Sorted nuclei were pelleted by centrifugation at 4°C (500rcf, 10min), supernatant discarded, and resuspended in 36 μ L of MissionBio Cell Buffer. The concentration of nuclei was determined by counting DAPI-positive nuclei with a hemocytometer on an EVOS FL (fluorescence) microscope (Thermo Fisher) while confirming that nuclei aggregates comprised <5% of total nuclei. Samples with <5% aggregate nuclei and a concentration within 2000–4000 nuclei/ μ L (diluting with additional MissionBio Cell Buffer where necessary) were used for snDNA-seq.

Library preparation was performed using the Tapestri platform (MissionBio) according to the manufacturers protocol (PN3354). Libraries were generated with a custom amplicon panel synthesized by MissionBio covering all exons of *KRIT1*, *CCM2*, *PDCD10*, and 7 amplicons covering somatic mutation hotspots in *PIK3CA*, per the COSMIC database. Up to three libraries were pooled and sequenced with a NextSeq Mid-Output 2 x 150bp kit (illumina). Data processing and QC was performed by the MissionBio cloud-based analysis pipeline. Data quality for each nuclei barcode was determined using MissionBio recommended filtering settings. Data from low quality nuclei barcodes were removed prior to mutation analysis.

To determine the cellular phase of somatic mutations detected in bulk sequencing, nuclei barcodes were selected that had a minimum of 20x coverage across all mutant regions to ensure that all nuclei included in the analysis have appropriate sensitivity to detect a mutation. For each nuclei barcode and each mutant position, reads containing the ref and alt alleles were counted. Mutant regions that had both a minimum of 10 alt reads and 10% allele frequency were marked as mutation

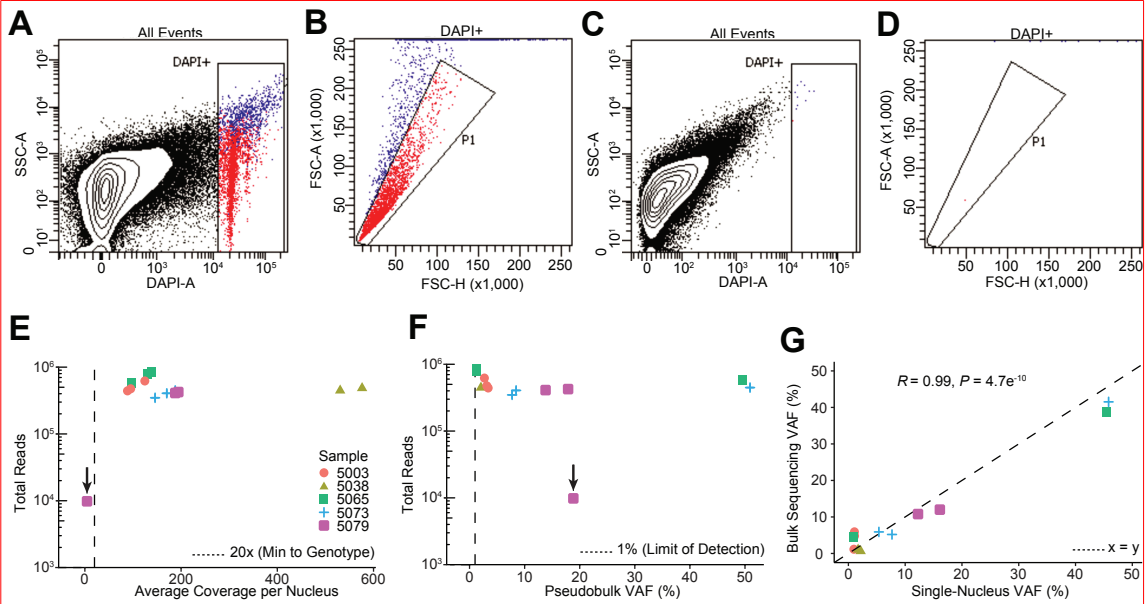


FIGURE 3.3: Correspondence of Bulk and Single-Nucleus Sequencing.

A–D, Representative FANS plots of DAPI stained (A–B) and unstained (C–D) CCM homogenate samples. Doublet discrimination by forward scatter profile for DAPI stained and unstained samples are shown in B and D respectively. **E**, Total reads and average coverage per nucleus from snDNAseq for each mutation detected by bulk sequencing. Dotted line shows 20x coverage, the minimum cutoff used for establishing genotype. **F**, Pseudobulk allele frequency from snDNA-seq for each mutation detected by bulk sequencing. Dotted line shows 1% allele frequency. Note the data point with * in E–F shows a mutation in sample 5079 detected in bulk sequencing which, due to poor amplification during snDNA-seq, received insufficient coverage per nucleus (4.5x) to establish nuclear genotypes however is clearly present in pseudobulk reads (1849/9814). **G**, Comparison of mutation allele frequency as detected by bulk and snDNA-seq. As nuclei are diploid for the relevant autosomes, the x-axis is equal to the fraction of mutant nuclei divided by two. Dotted line shows perfect correlation at $x=y$. R and P were calculated by Pearson's correlation coefficient.

positive. The number of nuclei barcodes with each possible genotype are recorded in Figure 3.2C.

The p value for each sample was determined by Chi-squared test comparing the observed number of triple mutant nuclei barcodes (or double mutant if only two mutations were identified) to the expected number of triple mutant nuclei barcodes

if the null hypothesis is true. In this test the null hypothesis is that the observed somatic mutations do not occur in the same cell and instead exist in two clonal populations where the proportion of each population = $2 \cdot$ variant allele frequency (assuming cells are diploid and heterozygous for the mutation). In samples where three somatic mutations were identified an alternative null hypothesis may be to use three clonal populations, however assuming that the three somatic mutations are partitioned into two clonal populations as asserted above is a more conservative test and therefore used here. To determine the expected number of triple mutant nuclei barcodes we first determined the expected number of droplets with two (or more) nuclei by approximating a Poisson distribution. The expected number of triple mutant nuclei barcodes is the product of the number of droplets with two nuclei, the proportion of mutant clone 1, and the proportion of mutant clone 2.

Here we report the Poisson estimation p value as this is the accepted method for estimating the rates of false-positive droplets when dealing with data generated using microfluidics. We can also consider a more intuitive upper bound for the p value by considering the extreme case where each droplet contains two nuclei. In this case the expected number of triple mutant nuclei barcodes is the product of the total number of nuclei barcodes, the proportion of mutant clone 1, and the proportion of mutant clone 2. Even in this extreme case the highest p value among our data is $< 1 \times 10^{-17}$.

3.5 Contributions and Acknowledgements

This chapter is adapted from a study published in *Nature* (Ren & Snellings et al., 2021) with the following authors: Aileen A. Ren, Daniel A. Snellings, Sophie Y. Su, Courtney C. Hong, Marco Castro, Alan T. Tang, Matthew R. Detter, Nicholas Hobson, Romuald Girard, Sharbel Romanos, Rhonda Lightle, Thomas Moore, Robert Shenkar, Christian Benavides, M. Makenzie Beaman, Helge Mueller-Fielitz, Mei

Chen, Patricia Mericko, Jisheng Yang, Derek C. Sung, Michael T. Lawton, Michael Ruppert, Markus Schwaninger, Jakob Körbelin, Michael Potente, Issam A. Awad, Douglas A. Marchuk and Mark L. Kahn. AAR and DAS contributed equally to this study. AAR designed and performed most of the mouse and tissue culture experiments and wrote the manuscript. DAS performed the genetic studies of human CCM lesions and wrote the manuscript. SYS created and performed the adult cranial window assays in mice. CCH, ATT and MRD contributed to mouse genetic studies. MC performed in vitro studies. NH, RG, SR, RL, TM, RS and IAA performed microCT CCM lesion imaging and quantification in a blinded manner. MC and PM assisted with mouse genetic studies. JY and DCS performed histologic studies. MTL provided surgically excised human CCM samples. MS and JK provided critical reagents. MP, IAA, DAM and MK designed experiments and wrote the manuscript.

We thank the members of the Kahn lab for their thoughtful comments and advice during this work. We thank Angioma Alliance for patient enrollment, and the University of Chicago PaleoCT core facility for its expertise in imaging and image quantitation. We thank the Penn CDB Microscopy Core for support with microscopy. Flow cytometry was performed in the Duke Human Vaccine Institute Research Flow Cytometry Shared Resource Facility. We thank Duke University School of Medicine for use of the Sequencing and Genomic Technologies Shared Resource for library preparation and sequencing. These studies were supported by National Institute of Health grants R01HL094326 and R01NS100949 (MK), P01NS092521 (MK, DM, IA) the Leducq Foundation (MK, MP), the AHA-Allen foundation (MK), T32 HL007150 (AR), F31HL152738 (DS), F31NS115256 (CH), F30NS100252 (AT), European Research Council (ERC) Synergy Grant-2019-WATCH-810331 (MS) and ERC Consolidator Grant EMERGE-773047 (MP).

4

Developmental Venous Anomalies Predispose to Malformation

This chapter is adapted from a study published in *bioRxiv* (Snellings et al., 2021)

4.1 Premise

Cerebral cavernous malformations (CCMs) are hemorrhagic neurovascular malformations that may lead to stroke, seizures and other clinical sequelae. CCM disease may be inherited by an autosomal dominant loss of function (LOF) mutation in the genes encoding components of the CCM signaling complex: *KRIT1* (Laberge-le Couteulx et al., 1999; Sahoo et al., 1999), *CCM2* (Liquori et al., 2003), or *PDCD10* (Bergametti et al., 2005). Solitary sporadic CCM lesions may also occur in the absence of inherited germline mutations in CCM complex genes. Previous studies have established that CCM pathogenesis follows a genetic two-hit model where somatic mutations cause biallelic LOF in *KRIT1*, *CCM2*, or *PDCD10* to initiate lesion formation (Akers et al., 2009; Gault et al., 2009, 2005; McDonald et al., 2014). Recent studies have found that somatic mutations in *PIK3CA* and *MAP3K3* also contribute to CCM pathogenesis (Hong et al., 2021; Ren et al., 2021; Weng et al., 2021). These discoveries opened new avenues for research and therapeutic development, but they also raised new questions about the roles of somatic mutations in familial versus sporadic lesions.

The presence of multiple somatic mutations in CCMs also helps explain a long-standing mystery: the association between sporadic CCM lesions and developmental venous anomalies (DVA). DVA are the most common vascular malformation present in 6–14% of the adult population (Brinjikji et al., 2017; Gokce et al., 2014; Jones et al., 2015; Linscott et al., 2016) with the majority developing prior to the age of 20 (Brinjikji et al., 2017). When assessed by magnetic resonance imaging, an adjacent DVA is identified in 24–32% of sporadic CCM cases (Abdulrauf et al., 1999; Porter et al., 1997; Wurm et al., 2005), and an even greater fraction of sporadic CCMs are found to be associated with a DVA at surgery (Abdulrauf et al., 1999; Porter et al., 1997). One study focused on DVA reported an adjacent sporadic CCM in 6.9% of all DVAs in a general population (116 of 1689) (Brinjikji et al., 2017). These studies

highlight the association between DVA and sporadic CCM. By contrast, familial CCM lesions have not been associated with DVA (Dammann et al., 2017). These combined data suggest that a DVA is not required for CCM formation but may be a predisposing factor in sporadic cases. We hypothesize that DVA are caused by somatic mutations, and that the genetic origin of DVA overlaps that of CCM. In this study we probe the relationship between mutations in *KRIT1*, *CCM2*, *PDCD10*, *PIK3CA*, and *MAP3K3* and explore a mechanism by which DVA act as a genetic primer for the genesis of sporadic CCM lesions.

4.2 Results

4.2.1 Mutations in *MAP3K3* and CCM Genes are Mutually Exclusive

To evaluate whether sporadic and familial CCMs have distinct somatic mutation spectra we identified somatic mutations present in 71 CCMs (20 familial CCMs and 51 sporadic/presumed sporadic CCMs). Mutations in *KRIT1*, *CCM2*, *PDCD10*, and *PIK3CA* were detected by targeted sequencing and/or droplet digital PCR (ddPCR) as previously described (Ren et al., 2021). The common gain of function mutation in *MAP3K3* (hg38 chr17:63691212, NM_002401.3, c.1323C>G; NP_002392, p.I441M) was detected by ddPCR using a previously published probe set (Couto et al., 2015).

The p.I441M mutation in *MAP3K3* was identified in 15/51 sporadic CCMs and 0/20 familial CCMs (Figure 4.1A). We also screened for *MAP3K3* p.I441M in 8 blood samples for which we were previously unable to identify a germline mutation in *KRIT1*, *CCM2*, *PDCD10*. None of the 8 blood samples harbored *MAP3K3* p.I441M. Notably 11/51 sporadic CCMs harbored at least 1 somatic mutation in *KRIT1*, *CCM2*, or *PDCD10*, however none of these CCMs also had a mutation in *MAP3K3* indicating that a mutual loss of the CCM complex and gain of function in MEKK3 (the protein product of *MAP3K3*) are not both required for CCM formation. As the CCM complex is known to be a direct inhibitor of MEKK3 activity (Zhou et al.,

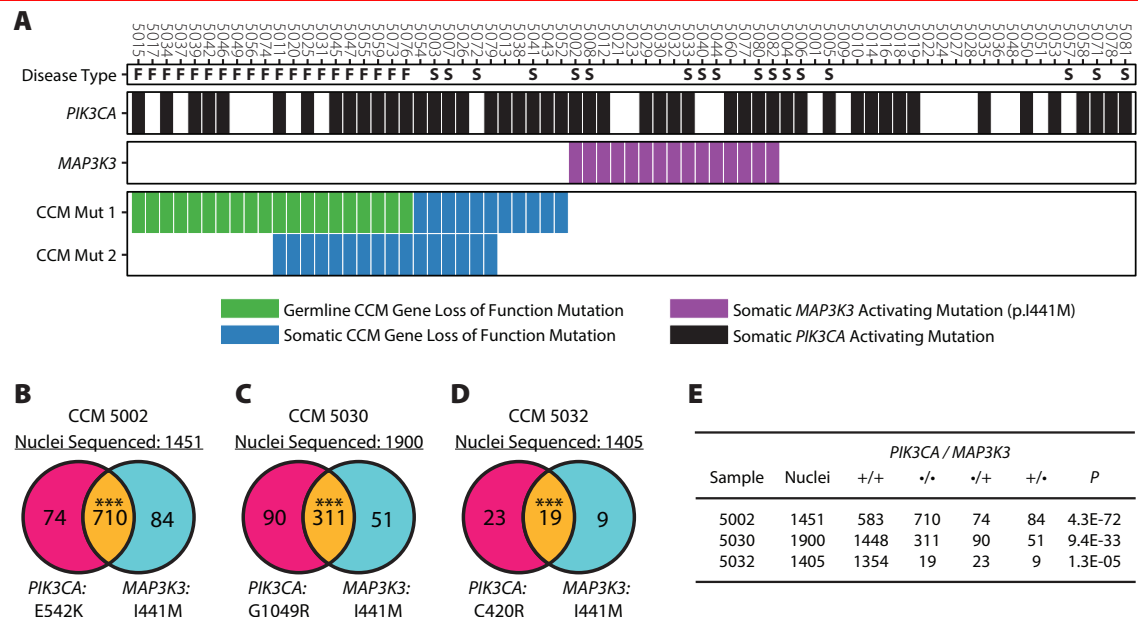


FIGURE 4.1: Mutations in *MAP3K3* are Mutually Exclusive with CCM Mutations and Occur in the Same Cells as *PIK3CA* Mutations.

A. Mutations present in 71 CCM samples. Disease type denotes whether the sample was familial (F), sporadic (S), or unknown (blank). The presence of somatic mutations in *PIK3CA* and *MAP3K3* are denoted by black and purple bars respectively. Germline and somatic mutations (green and blue respectively) in *KRIT1*, *CCM2*, or *PDCD10*, are shown in CCM Mut 1 with the second-hit mutation shown in CCM Mut 2 if present. **B–D.** Nuclei genotypes determined by snDNA-seq. The left and right circles in each Venn diagram shows the number of nuclei with the *PIK3CA* or *MAP3K3* mutations where the overlap shows nuclei harboring both mutations. *** P < 0.0001. **E.** Summary of data presented in B–D including P values determined by comparing the observed number of double mutant nuclei to the expected value derived from a Poisson distribution as done previously (Ren et al., 2021).

2015, 2016), these data strongly suggest identical functional consequences of these mutations.

The majority of CCM and verrucous venous malformations with a mutation in *MAP3K3* harbor the p.I441M variant (Couto et al., 2015; Hong et al., 2021; Weng et al., 2021), however an alternative variant p.Y544H has also been identified in a venous malformation (Al-Qattan et al., 2020). While ddPCR provides superior sen-

sitivity and specificity compared to targeted sequencing, it is restricted to detecting a single mutation per assay. To determine whether other mutations that contribute to CCM pathogenesis—either *MAP3K3* mutations besides p.I441M, or mutations in yet undiscovered genes—we performed whole-exome sequencing (mean depth 133x) on 8 sporadic CCMs for which no somatic mutations in *KRIT1*, *CCM2*, *PDCD10*, or *MAP3K3* were found. No additional mutations in *MAP3K3* were identified and no candidate variants in other genes passed QC filters (see Methods).

4.2.2 Cellular Phase of Somatic *MAP3K3* and *PIK3CA* Mutations

While somatic mutations in *KRIT1*, *CCM2*, *PDCD10*, and *MAP3K3* are mutually exclusive, somatic gain of function mutations in *PIK3CA* may co-occur with any other mutation (Figure 4.1A). We have previously shown that co-occurring mutations in *KRIT1/CCM2* and *PIK3CA* occur in the same clonal population of cells (Ren et al., 2021). To determine whether *MAP3K3* and *PIK3CA* mutations co-exist in the same cells we performed single-nucleus DNA-sequencing (snDNA-seq) on frozen tissue from three surgically resected CCMs determined to harbor both mutations (Figure 4.1B–D).

In CCMs 5002 and 5030, the vast majority of mutant nuclei harbor both mutations in *MAP3K3* and in *PIK3CA* indicating that these mutations co-exist in the same cells. In CCM 5032, 37% (19/51) of mutant nuclei harbor both mutations. While this is a far lower fraction compared to other samples, it is significantly higher than may be expected by chance when sampling from 1405 total nuclei ($P = 1.3 \times 10^{-5}$, Figure 4.1E). In bulk genetic analysis, the allele frequencies of *PIK3CA* and *MAP3K3* mutations detected in CCM 5002 were 19% and 13% respectively. In snDNA-seq the allele frequencies of these mutations increased to 54% and 55% respectively. This difference likely reflects the mosaic nature of CCMs. As snDNA-seq requires nuclei harvested from frozen tissue, we must sample a new area of the

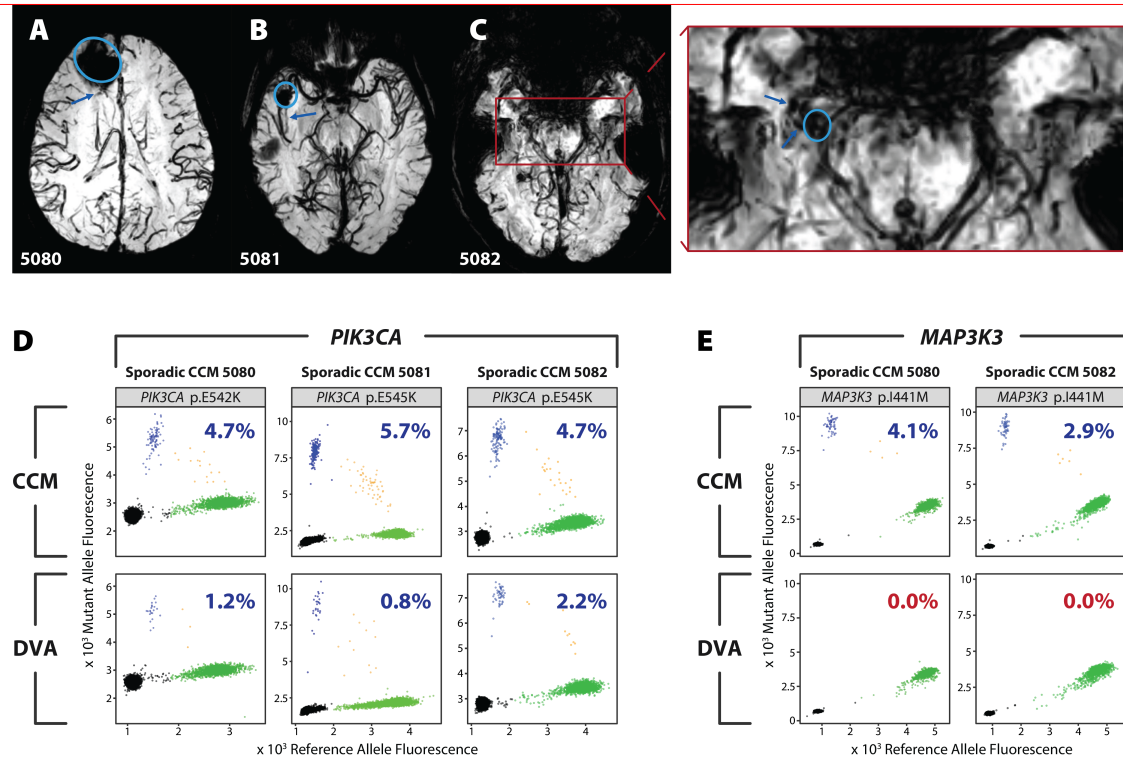


FIGURE 4.2: CCM and Adjacent DVA Harbor Identical Somatic Mutations in *PIK3CA*.

A–C. Axial magnetic resonance (MR) susceptibility weighted images acquired at 3 Tesla showing CCM (circle) and associated DVA branches sampled during surgery (arrow) in individuals with CCM 5080 (A) or 5081 (B) or 5082(C). The inset red box in C shows the region expanded to the right with the CCM and DVA marked. **D–E.** Somatic mutations in *PIK3CA* (D) and *MAP3K3* (E) in CCM (top panels) and the associated DVA (bottom panels) from samples 5081, 5082, and 5083. Mutations were detected by droplet digital PCR (ddPCR) and shown as the fluorescence of the reference probe on the x-axis, and the mutant probe on the y-axis. Droplets containing the reference allele, mutant allele, both, or neither, are colored in green, blue, orange, and black respectively. Percentage inset into each graph shows the variant allele frequency for the displayed mutation. If the mutation was determined to be present, the percentage is blue, else the percentage is red.

frozen lesion than was sampled for bulk sequencing. Sampling from different sites of the same lesion often results in minor changes in allele frequency, however the drastic change in allele frequency we find in CCM 5002 suggests either that our initial sample of the lesion for bulk sequencing contained largely non-lesion tissue, or an uneven distribution of mutant cells in the lesion.

4.2.3 CCMs and DVA Harbor a Shared Mutation in *PIK3CA*

Many sporadic CCMs are found in the vicinity of a developmental venous anomaly (DVA). We hypothesized that CCM and DVA may have a common genetic origin, specifically that DVA may be a genetic precursor to CCM. To determine whether DVA and CCMs originate from a shared mutation, we collected three sporadic CCMs and sampled a portion of the associated DVA obtained during surgery (Figure 4.2A–C). Assays for mutations via ddPCR revealed that all three CCMs have a somatic activating mutation in *PIK3CA* and that the same mutation is present within the paired DVA samples at lower frequency (Figure 4.2D). Furthermore, ddPCR revealed that two of the CCMs harbored a mutation in *MAP3K3* in addition to the previously noted mutation in *PIK3CA*. However, unlike the *PIK3CA* mutation, the *MAP3K3* mutation was entirely absent from both DVA samples (Figure 4.2E). The presence of the *PIK3CA*, but not the *MAP3K3*, mutation in the DVA confirms that the *PIK3CA* mutation in the DVA did not arise via cross-sample contamination. The presence of multiple somatic mutations in these CCMs allows us to infer the developmental history of the lesion. The cancer field commonly uses the presence or absence of somatic mutations in clonal populations to track the evolutionary history of a tumor (Jiao et al., 2014; Jolly & Van Loo, 2018). Recent studies have expanded on this approach to use somatic mutations as endogenous barcodes to track embryonic development (Bizzotto et al., 2021). Using this same approach, we infer that the DVA was the first lesion to develop and that the associated CCM is derived from cells of the DVA following a somatic mutation in *MAP3K3*.

4.2.4 Plasma miRNAs Reflect PI3K Activation in DVA Patients

In addition to assaying the presence of *PIK3CA* mutations in DVA associated with CCM, we would ideally also assay DVA that are not associated with CCM. Unfortunately, DVA are benign malformations and are not resected unless associated

with an additional pathology. This has precluded the direct assessment of *PIK3CA* mutations in DVA without a CCM. To address this limitation, we sought another source of tissue that could be assayed for indirect evidence of *PIK3CA* activation. Thus, we collected plasma from individuals with DVA without a CCM and measured circulating miRNAs that might serve as biomarkers reflecting *PIK3CA* activity (Mori et al., 2019).

We sequenced the plasma miRNomes of 12 individuals with a sporadic CCM associated with a DVA (CCM + DVA), 6 individuals with a DVA without a CCM (DVA only), and 7 healthy controls. Three plasma miRNAs were DE in the DVA only group when compared to healthy controls ($P < 0.05$; false discovery rate (FDR) corrected). Two of these DE miRNAs, *miR-134-5p* (FC = 0.10) and *miR-92a-3p* (FC = 3.10), putatively target *PIK3CA* and *PIK3CB* respectively, which are both components of the PI3K/AKT/mTOR pathway (Figure 4.3).

In addition, 18 plasma miRNAs were DE in CCM + DVA when compared to DVA only ($P < 0.05$; FDR corrected). Two of the 18 DE miRNAs, *miR-122-5p* (FC = 5.25) and *miR-182-5p* (FC = 0.21), target *AKT3* and *MAP3K3* respectively, linking them to both the PI3K/AKT/mTOR and MAPK/ERK pathways. Additionally, *let-7c-5p* (FC = 12.64) targets both *PIK3CA* and *MAP3K3*, consistent with the role of these two pathways in sporadic CCM pathogenesis (Figure 4.3). Of interest, *let-7c-5p* also targets *COL1A1*, a DEG within the transcriptome of human sporadic CCM lesions (see Supplementary Data). This gene is associated with PI3K/AKT signaling, platelet activation, and ECM-receptor interaction KEGG pathways (Kanehisa et al., 2021; Kanehisa & Goto, 2000), all of which have previously been implicated in CCM disease (Faurobert et al., 2013; Hong et al., 2021; Lopez-Ramirez et al., 2019; Ren et al., 2021).

Additionally, 28 DE plasma miRNAs were identified between CCM + DVA and healthy controls ($P < 0.05$; FDR corrected). Four of these miRNAs putatively target

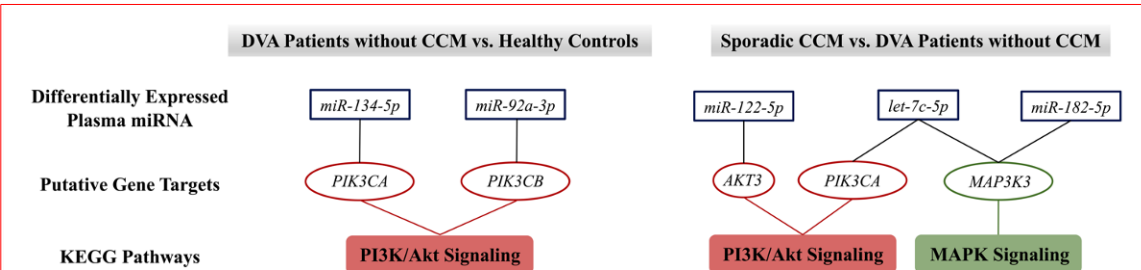


FIGURE 4.3: Differentially Expressed micro-RNAs in CCM and DVA.

Two miRNAs differentially expressed (DE) in the plasma of individuals with DVA without a CCM, *miR-134-5p* and *miR-92a-3p*, putatively target genes in the Kyoto Encyclopedia of Genes and Genomes (KEGG) PI3K/AKT signaling pathway. In the plasma of individuals with sporadic CCMs with an associated DVA, *miR-122-5p*, *miR-182-5p*, and *let-7c-5p* were DE and found to target genes within both PI3K/AKT and MAPK signaling KEGG pathways. All results were $P < 0.05$; false discovery rate corrected.

PIK3CA: *miR-148a-3p* ($FC = 3.27$), *miR-148b-3p* ($FC = 2.64$), *miR-128-3p* ($FC = 2.55$) and *let-7c-5p* ($FC = 4.20$), which also targets *MAP3K3*.

4.2.5 Relative Probability of Multiple Somatic Mutations

The association between DVA and sporadic—but not familial—CCMs suggests that there are at least two genetic trajectories by which a CCM may develop. The first trajectory is via a quiescent CCM caused by an initial mutation in *KRIT1*, *CCM2*, *PDCD10*, or *MAP3K3*. The second trajectory is via a DVA caused by an initial mutation in *PIK3CA* with subsequent mutations in *KRIT1*, *CCM2*, *PDCD10*, or *MAP3K3* leading to CCM formation. To understand whether one trajectory is favored in familial vs sporadic CCMs we use a simplified model to estimate the relative probability of CCM complex LOF (*KRIT1*, *CCM2*, *PDCD10*), *MAP3K3* GOF, and *PIK3CA* GOF.

Somatic mutagenesis is a complex process that depends on many variables including cell turnover rates, age, exposure to mutagens, and numerous genetic factors which facilitate DNA synthesis and repair. As a result, estimating absolute mutation

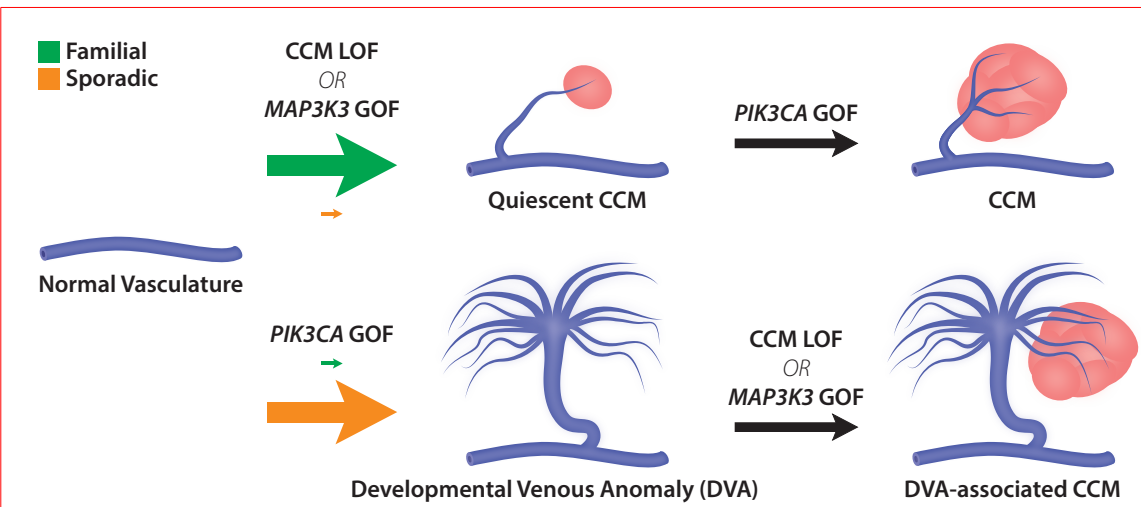


FIGURE 4.4: Genetic Model of CCM Pathogenesis.

The genetic trajectories that underly familial and sporadic CCM pathogenesis. The initial path of familial and sporadic CCMs are denoted by arrow colors (green and orange respectively) with the relative probability of each path denoted by the size of the arrow. Familial CCM preferentially develop via a LOF mutation in the CCM complex (*KRIT1*, *CCM2*, *PDCD10*) to develop a quiescent CCM that may acquire an additional mutation in *PIK3CA* that drives lesion growth. Sporadic CCM are more likely to develop via a DVA caused by a *PIK3CA* mutation creating a clonal population of cells that may subsequently acquire a CCM complex LOF or *MAP3K3* GOF.

rate is not feasible. However, by assuming a uniform mutation rate across these genes, we can determine the relative rate of CCM complex LOF, *MAP3K3* GOF, and *PIK3CA* GOF as simply the number of mutations that result in LOF or GOF. Determining this value for *MAP3K3* and *PIK3CA* is straightforward. To date there is only a single mutation in *MAP3K3* (p.I441M) that has been reported in CCMs. The spectrum of mutations in *PIK3CA* has been well documented in the catalogue of somatic mutations in cancer (COSMIC). In the absence of functional assays for each mutation, we define a GOF mutation as any mutation that accounts for >1% of all *PIK3CA* mutations COSMIC which was determined to be 10 mutations. The number of CCM complex LOF mutations was determined by considering all possible single nucleotide variants that would result in a premature stop codon or disrupt a

canonical splice site (see Methods). The average of these values for all three genes is 430 mutations (*KRIT1* = 718, *CCM2* = 353, *PDCD10* = 220). This is a very conservative estimate and should be considered a lower bound, since the majority of CCM complex LOF mutations are the result of frameshift mutations which are not accounted for here.

From the relative probability of each mutation, it is clear that familial CCMs will almost always develop via CCM complex LOF (Figure 4.4 top), consistent with the lack of association between familial CCM and DVA. The probability of two CCM complex LOF mutations in trans and in the same cell (as required for CCM complex LOF in sporadic CCMs) is far lower than for a single mutation (as required for CCM complex LOF in familial CCMs). In this study we identified 6 sporadic CCMs with biallelic somatic mutations in a CCM complex gene, therefore probability of this event is likely of similar magnitude to *MAP3K3* GOF which we identified in 15 sporadic CCMs. Assuming the same relative probability for CCM complex LOF as *MAP3K3* GOF in sporadic CCMs, we determine that sporadic CCM are at least 5x more likely to develop via *PIK3CA* GOF than CCM complex LOF or *MAP3K3* GOF (Figure 4.4 bottom). This finding is consistent with the strong association between DVA and sporadic CCM.

4.3 Discussion

4.3.1 *MAP3K3* GOF and CCM LOF Have Similar Molecular Effects

In this study we have further interrogated the relationship between somatic mutations in *KRIT1*, *CCM2*, *PDCD10*, *MAP3K3*, and *PIK3CA* which contribute to the pathogenesis of CCM. We find that somatic mutations in *MAP3K3* are not present in CCMs from individuals with familial CCM, consistent with a recent study (Weng et al., 2021). We find that sporadic CCMs may harbor mutations in *MAP3K3*, *KRIT1*, *CCM2*, or *PDCD10*, but that the lesion will only have mutations in one

of these genes. This implies that mutations in any of *MAP3K3*, *KRIT1*, *CCM2*, or *PDCD10* are sufficient for CCM formation, without the need for mutations in a second gene. As *KRIT1*, *CCM2*, and *PDCD10* are all members of the CCM signaling complex, this reflects the fact that the loss of any component of the complex prevents normal signal transduction. Similarly, as the CCM complex is a direct inhibitor of *MAP3K3* activity (Zhou et al., 2015), this pathway may be activated by either CCM complex LOF or by *MAP3K3* GOF, but the mutual exclusivity of mutations in these genes suggests that only one of these events is necessary for lesion formation.

4.3.2 DVA Clonal Expansion Promotes Additional Mutations

CCMs often develop as the result of multiple somatic mutations that co-exist within the same cells as we show with snDNA-seq. Although several somatic mutations occur in every cell division (Rodin et al., 2021), the specificity of the mutations in CCM translates to a very low chance of acquiring these mutations within a single cell. This is especially true of somatic mutations in *MAP3K3* and *PIK3CA*, both of which have very narrow spectra of activating mutations. Despite this improbability, the accumulation of these mutations in CCM seems to occur frequently. One possible explanation for this phenomenon is that CCMs have an increased rate of somatic mutations. There is little evidence supporting this theory and such a mechanism is difficult to conceive in cases of sporadic CCM where individuals have no known genetic predisposition to CCM. An alternative explanation is that after an initial somatic mutation, the singly-mutated cell undergoes clonal expansion to form an intermediate lesion. In this study we identify 7 CCMs with either biallelic LOF in a CCM complex gene or *MAP3K3* GOF in the absence a *PIK3CA* mutation, suggesting that *PIK3CA* activation is not required for CCM formation. Furthermore, previous work in mouse models has shown that loss of a CCM complex gene (with WT *Pik3ca*) leads to clonal expansion of the mutant cells and in later stages of growth,

incorporation of WT endothelial cells (Detter et al., 2018; Malinverno et al., 2019). As a result of this clonal expansion, the probability of creating a double-mutant cell increases by a factor of the clonal population size as there are more cells in which the second mutation may occur. Somatic mutations in this clonal population may be acquired by genome replication during expansion or after expansion as mutations accumulate via DNA damage and error-prone repair as has been reported in other quiescent cell types (Lodato et al., 2018).

The data presented in this study suggest that DVA are an intermediate lesion as posited by the latter explanation. Genetic analysis of DVA and paired CCM show that at least some DVA develop following a somatic activating mutation in *PIK3CA*. Furthermore, plasma miRNA analysis of individuals with DVA-associated CCM revealed differentially expressed miRNAs that putatively target *PIK3CA* and *MAP3K3*, the same genes that are mutated in these lesions. By contrast, individuals with DVA but no CCM differentially expressed miRNAs that putatively target *PIK3CA*, but not *MAP3K3*. These data are consistent with the distribution of mutations we observe in CCM and DVA, and the differential regulation of these miRNAs may reflect an attempt to compensate for dysregulation of PI3K and MAPK signaling due to the somatic mutations.

The presence of *PIK3CA* mutations in DVA suggests that DVA act as a genetic precursor to CCM, which would account for the strong association between sporadic CCM and DVA. Likewise, DVA are not associated with familial CCM because the presence of an inherited germline mutation in a CCM gene strongly biases probability towards a CCM gene somatic mutation occurring first, as there exist many different mutations that may cause LOF, but far fewer that would cause GOF in *PIK3CA*.

This study is the first to collect CCM and associated DVA for genetic analysis. Collecting tissue from CCM-associated DVA is challenging; however, collecting tissue from DVA not associated with CCM is yet more challenging as DVA are considered

benign and are therefore not resected. We have attempted to address this limitation by studying biomarkers of PI3K activity which can be assayed noninvasively in blood plasma. Assaying the presence of *PIK3CA* mutations in DVA not associated with CCM will be the domain of future studies, but the data we present here demonstrate a clear link between DVA and *PIK3CA*, and suggest a model that explains the long recognized—but poorly understood—association between CCM and DVA.

4.3.3 DVA May Contribute to Additional Phenotypes

While we are unable to address the presence of *PIK3CA* mutations in DVA not associated with CCM, it is worth noting that DVAs have been associated with other PI3K-related disorders(Brinjikji et al., 2018; Dhamija et al., 2018; Rasalkar & Paunipagar, 2010; Roux et al., 2020; Santucci et al., 2008; Tan et al., 2007; Ucler, 2019) including some cancers and neurological malformations, suggesting that DVA may have a role, possibly even as a genetic primer, in these other diseases.

4.4 Methods

Sample Collection

Surgically resected CCMs were obtained from the University of Chicago, the Barrow Neurological Institute, and the Angioma Alliance biobank. Additional DVA tissue was discretely dissected from the lesion during surgical resection of the associated CCM at the University of Chicago. This study was approved by each institution's respective Institutional Review Board.

DNA Extraction

DNA from CCM and DVA samples was extracted using the DNeasy blood and tissue kit (QIAGEN, catalog number 69504) per the manufacturers protocol. DNA purity was determined by Nanodrop and concentration was determined using the Qubit

dsDNA BR assay kit (Invitrogen, catalog number Q32850) per the manufacturers protocol.

Droplet Digital PCR

Detection of *MAP3K3* p.I441M was performed via ddPCR using a previously described probe set(Couto et al., 2015). Assays were performed using 30–100ng of DNA with the QX200 AutoDG system (BioRad) and quantified with the QX200 droplet reader (BioRad). Analysis was performed with the QuantaSoft software (BioRad).

Sequencing

A total of 8 sporadic CCMs with no identified mutation in *KRIT1*, *CCM2*, *PDCD10*, or *MAP3K3* (5001, 5005, 5006, 5022, 5024, 5036, 5078, and 5081) were used for whole-exome sequencing prepared using the SureSelect Human All Exon V7 probe set (Agilent, Design ID S31285117) per the manufacturers protocol. Prepared libraries were sequenced on one lane of a NovaSeq 6000 S4 flow cell for a mean depth of 133x.

Sequence Analysis

Sequencing data was processed using the Gene Analysis Toolkit (GATK, Broad Institute) while following the GATK best practices for somatic short variant discovery using Mutect2. Secondary variant detection was performed using gonomics (<https://github.com/vertgenlab/gonomics>) and bcftools mpileup to manually examine *KRIT1*, *CCM2*, *PDCD10*, and *MAP3K3* for somatic variants. Putative variants were annotated using Funcotator (GATK), the catalog of somatic mutation in cancer (COSMIC), and the genome aggregation database (gnomAD). Putative variants were filtered according to the following criteria: greater than 50x total coverage, less than 90% strand specificity, greater than 5 reads supporting the alternate allele, greater

than 1% alternate allele frequency, less than 1% population allele frequency, and predicted protein/splicing change.

Single-Nucleus DNA Sequencing

Nuclei isolation, snDNA-seq, and analysis were performed as previously described(Ren et al., 2021).

miRNA Extraction and Sequencing

Total plasma RNA was extracted from the plasma of 12 individuals with a sporadic CCM and an associated DVA (CCM + DVA), 6 individuals with DVA and without a CCM (DVA only), and 7 healthy controls using the miRNeasy Serum/Plasma Kit (Qiagen, Hilden, Germany) following the manufacturer isolation protocol. Diagnosis of CCM with an associated DVA, as well as DVA without a CCM lesion was confirmed on susceptibility weighted MR imaging. Illumina small RNA-Seq kits (Clontech, Mountain View, CA, USA) were then used to generate cDNA libraries, and sequencing was completed with the Illumina HiSeq 4000 platform (Illumina, San Diego, CA, USA), with single-end 50bp reads, at the University of Chicago Genomics Core. Differential miRNA analyses were completed between (1) CCM + DVA to DVA only and then (2) DVA only to healthy controls. The differentially expressed miRNAs were identified having $P < 0.05$, FDR-corrected. All analyses were completed using the sRNAToolbox and DESeq2 R packages(Love et al., 2014; Rueda et al., 2015).

Identification of Putative Targets

miRWalk 3.0 was used to identify the putative gene targets of each of the DE miRNAs, using a random forest tree algorithm with a bonding prediction probability higher than 95% on the 3 different gene locations (3' UTR, 5' UTR, and CDS)(Sticht et al., 2018). Putative gene targets of the DE miRNAs were identified in at least 2

of the 3 databases. DE miRNAs between (1) CCM + DVA and DVA only as well as (2) DVA only and healthy controls were then analyzed for potential targeting of the PI3K, AKT, and MAPK gene families.

Estimating Possible LOF Mutations in KRIT1, CCM2, and PDCD10

The majority of LOF mutations in *KRIT1*, *CCM2*, and *PDCD10* result in either: creation of a premature stop codon (nonsense); disruption of a canonical splice site; or a frameshift. The first two of these are typically caused by a single nucleotide variant (SNV) and can be determined from the gene sequence. However, frameshift variants resulting from insertions and deletions may occur in any exon regardless of sequence context. This prevents a meaningful comparison between indel and SNV events, without making assumptions about the rate of somatic SNV and indel events. To determine a conservative lower bound for the number of LOF mutations in the CCM complex genes, we only consider nonsense and splice site mutations. The number of nonsense and splice site mutations were determined from the sequences of *KRIT1* (ENST00000394507.5), *CCM2* (ENST00000258781.11), and *PDCD10* (ENST00000392750.7). Nonsense mutations were considered any SNV in the coding sequence that would result in an in frame stop codon prior to the stop codon in the reference sequence. Splice site mutations were considered any SNV in the nearly invariant sequences at each exon-intron boundary that mediate canonical splicing.

Sporadic CCM Transcriptome

Laser micro-dissected neurovascular units (NVUs) from sporadic CCM lesions were sequenced for transcriptomic analyses in comparison to micro-dissected NVUs from human brain microvasculature. The differential analyses identified 426 DE genes (DEGs) ($P < 0.05$; FDR corrected; $FC > |1.5|$). Additionally, 8 pathways from the

Kyoto Encyclopedia of Genes and Genomes (KEGG) were enriched ($P < 0.05$, FDR corrected).

Sporadic Transcriptome and KEGG Pathway Analyses

Six human sporadic CCM lesions were surgically resected prior to embedding in optimal cutting temperature, snap-freezing, and storing at -80°C. Control brain tissue was collected during autopsy from three subjects lacking neurological disease, fixed in formalin, and embedded in paraffin blocks. Five- μm tissue sections were mounted on Leica glass slides (Leica Biosystems Inc) and were stained, in accordance with the manufacturer's protocols, with HistoGene (Applied Biosystems) for frozen tissue and Paradise stain (Applied Biosystems) for paraffin-embedded tissue. The neurovascular units (NVUs) from sporadic CCM lesions and normal brain capillaries were then collected using laser capture microdissection and stored at -80°C. RNA was isolated using an RNA extraction kit (RNeasy Micro Kit, Qiagen). cDNA libraries were then generated with low-input strand-specific RNA-Seq kits (Clontech) and sequenced using the Illumina HiSeq 4000 platform with single-end 50bp reads. Differentially expressed genes were defined as $P < 0.05$, FDR corrected.

Enriched Kyoto Encyclopedia of Genes and Genomes (KEGG) pathways (Kanehisa et al., 2021; Kanehisa & Goto, 2000) were obtained for the DE genes (DEGs) in the sporadic transcriptome with fold change values greater than 1.5 ($P < 0.05$, FDR corrected). The sporadic transcriptome was compared to the putative targets of the DE miRNAs between (1) CCM + DVA and DVA only as well as (2) DVA only and healthy controls to obtain a set of overlapping genes. Enriched Kyoto Encyclopedia of Genes and Genomes (KEGG) pathways were obtained for the overlapping genes, using a database and knowledge extraction engine with a Bayes factor greater than 3.

4.5 Contributions and Acknowledgements

This chapter is adapted from a study published in *bioRxiv* (Snellings et al., 2021) with the following authors: Daniel A. Snellings, Romuald Girard, Rhonda Lightle, Abhinav Srinath, Sharbel Romanos, Ying Li, Chang Chen, Aileen A. Ren, Mark L. Kahn, Issam A. Awad, Douglas A. Marchuk. DAS designed and performed the genetic studies of human CCM lesions and wrote the manuscript. IAA performed surgical resection of CCM and DVA samples used in this study. RG, RL, AS, SR, YL, CC and IAA performed plasma miRNA sequencing and analysis. AAR and MLK assisted with experimental design. RG, IAA, and DAM designed experiments and wrote the manuscript.

We thank the patients who donated tissue for this study. We thank Angioma Alliance, the Barrow Neurological Institute, and the University of Chicago for patient enrollment and sample collection. Nucleus sorting was performed in the Duke Human Vaccine Institute Research Flow Cytometry Shared Resource Facility. We thank Duke University School of Medicine for use of the Sequencing and Genomic Technologies Shared Resource for library preparation and sequencing. These studies were supported by National Institute of Health grants, P01NS092521 (DM, IA, MK), F31HL152738 (DS).

Conclusions & Musings

5.1 HHT Pathogenesis

5.2 CCM Pathogenesis

5.2.1 *Regrowth after Surgical Resection*

5.2.2 *CCM & Meningioma*

Although the vascular lesions are the primary sequelae of familial CCM, many groups have noted an increased prevalence of meningioma in individuals with familial CCM—especially those with a mutation in *PDCD10* (Labauge et al., 2009; Riant et al., 2013; Garaci et al., 2015). In addition, we have previously been contacted by an individual whose child had a sporadic CCM that regrew into a meningioma. Unfortunately we were unable to acquire a tissue sample for genetic analysis, however this case along with the strong link between familial CCM and meningioma has fueled my interest in understanding the link between CCM and meningioma.

Kruppel-like factor 4 (KLF4)

KLF4 is a transcription factor with key roles in the pathogenesis of both CCM and meningioma. In CCM, *KLF4* (along with *KLF2*) is a key player in CCM

signaling that is upregulated by loss of the CCM complex or gain of function in *MAP3K3* (Cuttano et al., 2016; Zhou et al., 2016). Indeed, overexpression of *KLF4* in mouse models leads to an aggressive CCM-like phenotype (Ren et al., 2021). In meningioma, mutations in *KLF4* are common and often co-occur with mutations in *TRAF7* (Reuss et al., 2013). In addition, *KLF4* mutated meningioma have been shown to be responsive to treatment with temsirolimus (von Spreckelsen et al., 2020)—a derivative of rapamycin (sirolimus) which has been shown to be effective in treating CCM in mice (Ren et al., 2021). The importance of *KLF4* in both CCM and meningioma suggests that dysregulation of *KLF4* may underlie the development of meningioma in individuals with familial CCM.

The majority of *KLF4* mutations found in the catalog of somatic mutations in cancer (COSMIC) result in p.K409Q (Figure 5.1A). This narrow spectrum of mutations suggests that the p.K409Q variant results in *KLF4* gain of function. Notably, the p.K409Q mutation is highly specific to meningioma, occurring in very few other cancer types (Figure 5.1B). The *KLF4* protein contains 3 DNA-binding zinc-finger domains that contribute to its activity as a transcription factor. The p.K409Q mutation occurs in the first of the three zinc-finger domains (Figure 5.1C). A structural study of *KLF4* determined that the second two zinc-finger domains consistently bind DNA, however the first zinc-finger only sometimes participates in DNA binding (Schuetz et al., 2011). They determined that the second and third domains are required for site specificity, but the third "inhibits cryptic self-renewal and block of differentiation activity". This immediately suggests a mechanism by which the p.K409Q mutation may disrupt the inhibitory capacity of *KLF4* while retaining its functions that are independent of the first zinc-finger domain.

I thought that since overexpression of *KLF4* is sufficient to cause CCM in mice, the p.K409Q mutation may cause some sporadic CCMs in humans. To test this, I developed a ddPCR assay to test for this mutation in 30 mutation-negative sporadic

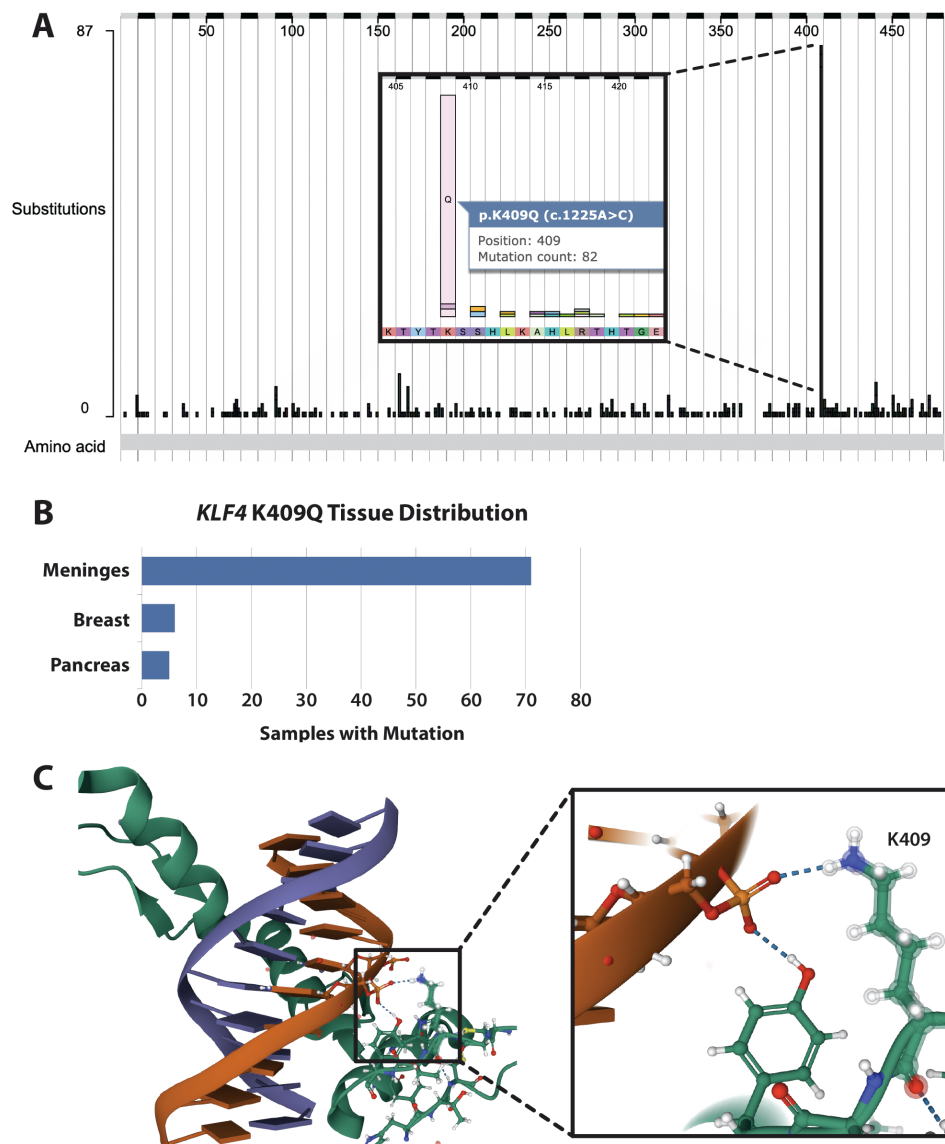


FIGURE 5.1: *KLF4* Mutations in COSMIC.

A. Distribution of somatic mutations in *KLF4* that are present in the catalog of somatic mutations in cancer (COSMIC). The location of the most frequent mutation (p.K409Q) is expanded in the inset. B. Distribution of *KLF4* p.K409Q in tissue types present in COSMIC. C. Structure of *KLF4* zinc-finger domains bound to DNA (pdb: 2WBU). Border box denotes the expanded region to the right showing the interaction between K409 and the DNA backbone.

CCM, however I did not find evidence for this mutation in any of these samples. This may be a reflection of the highly specific functions of the first zinc-finger domain in *KLF4* as discussed above. This function may be critical for meningioma development, but less important for CCM development. However, the inverse is not necessarily true—i.e. while the p.K409Q mutation may not cause CCMs, overexpression of *KLF4* may cause meningioma. This is currently unknown, though if true, may account for the presence of meningioma in familial CCM. One straightforward way to test this hypothesis would be to sequence tissue from meningioma in individuals with familial CCM. I suspect that these meningioma harbor a somatic loss of function mutation in *KRIT1/CCM2/PDCD10* leading to biallelic loss of a CCM gene resulting in upregulation of *KLF4*. These meningioma may also harbor a second mutation in *TRAF7* which have often been found in non-CCM meningioma. Unfortunately, tissue samples of meningioma from individuals with familial CCM have been difficult to acquire, thus I have been unable to test this hypothesis. However, I expect that future studies will find that *KLF4* is a critical link between CCM and meningioma.

5.3 Developmental Venous Anomalies as a Primer for Disease

5.3.1 *Association with Sporadic CCM*

5.3.2 *Association with Other Diseases*

5.3.3 *Cowden Syndrome*

5.3.4 *Implications*

5.4 Other Vascular Malformations

5.4.1 *Classification of Vascular Malformations and Vascular Tumors*

5.4.2 *Sturge-Weber Syndrome and Somatic Mutations in GNAQ*

Happle's hypothesis

GNAQ in uveal melanoma and circumscribed choroidal hemangioma

Link between SWS, UM, and CCH?

5.4.3 *The Curious Case of Infantile Hemangioma*

Infantile hemangioma (IH) are one of the most common vascular malformations.

They occur in children and are typically present at birth as a red spot flush with the surrounding skin. Soon after birth the hemangioma rapidly grows and becomes raised from the skin. They are generally benign and are typically left alone unless they cover the child's mouth, nose, or eyes. What makes IH so interesting compared to other types of vascular malformations is that they almost always completely regress within the first few years of the child's life. While other types of vascular malformations may spontaneously regress (telangiectasia and AVMs), none do so with the consistency of IH. This phenomenon has been of great interest, not for the purpose of developing therapeutics for IH (propranolol is an extremely effective treatment for IH) but for uncovering the mechanism of regression in the hopes that what we learn can be applied to regress other, more nefarious, vascular malformations.

GLUT1 in IH endothelium

Perhaps one of the most provocative discoveries into the mechanism of IH pathogenesis is the fact that endothelial cells from IHs highly express GLUT1 (North et al., 2000, 2001). GLUT1 is a glucose transporter that has remarkable specificity for the placental endothelium. This finding suggested that the IH may be comprised of cells that dislodged from the maternal placenta, then became hyper-proliferative in a post-fetal environment. If this hypothesis is correct, one would expect to find that the IH is a genetically chimeric growth between fetal and maternal cells. This hypothesis was put to the test using fluorescence *in situ* hybridization to assay the presence of XX cells in IH from a male infant with confirmation by sequencing microsatellites and SNPs that were divergent between mother and child. This analysis found no evidence for maternal-fetal chimerism in IH (Pittman et al., 2006). Despite this counter-evidence, the presence of GLUT1 in IH is strongly indicative of some link with the placenta though unfortunately this link currently remains elusive. The current literature has very clearly shown the presence of GLUT1 in IH endothelial cells, however the extent of the placental transcriptional program is unclear. Epigenomic profiling of paired IH and maternal placental samples may give valuable insights into the mechanism of IH.

Efforts to find somatic mutations in IH

As it is quickly becoming clear that the vast majority of vascular malformations are the result of somatic mutations—many occurring in known oncogenes—I thought that somatic mutations may also underlie IH. To test this, I sequenced 61 IH lesions on an ‘oncopanel’ covering many genes that are highly mutated in cancers as well as several genes previously implicated in vascular malformations (*KRIT1*, *CCM2*, *PDCD10*, *ACVRL1*, *ENG*, *SMAD4*, etc.) Unfortunately after filtering putative variants, no there were no variants with likely functional significance and that occurred in

more than a single sample. I am aware of at least 1 other group that has attempted to identify somatic mutations in IH via whole-exome sequencing, however to date there are no known somatic mutations in IH. One important aspect of these studies that must be noted is that they are invariably focused on coding regions of the genome. Non-coding variants are more than capable of causing disease however discovery-focused sequencing studies often ignore non-coding regions both because of the cost of sequencing the entire genome to a depth sufficient to detect somatic mutations, and the challenges associated with functional analysis of non-coding variants. Further studies may find that somatic mutations do cause IH, but they occur in a region of the genome that is missed by the majority of sequencing studies.

5.5 The Molecular Basis of Genetic Dominance

5.5.1 *Phenotypic Dominance ≠ Genetic Dominance*

5.5.2 *Knudsons Fingerprint*

5.5.3 *The Diverse Functional Effects of Genetic Mutations*

5.6 The Intersection of Somatic Mutagenesis and Evolution

5.6.1 *The Creation of New Alleles*

5.6.2 *The Relationship Between Mutability and Fitness Landscape*

5.6.3 *Recurring Mutations & Convergent Evolution*

5.6.4 *Clonal Evolution of Somatic Mutants*

5.6.5 *Cancer*

5.7 Somatic Mutations

5.7.1 *The Role of Somatic Mutations in Aging*

5.7.2 *Constitutional Intolerance & Somatic Permissiveness*

5.7.3 *Somatic Reversion of Pathogenic Mutations*

5.7.4 *What is the Consequence of RNA Mutations?*

5.8 Innovation in the Sequencing Era

5.8.1 *Detection of Somatic Mutations*

5.8.2 *Single Cell Sequencing*

5.8.3 *Utility of Rare Disease Research in Mechanistic Discovery*

5.8.4 *Data Democratization & Individual Privacy*

5.8.5 *Growing Importance of Informatics in Biology*

Appendix A

Probability of Multiple Somatic Mutations

Bibliography

- Abdalla, S. A., Pece-Barbara, N., Vera, S., Tapia, E., Paez, E., Bernabeu, C., & Letarte, M. (2000). Analysis of ALK-1 and endoglin in newborns from families with hereditary hemorrhagic telangiectasia type 2. *Hum Mol Genet*, 9(8), 1227–37.
URL <https://www.ncbi.nlm.nih.gov/pubmed/10767348>
- Abdulrauf, S. I., Kaynar, M. Y., & Awad, I. A. (1999). A comparison of the clinical profile of cavernous malformations with and without associated venous malformations. *Neurosurgery*, 44(1), 41–6; discussion 46–7.
URL <https://www.ncbi.nlm.nih.gov/pubmed/9894962>
- Akers, A., Al-Shahi Salman, R., I, A. A., Dahlem, K., Flemming, K., Hart, B., Kim, H., Jusue-Torres, I., Kondziolka, D., Lee, C., Morrison, L., Rigamonti, D., Rebeiz, T., Tournier-Lasserve, E., Waggoner, D., & Whitehead, K. (2017). Synopsis of Guidelines for the Clinical Management of Cerebral Cavernous Malformations: Consensus Recommendations Based on Systematic Literature Review by the Angioma Alliance Scientific Advisory Board Clinical Experts Panel. *Neurosurgery*, 80(5), 665–680.
URL <https://www.ncbi.nlm.nih.gov/pubmed/28387823>
- Akers, A. L., Johnson, E., Steinberg, G. K., Zabramski, J. M., & Marchuk, D. A. (2009). Biallelic somatic and germline mutations in cerebral cavernous malformations (CCMs): evidence for a two-hit mechanism of CCM pathogenesis. *Hum Mol Genet*, 18(5), 919–30.
URL <https://www.ncbi.nlm.nih.gov/pubmed/19088123>
- Al-Olabi, L., Polubothu, S., Dowsett, K., Andrews, K. A., Stadnik, P., Joseph, A. P., Knox, R., Pittman, A., Clark, G., Baird, W., Bulstrode, N., Glover, M., Gordon, K., Hargrave, D., Huson, S. M., Jacques, T. S., James, G., Kondolf, H., Kangesu, L., Keppler-Noreuil, K. M., Khan, A., Lindhurst, M. J., Lipson, M., Mansour, S., O'Hara, J., Mahon, C., Mosica, A., Moss, C., Murthy, A., Ong, J., Parker, V. E., Riviere, J. B., Sapp, J. C., Sebire, N. J., Shah, R., Sivakumar, B., Thomas, A., Virasami, A., Waelchli, R., Zeng, Z., Biesecker, L. G., Barnacle, A., Topf, M., Semple, R. K., Patton, E. E., & Kinsler, V. A. (2018). Mosaic RAS/MAPK variants cause sporadic vascular malformations which respond to targeted therapy.

J Clin Invest, 128(4), 1496–1508.

URL <https://www.ncbi.nlm.nih.gov/pubmed/29461977>

Al-Qattan, M. M., Al-Balwi, M. A., Al-Zayed, E. M., Al-Sohaibani, M., Gelidan, A. G., & Alsheibani, S. (2020). Late-onset multiple venous malformations confined to the upper limb: link to somatic MAP3K3 mutations. *J Hand Surg Eur Vol*, 45(10), 1023–1027.

URL <https://www.ncbi.nlm.nih.gov/pubmed/32380920>

Al-Shahi Salman, R., Hall, J. M., Horne, M. A., Moultrie, F., Josephson, C. B., Bhattacharya, J. J., Counsell, C. E., Murray, G. D., Papanastassiou, V., Ritchie, V., Roberts, R. C., Sellar, R. J., Warlow, C. P., & Scottish Audit of Intracranial Vascular Malformations, c. (2012). Untreated clinical course of cerebral cavernous malformations: a prospective, population-based cohort study. *Lancet Neurol*, 11(3), 217–24.

URL <https://www.ncbi.nlm.nih.gov/pubmed/22297119>

Argyriou, L., Twelkemeyer, S., Panchulidze, I., Wehner, L. E., Teske, U., Engel, W., & Nayernia, K. (2006). Novel mutations in the ENG and ACVRL1 genes causing hereditary hemorrhagic telangiectasia. *Int J Mol Med*, 17(4), 655–9.

URL <https://www.ncbi.nlm.nih.gov/pubmed/16525724>

Awad, I. A., & Polster, S. P. (2019). Cavernous angiomas: deconstructing a neurosurgical disease. *J Neurosurg*, 131(1), 1–13.

URL <https://www.ncbi.nlm.nih.gov/pubmed/31261134>

Bailey, M. H., Tokheim, C., Porta-Pardo, E., Sengupta, S., Bertrand, D., Weerasinghe, A., Colaprico, A., Wendl, M. C., Kim, J., Reardon, B., Ng, P. K., Jeong, K. J., Cao, S., Wang, Z., Gao, J., Gao, Q., Wang, F., Liu, E. M., Mularoni, L., Rubio-Perez, C., Nagarajan, N., Cortes-Ciriano, I., Zhou, D. C., Liang, W. W., Hess, J. M., Yellapantula, V. D., Tamborero, D., Gonzalez-Perez, A., Suphavilai, C., Ko, J. Y., Khurana, E., Park, P. J., Van Allen, E. M., Liang, H., Group, M. C. W., Cancer Genome Atlas Research, N., Lawrence, M. S., Godzik, A., Lopez-Bigas, N., Stuart, J., Wheeler, D., Getz, G., Chen, K., Lazar, A. J., Mills, G. B., Karchin, R., & Ding, L. (2018). Comprehensive Characterization of Cancer Driver Genes and Mutations. *Cell*, 173(2), 371–385 e18.

URL <https://www.ncbi.nlm.nih.gov/pubmed/29625053>

Bergametti, F., Denier, C., Labauge, P., Arnoult, M., Boetto, S., Clanet, M., Coubes, P., Echenne, B., Ibrahim, R., Irthum, B., Jacquet, G., Lonjon, M., Moreau, J. J., Neau, J. P., Parker, F., Tremoulet, M., Tournier-Lasserve, E., & Societe Francaise de, N. (2005). Mutations within the programmed cell death 10 gene cause cerebral cavernous malformations. *Am J Hum Genet*, 76(1), 42–51.

URL <https://www.ncbi.nlm.nih.gov/pubmed/15543491>

- Bizzotto, S., Dou, Y., Ganz, J., Doan, R. N., Kwon, M., Bohrson, C. L., Kim, S. N., Bae, T., Abyzov, A., Network, N. B. S. M., Park, P. J., & Walsh, C. A. (2021). Landmarks of human embryonic development inscribed in somatic mutations. *Science*, 371(6535), 1249–1253.
URL <https://www.ncbi.nlm.nih.gov/pubmed/33737485>
- Bossler, A. D., Richards, J., George, C., Godmilow, L., & Ganguly, A. (2006). Novel mutations in ENG and ACVRL1 identified in a series of 200 individuals undergoing clinical genetic testing for hereditary hemorrhagic telangiectasia (HHT): correlation of genotype with phenotype. *Hum Mutat*, 27(7), 667–75.
URL <https://www.ncbi.nlm.nih.gov/pubmed/16752392>
- Bourdeau, A., Cymerman, U., Paquet, M. E., Meschino, W., McKinnon, W. C., Guttmacher, A. E., Becker, L., & Letarte, M. (2000). Endoglin expression is reduced in normal vessels but still detectable in arteriovenous malformations of patients with hereditary hemorrhagic telangiectasia type 1. *Am J Pathol*, 156(3), 911–23.
URL <https://www.ncbi.nlm.nih.gov/pubmed/10702408>
- Bourdeau, A., Dumont, D. J., & Letarte, M. (1999). A murine model of hereditary hemorrhagic telangiectasia. *J Clin Invest*, 104(10), 1343–51.
URL <https://www.ncbi.nlm.nih.gov/pubmed/10562296>
- Brinjikji, W., El-Rida El-Masri, A., Wald, J. T., & Lanzino, G. (2017). Prevalence of Developmental Venous Anomalies Increases With Age. *Stroke*, 48(7), 1997–1999.
URL <https://www.ncbi.nlm.nih.gov/pubmed/28536179>
- Brinjikji, W., Hilditch, C. A., Tsang, A. C., Nicholson, P. J., Krings, T., & Agid, R. (2018). Facial Venous Malformations Are Associated with Cerebral Developmental Venous Anomalies. *AJNR Am J Neuroradiol*, 39(11), 2103–2107.
URL <https://www.ncbi.nlm.nih.gov/pubmed/30237297>
- Castel, P., Carmona, F. J., Grego-Bessa, J., Berger, M. F., Viale, A., Anderson, K. V., Bague, S., Scaltriti, M., Antonescu, C. R., Baselga, E., & Baselga, J. (2016). Somatic PIK3CA mutations as a driver of sporadic venous malformations. *Sci Transl Med*, 8(332), 332ra42.
URL <https://www.ncbi.nlm.nih.gov/pubmed/27030594>
- Castillo, S. D., Baselga, E., & Graupera, M. (2019). PIK3CA mutations in vascular malformations. *Curr Opin Hematol*, 26(3), 170–178.
URL <https://www.ncbi.nlm.nih.gov/pubmed/30855339>
- Castillo, S. D., Tzouanacou, E., Zaw-Thin, M., Berenjeno, I. M., Parker, V. E., Chivite, I., Mila-Guasch, M., Pearce, W., Solomon, I., Angulo-Urarte, A., Figueiredo, A. M., Dewhurst, R. E., Knox, R. G., Clark, G. R., Scudamore, C. L.,

- Badar, A., Kalber, T. L., Foster, J., Stuckey, D. J., David, A. L., Phillips, W. A., Lythgoe, M. F., Wilson, V., Semple, R. K., Sebire, N. J., Kinsler, V. A., Graupera, M., & Vanhaesebroeck, B. (2016). Somatic activating mutations in Pik3ca cause sporadic venous malformations in mice and humans. *Sci Transl Med*, 8(332), 332ra43.
- URL <https://www.ncbi.nlm.nih.gov/pubmed/27030595>
- Cavalcanti, D. D., Kalani, M. Y., Martirosyan, N. L., Eales, J., Spetzler, R. F., & Preul, M. C. (2012). Cerebral cavernous malformations: from genes to proteins to disease. *J Neurosurg*, 116(1), 122–32.
- URL <https://www.ncbi.nlm.nih.gov/pubmed/21962164>
- Choi, E. J., Chen, W., Jun, K., Arthur, H. M., Young, W. L., & Su, H. (2014). Novel brain arteriovenous malformation mouse models for type 1 hereditary hemorrhagic telangiectasia. *PLoS One*, 9(2), e88511.
- URL <https://www.ncbi.nlm.nih.gov/pubmed/24520391>
- Choi, E. J., Walker, E. J., Shen, F., Oh, S. P., Arthur, H. M., Young, W. L., & Su, H. (2012). Minimal homozygous endothelial deletion of Eng with VEGF stimulation is sufficient to cause cerebrovascular dysplasia in the adult mouse. *Cerebrovasc Dis*, 33(6), 540–7.
- URL <https://www.ncbi.nlm.nih.gov/pubmed/22571958>
- Church, D. M., Stotler, C. J., Rutter, J. L., Murrell, J. R., Trofatter, J. A., & Buckler, A. J. (1994). Isolation of genes from complex sources of mammalian genomic DNA using exon amplification. *Nat Genet*, 6(1), 98–105.
- URL <https://www.ncbi.nlm.nih.gov/pubmed/8136842>
- Couto, J. A., Huang, A. Y., Konczyk, D. J., Goss, J. A., Fishman, S. J., Mulliken, J. B., Warman, M. L., & Greene, A. K. (2017). Somatic MAP2K1 Mutations Are Associated with Extracranial Arteriovenous Malformation. *Am J Hum Genet*, 100(3), 546–554.
- URL <https://www.ncbi.nlm.nih.gov/pubmed/28190454>
- Couto, J. A., Vivero, M. P., Kozakewich, H. P., Taghinia, A. H., Mulliken, J. B., Warman, M. L., & Greene, A. K. (2015). A somatic MAP3K3 mutation is associated with verrucous venous malformation. *Am J Hum Genet*, 96(3), 480–6.
- URL <https://www.ncbi.nlm.nih.gov/pubmed/25728774>
- Cuttano, R., Rudini, N., Bravi, L., Corada, M., Giampietro, C., Papa, E., Morini, M. F., Maddaluno, L., Baeyens, N., Adams, R. H., Jain, M. K., Owens, G. K., Schwartz, M., Lampugnani, M. G., & Dejana, E. (2016). KLF4 is a key determinant in the development and progression of cerebral cavernous malformations. *EMBO Mol Med*, 8(1), 6–24.
- URL <https://www.ncbi.nlm.nih.gov/pubmed/26612856>

- Dammann, P., Wrede, K., Zhu, Y., Matsushige, T., Maderwald, S., Umutlu, L., Quick, H. H., Hehr, U., Rath, M., Ladd, M. E., Felbor, U., & Sure, U. (2017). Correlation of the venous angioarchitecture of multiple cerebral cavernous malformations with familial or sporadic disease: a susceptibility-weighted imaging study with 7-Tesla MRI. *J Neurosurg*, *126*(2), 570–577.
URL <https://www.ncbi.nlm.nih.gov/pubmed/27153162>
- Davis, S., Ware, M. A., Zeiger, J., Deardorff, M. A., Grand, K., Grimberg, A., Hsu, S., Kelsey, M., Majidi, S., Matthew, R. P., Napier, M., Nokoff, N., Prasad, C., Riggs, A. C., McKinnon, M. L., & Mirzaa, G. (2020). Growth hormone deficiency in megalencephaly-capillary malformation syndrome: An association with activating mutations in PIK3CA. *Am J Med Genet A*, *182*(1), 162–168.
URL <https://www.ncbi.nlm.nih.gov/pubmed/31729162>
- Desmet, F. O., Hamroun, D., Lalande, M., Collod-Beroud, G., Claustres, M., & Beroud, C. (2009). Human Splicing Finder: an online bioinformatics tool to predict splicing signals. *Nucleic Acids Res*, *37*(9), e67.
URL <https://www.ncbi.nlm.nih.gov/pubmed/19339519>
- Detter, M. R., Snellings, D. A., & Marchuk, D. A. (2018). Cerebral Cavernous Malformations Develop Through Clonal Expansion of Mutant Endothelial Cells. *Circ Res*, *123*(10), 1143–1151.
URL <https://www.ncbi.nlm.nih.gov/pubmed/30359189>
- Dhamija, R., Weindling, S. M., Porter, A. B., Hu, L. S., Wood, C. P., & Hoxworth, J. M. (2018). Neuroimaging abnormalities in patients with Cowden syndrome: Retrospective single-center study. *Neurol Clin Pract*, *8*(3), 207–213.
URL <https://www.ncbi.nlm.nih.gov/pubmed/30105160>
- Dogruluk, T., Tsang, Y. H., Espitia, M., Chen, F., Chen, T., Chong, Z., Appadurai, V., Dogruluk, A., Eterovic, A. K., Bonnen, P. E., Creighton, C. J., Chen, K., Mills, G. B., & Scott, K. L. (2015). Identification of Variant-Specific Functions of PIK3CA by Rapid Phenotyping of Rare Mutations. *Cancer Res*, *75*(24), 5341–54.
URL <https://www.ncbi.nlm.nih.gov/pubmed/26627007>
- Eleftheriou, N. M., Sjolund, J., Bocci, M., Cortez, E., Lee, S. J., Cunha, S. I., & Pietras, K. (2016). Compound genetically engineered mouse models of cancer reveal dual targeting of ALK1 and endoglin as a synergistic opportunity to impinge on angiogenic TGF-beta signaling. *Oncotarget*, *7*(51), 84314–84325.
URL <https://www.ncbi.nlm.nih.gov/pubmed/27741515>
- Faurobert, E., Rome, C., Lisowska, J., Manet-Dupe, S., Boulday, G., Malbouyres, M., Balland, M., Bouin, A. P., Keramidas, M., Bouvard, D., Coll, J. L., Ruggiero, F., Tournier-Lasserve, E., & Albiges-Rizo, C. (2013). CCM1-ICAP-1 complex controls beta1 integrin-dependent endothelial contractility and fibronectin

- remodeling. *J Cell Biol*, 202(3), 545–61.
URL <https://www.ncbi.nlm.nih.gov/pubmed/23918940>
- Fischer, A., Zalvide, J., Faurobert, E., Albiges-Rizo, C., & Tournier-Lasserve, E. (2013). Cerebral cavernous malformations: from CCM genes to endothelial cell homeostasis. *Trends Mol Med*, 19(5), 302–8.
URL <https://www.ncbi.nlm.nih.gov/pubmed/23506982>
- Fisher, O. S., & Boggon, T. J. (2014). Signaling pathways and the cerebral cavernous malformations proteins: lessons from structural biology. *Cell Mol Life Sci*, 71(10), 1881–92.
URL <https://www.ncbi.nlm.nih.gov/pubmed/24287896>
- Francis, J. H., Milman, T., Grossniklaus, H., Albert, D., Folberg, R., Levitin, G., Coupland, S., Catalanotti, F., Rabady, D., Kandoth, C., Busam, K., & Abramson, D. (2019). GNAQ Mutations in Diffuse and Solitary Choroidal Hemangiomas. *Ophthalmology*, 126(5), 759–763.
URL <https://www.ncbi.nlm.nih.gov/pubmed/30537484>
- Gallione, C. J., Klaus, D. J., Yeh, E. Y., Stenzel, T. T., Xue, Y., Anthony, K. B., McAllister, K. A., Baldwin, M. A., Berg, J. N., Lux, A., Smith, J. D., Vary, C. P., Craigen, W. J., Westermann, C. J., Warner, M. L., Miller, Y. E., Jackson, C. E., Guttmacher, A. E., & Marchuk, D. A. (1998). Mutation and expression analysis of the endoglin gene in hereditary hemorrhagic telangiectasia reveals null alleles. *Hum Mutat*, 11(4), 286–94.
URL <https://www.ncbi.nlm.nih.gov/pubmed/9554745>
- Gallione, C. J., Repetto, G. M., Legius, E., Rustgi, A. K., Schelley, S. L., Tejpar, S., Mitchell, G., Drouin, E., Westermann, C. J., & Marchuk, D. A. (2004). A combined syndrome of juvenile polyposis and hereditary haemorrhagic telangiectasia associated with mutations in MADH4 (SMAD4). *Lancet*, 363(9412), 852–9.
URL <https://www.ncbi.nlm.nih.gov/pubmed/15031030>
- Garaci, F., Marsili, L., Riant, F., Marziali, S., Cecillon, M., Pasquarelli, R., Sangiuolo, F., Floris, R., Novelli, G., Tournier-Lasserve, E., & Brancati, F. (2015). Cerebral cavernous malformations associated to meningioma: High penetrance in a novel family mutated in the PDCD10 gene. *Neuroradiol J*, 28(3), 289–93.
URL <https://www.ncbi.nlm.nih.gov/pubmed/26246098>
- Garrido-Martin, E. M., Nguyen, H. L., Cunningham, T. A., Choe, S. W., Jiang, Z., Arthur, H. M., Lee, Y. J., & Oh, S. P. (2014). Common and distinctive pathogenetic features of arteriovenous malformations in hereditary hemorrhagic telangiectasia 1 and hereditary hemorrhagic telangiectasia 2 animal models—brief report. *Arterioscler Thromb Vasc Biol*, 34(10), 2232–6.
URL <https://www.ncbi.nlm.nih.gov/pubmed/25082229>

- Gault, J., Awad, I. A., Recksiek, P., Shenkar, R., Breeze, R., Handler, M., & Kleinschmidt-DeMasters, B. K. (2009). Cerebral cavernous malformations: somatic mutations in vascular endothelial cells. *Neurosurgery*, *65*(1), 138–44; discussion 144–5.
URL <https://www.ncbi.nlm.nih.gov/pubmed/19574835>
- Gault, J., Shenkar, R., Recksiek, P., & Awad, I. A. (2005). Biallelic somatic and germ line CCM1 truncating mutations in a cerebral cavernous malformation lesion. *Stroke*, *36*(4), 872–4.
URL <https://www.ncbi.nlm.nih.gov/pubmed/15718512>
- Girard, R., Zeineddine, H. A., Koskimaki, J., Fam, M. D., Cao, Y., Shi, C., Moore, T., Lightle, R., Stadnik, A., Chaudagar, K., Polster, S., Shenkar, R., Duggan, R., Leclerc, D., Whitehead, K. J., Li, D. Y., & Awad, I. A. (2018). Plasma Biomarkers of Inflammation and Angiogenesis Predict Cerebral Cavernous Malformation Symptomatic Hemorrhage or Lesional Growth. *Circ Res*, *122*(12), 1716–1721.
URL <https://www.ncbi.nlm.nih.gov/pubmed/29720384>
- Gokce, E., Acu, B., Beyhan, M., Celikyay, F., & Celikyay, R. (2014). Magnetic resonance imaging findings of developmental venous anomalies. *Clin Neuroradiol*, *24*(2), 135–43.
URL <https://www.ncbi.nlm.nih.gov/pubmed/24240482>
- Gonzalez, C. D., Cipriano, S. D., Topham, C. A., Stevenson, D. A., Whitehead, K. J., Vanderhoof, S., Presson, A. P., & McDonald, J. (2019). Localization and age distribution of telangiectases in children and adolescents with hereditary hemorrhagic telangiectasia: A retrospective cohort study. *J Am Acad Dermatol*.
URL <https://www.ncbi.nlm.nih.gov/pubmed/30819528>
- Goss, J. A., Huang, A. Y., Smith, E., Konczyk, D. J., Smits, P. J., Sudduth, C. L., Stapleton, C., Patel, A., Alexandrescu, S., Warman, M. L., & Greene, A. K. (2019). Somatic mutations in intracranial arteriovenous malformations. *PLoS One*, *14*(12), e0226852.
URL <https://www.ncbi.nlm.nih.gov/pubmed/31891627>
- Grosse, S. D., Boulet, S. L., Grant, A. M., Hulihan, M. M., & Faughnan, M. E. (2014). The use of US health insurance data for surveillance of rare disorders: hereditary hemorrhagic telangiectasia. *Genet Med*, *16*(1), 33–9.
URL <https://www.ncbi.nlm.nih.gov/pubmed/23703685>
- Heiskanen, O. (1993). Treatment of spontaneous intracerebral and intracerebellar hemorrhages. *Stroke*, *24*(12 Suppl), I94–5; discussion I107–8.
URL <https://www.ncbi.nlm.nih.gov/pubmed/8249028>

- Hong, T., Xiao, X., Ren, J., Cui, B., Zong, Y., Zou, J., Kou, Z., Jiang, N., Meng, G., Zeng, G., Shan, Y., Wu, H., Chen, Z., Liang, J., Xiao, X., Tang, J., Wei, Y., Ye, M., Sun, L., Li, G., Hu, P., Hui, R., Zhang, H., & Wang, Y. (2021). Somatic MAP3K3 and PIK3CA mutations in sporadic cerebral and spinal cord cavernous malformations. *Brain*.
- URL <https://www.ncbi.nlm.nih.gov/pubmed/33729480>
- Horne, M. A., Flemming, K. D., Su, I. C., Stafp, C., Jeon, J. P., Li, D., Maxwell, S. S., White, P., Christianson, T. J., Agid, R., Cho, W. S., Oh, C. W., Wu, Z., Zhang, J. T., Kim, J. E., Ter Brugge, K., Willinsky, R., Brown, J., R. D., Murray, G. D., Al-Shahi Salman, R., & Cerebral Cavernous Malformations Individual Patient Data Meta-analysis, C. (2016). Clinical course of untreated cerebral cavernous malformations: a meta-analysis of individual patient data. *Lancet Neurol*, 15(2), 166–173.
- URL <https://www.ncbi.nlm.nih.gov/pubmed/26654287>
- Hurst, C. D., Zuiverloon, T. C., Hafner, C., Zwarthoff, E. C., & Knowles, M. A. (2009). A SNaPshot assay for the rapid and simple detection of four common hotspot codon mutations in the PIK3CA gene. *BMC Res Notes*, 2, 66.
- URL <https://www.ncbi.nlm.nih.gov/pubmed/19402901>
- Jiao, W., Vembu, S., Deshwar, A. G., Stein, L., & Morris, Q. (2014). Inferring clonal evolution of tumors from single nucleotide somatic mutations. *BMC Bioinformatics*, 15, 35.
- URL <https://www.ncbi.nlm.nih.gov/pubmed/24484323>
- Jin, Y., Muhl, L., Burmakin, M., Wang, Y., Duchez, A. C., Betsholtz, C., Arthur, H. M., & Jakobsson, L. (2017). Endoglin prevents vascular malformation by regulating flow-induced cell migration and specification through VEGFR2 signalling. *Nat Cell Biol*, 19(6), 639–652.
- URL <https://www.ncbi.nlm.nih.gov/pubmed/28530660>
- Johnson, D. W., Berg, J. N., Baldwin, M. A., Gallione, C. J., Marondel, I., Yoon, S. J., Stenzel, T. T., Speer, M., Pericak-Vance, M. A., Diamond, A., Guttmacher, A. E., Jackson, C. E., Attisano, L., Kucherlapati, R., Porteous, M. E., & Marchuk, D. A. (1996). Mutations in the activin receptor-like kinase 1 gene in hereditary haemorrhagic telangiectasia type 2. *Nat Genet*, 13(2), 189–95.
- URL <https://www.ncbi.nlm.nih.gov/pubmed/8640225>
- Johnson, D. W., Berg, J. N., Gallione, C. J., McAllister, K. A., Warner, J. P., Helmbold, E. A., Markel, D. S., Jackson, C. E., Porteous, M. E., & Marchuk, D. A. (1995). A second locus for hereditary hemorrhagic telangiectasia maps to chromosome 12. *Genome Res*, 5(1), 21–8.
- URL <https://www.ncbi.nlm.nih.gov/pubmed/8717052>

- Jolly, C., & Van Loo, P. (2018). Timing somatic events in the evolution of cancer. *Genome Biol*, 19(1), 95.
URL <https://www.ncbi.nlm.nih.gov/pubmed/30041675>
- Jones, B. V., Linscott, L., Koberlein, G., Hummel, T. R., & Leach, J. L. (2015). Increased Prevalence of Developmental Venous Anomalies in Children with Intracranial Neoplasms. *AJNR Am J Neuroradiol*, 36(9), 1782–5.
URL <https://www.ncbi.nlm.nih.gov/pubmed/26021620>
- Kanehisa, M., Furumichi, M., Sato, Y., Ishiguro-Watanabe, M., & Tanabe, M. (2021). KEGG: integrating viruses and cellular organisms. *Nucleic Acids Res*, 49(D1), D545–D551.
URL <https://www.ncbi.nlm.nih.gov/pubmed/33125081>
- Kanehisa, M., & Goto, S. (2000). KEGG: kyoto encyclopedia of genes and genomes. *Nucleic Acids Res*, 28(1), 27–30.
URL <https://www.ncbi.nlm.nih.gov/pubmed/10592173>
- Kim, Y. H., Choe, S. W., Chae, M. Y., Hong, S., & Oh, S. P. (2018). SMAD4 Deficiency Leads to Development of Arteriovenous Malformations in Neonatal and Adult Mice. *J Am Heart Assoc*, 7(21), e009514.
URL <https://www.ncbi.nlm.nih.gov/pubmed/30571376>
- Koren, S., Reavie, L., Couto, J. P., De Silva, D., Stadler, M. B., Roloff, T., Britschgi, A., Eichlisberger, T., Kohler, H., Aina, O., Cardiff, R. D., & Bentires-Alj, M. (2015). PIK3CA(H1047R) induces multipotency and multi-lineage mammary tumours. *Nature*, 525(7567), 114–8.
URL <https://www.ncbi.nlm.nih.gov/pubmed/26266975>
- Koskimaki, J., Zhang, D., Li, Y., Saadat, L., Moore, T., Lightle, R., Polster, S. P., Carrion-Penagos, J., Lyne, S. B., Zeineddine, H. A., Shi, C., Shenkar, R., Romanos, S., Avner, K., Srinath, A., Shen, L., Detter, M. R., Snellings, D., Cao, Y., Lopez-Ramirez, M. A., Fonseca, G., Tang, A. T., Faber, P., Andrade, J., Ginsberg, M., Kahn, M. L., Marchuk, D. A., Girard, R., & Awad, I. A. (2019). Transcriptome clarifies mechanisms of lesion genesis versus progression in models of Ccm3 cerebral cavernous malformations. *Acta Neuropathol Commun*, 7(1), 132.
URL <https://www.ncbi.nlm.nih.gov/pubmed/31426861>
- Labauge, P., Fontaine, B., Neau, J. P., Bergametti, F., Riant, F., Blecon, A., Marchelli, F., Arnoult, M., Lannuzel, A., Clanet, M., Olschwang, S., Denier, C., & Tournier-Lasserve, E. (2009). Multiple dural lesions mimicking meningiomas in patients with CCM3/PDCD10 mutations. *Neurology*, 72(23), 2044–6.
URL <https://www.ncbi.nlm.nih.gov/pubmed/19506228>
- Laberge-le Couteulx, S., Jung, H. H., Labauge, P., Houtteville, J. P., Lescoat, C., Cecillon, M., Marechal, E., Joutel, A., Bach, J. F., & Tournier-Lasserve, E. (1999).

- Truncating mutations in CCM1, encoding KRIT1, cause hereditary cavernous angiomas. *Nat Genet*, 23(2), 189–93.
URL <https://www.ncbi.nlm.nih.gov/pubmed/10508515>
- Lapinski, P. E., Doosti, A., Salato, V., North, P., Burrows, P. E., & King, P. D. (2018). Somatic second hit mutation of RASA1 in vascular endothelial cells in capillary malformation-arteriovenous malformation. *Eur J Med Genet*, 61(1), 11–16.
URL <https://www.ncbi.nlm.nih.gov/pubmed/29024832>
- Laver, T. W., Caswell, R. C., Moore, K. A., Poschmann, J., Johnson, M. B., Owens, M. M., Ellard, S., Paszkiewicz, K. H., & Weedon, M. N. (2016). Pitfalls of haplotype phasing from amplicon-based long-read sequencing. *Sci Rep*, 6, 21746.
URL <https://www.ncbi.nlm.nih.gov/pubmed/26883533>
- Letteboer, T. G., Mager, H. J., Snijder, R. J., Lindhout, D., Ploos van Amstel, H. K., Zanen, P., & Westermann, K. J. (2008). Genotype-phenotype relationship for localization and age distribution of telangiectases in hereditary hemorrhagic telangiectasia. *Am J Med Genet A*, 146A(21), 2733–9.
URL <https://www.ncbi.nlm.nih.gov/pubmed/18831062>
- Limaye, N., Kangas, J., Mendola, A., Godfraind, C., Schlogel, M. J., Helaers, R., Eklund, L., Boon, L. M., & Viikkula, M. (2015). Somatic Activating PIK3CA Mutations Cause Venous Malformation. *Am J Hum Genet*, 97(6), 914–21.
URL <https://www.ncbi.nlm.nih.gov/pubmed/26637981>
- Limaye, N., Wouters, V., Uebelhoer, M., Tuominen, M., Wirkkala, R., Mulliken, J. B., Eklund, L., Boon, L. M., & Viikkula, M. (2009). Somatic mutations in angiopoietin receptor gene TEK cause solitary and multiple sporadic venous malformations. *Nat Genet*, 41(1), 118–24.
URL <https://www.ncbi.nlm.nih.gov/pubmed/19079259>
- Linscott, L. L., Leach, J. L., Jones, B. V., & Abruzzo, T. A. (2016). Developmental venous anomalies of the brain in children – imaging spectrum and update. *Pediatr Radiol*, 46(3), 394–406; quiz 391–3.
URL <https://www.ncbi.nlm.nih.gov/pubmed/26795616>
- Liquori, C. L., Berg, M. J., Siegel, A. M., Huang, E., Zawistowski, J. S., Stoffer, T., Verlaan, D., Balogun, F., Hughes, L., Leedom, T. P., Plummer, N. W., Cannella, M., Maglione, V., Squitieri, F., Johnson, E. W., Rouleau, G. A., Ptacek, L., & Marchuk, D. A. (2003). Mutations in a gene encoding a novel protein containing a phosphotyrosine-binding domain cause type 2 cerebral cavernous malformations. *Am J Hum Genet*, 73(6), 1459–64.
URL <https://www.ncbi.nlm.nih.gov/pubmed/14624391>

- Lo Sardo, V., Ferguson, W., Erikson, G. A., Topol, E. J., Baldwin, K. K., & Torkamani, A. (2017). Influence of donor age on induced pluripotent stem cells. *Nat Biotechnol*, 35(1), 69–74.
URL <https://www.ncbi.nlm.nih.gov/pubmed/27941802>
- Lodato, M. A., Rodin, R. E., Bohrson, C. L., Coulter, M. E., Barton, A. R., Kwon, M., Sherman, M. A., Vitzthum, C. M., Luquette, L. J., Yandava, C. N., Yang, P., Chittenden, T. W., Hatem, N. E., Ryu, S. C., Woodworth, M. B., Park, P. J., & Walsh, C. A. (2018). Aging and neurodegeneration are associated with increased mutations in single human neurons. *Science*, 359(6375), 555–559.
URL <https://www.ncbi.nlm.nih.gov/pubmed/29217584>
- Lodato, M. A., Woodworth, M. B., Lee, S., Evrony, G. D., Mehta, B. K., Karger, A., Lee, S., Chittenden, T. W., D'Gama, A. M., Cai, X., Luquette, L. J., Lee, E., Park, P. J., & Walsh, C. A. (2015). Somatic mutation in single human neurons tracks developmental and transcriptional history. *Science*, 350(6256), 94–98.
URL <https://www.ncbi.nlm.nih.gov/pubmed/26430121>
- Lopez-Ramirez, M. A., Pham, A., Girard, R., Wyseure, T., Hale, P., Yamashita, A., Koskimaki, J., Polster, S., Saadat, L., Romero, I. A., Esmon, C. T., Lagarrigue, F., Awad, I. A., Mosnier, L. O., & Ginsberg, M. H. (2019). Cerebral cavernous malformations form an anticoagulant vascular domain in humans and mice. *Blood*, 133(3), 193–204.
URL <https://www.ncbi.nlm.nih.gov/pubmed/30442679>
- Love, M. I., Huber, W., & Anders, S. (2014). Moderated estimation of fold change and dispersion for RNA-seq data with DESeq2. *Genome Biol*, 15(12), 550.
URL <https://www.ncbi.nlm.nih.gov/pubmed/25516281>
- Luks, V. L., Kamitaki, N., Vivero, M. P., Uller, W., Rab, R., Bovee, J. V., Rialon, K. L., Guevara, C. J., Alomari, A. I., Greene, A. K., Fishman, S. J., Kozakewich, H. P., Maclellan, R. A., Mulliken, J. B., Rahbar, R., Spencer, S. A., Trenor, r., C. C., Upton, J., Zurakowski, D., Perkins, J. A., Kirsh, A., Bennett, J. T., Dobyns, W. B., Kurek, K. C., Warman, M. L., McCarroll, S. A., & Murillo, R. (2015). Lymphatic and other vascular malformative/overgrowth disorders are caused by somatic mutations in PIK3CA. *J Pediatr*, 166(4), 1048–54 e1–5.
URL <https://www.ncbi.nlm.nih.gov/pubmed/25681199>
- Lyne, S. B., Girard, R., Koskimaki, J., Zeineddine, H. A., Zhang, D., Cao, Y., Li, Y., Stadnik, A., Moore, T., Lightle, R., Shi, C., Shenkar, R., Carrion-Penagos, J., Polster, S. P., Romanos, S., Akers, A., Lopez-Ramirez, M., Whitehead, K. J., Kahn, M. L., Ginsberg, M. H., Marchuk, D. A., & Awad, I. A. (2019). Biomarkers of cavernous angioma with symptomatic hemorrhage. *JCI Insight*, 4(12).
URL <https://www.ncbi.nlm.nih.gov/pubmed/31217347>

- Macmurdo, C. F., Wooderchak-Donahue, W., Bayrak-Toydemir, P., Le, J., Wallenstein, M. B., Milla, C., Teng, J. M., Bernstein, J. A., & Stevenson, D. A. (2016). RASA1 somatic mutation and variable expressivity in capillary malformation/arteriovenous malformation (CM/AVM) syndrome. *Am J Med Genet A*, *170*(6), 1450–4.
URL <https://www.ncbi.nlm.nih.gov/pubmed/26969842>
- Mahmoud, M., Allinson, K. R., Zhai, Z., Oakenfull, R., Ghandi, P., Adams, R. H., Fruttiger, M., & Arthur, H. M. (2010). Pathogenesis of arteriovenous malformations in the absence of endoglin. *Circ Res*, *106*(8), 1425–33.
URL <https://www.ncbi.nlm.nih.gov/pubmed/20224041>
- Malinverno, M., Maderna, C., Abu Taha, A., Corada, M., Orsenigo, F., Valentino, M., Pisati, F., Fusco, C., Graziano, P., Giannotta, M., Yu, Q. C., Zeng, Y. A., Lampugnani, M. G., Magnusson, P. U., & Dejana, E. (2019). Endothelial cell clonal expansion in the development of cerebral cavernous malformations. *Nat Commun*, *10*(1), 2761.
URL <https://www.ncbi.nlm.nih.gov/pubmed/31235698>
- McAllister, K. A., Grogg, K. M., Johnson, D. W., Gallione, C. J., Baldwin, M. A., Jackson, C. E., Helmbold, E. A., Markel, D. S., McKinnon, W. C., Murrell, J., & et al. (1994). Endoglin, a TGF-beta binding protein of endothelial cells, is the gene for hereditary haemorrhagic telangiectasia type 1. *Nat Genet*, *8*(4), 345–51.
URL <https://www.ncbi.nlm.nih.gov/pubmed/7894484>
- McDonald, D. A., Shi, C., Shenkar, R., Gallione, C. J., Akers, A. L., Li, S., De Castro, N., Berg, M. J., Corcoran, D. L., Awad, I. A., & Marchuk, D. A. (2014). Lesions from patients with sporadic cerebral cavernous malformations harbor somatic mutations in the CCM genes: evidence for a common biochemical pathway for CCM pathogenesis. *Hum Mol Genet*, *23*(16), 4357–70.
URL <https://www.ncbi.nlm.nih.gov/pubmed/24698976>
- McGranahan, N., Favero, F., de Bruin, E. C., Birkbak, N. J., Szallasi, Z., & Swanton, C. (2015). Clonal status of actionable driver events and the timing of mutational processes in cancer evolution. *Sci Transl Med*, *7*(283), 283ra54.
URL <https://www.ncbi.nlm.nih.gov/pubmed/25877892>
- Milholland, B., Dong, X., Zhang, L., Hao, X., Suh, Y., & Vijg, J. (2017). Differences between germline and somatic mutation rates in humans and mice. *Nat Commun*, *8*, 15183.
URL <https://www.ncbi.nlm.nih.gov/pubmed/28485371>
- Mori, M. A., Ludwig, R. G., Garcia-Martin, R., Brandao, B. B., & Kahn, C. R. (2019). Extracellular miRNAs: From Biomarkers to Mediators of Physiology and Disease. *Cell Metab*, *30*(4), 656–673.
URL <https://www.ncbi.nlm.nih.gov/pubmed/31447320>

- Nikolaev, S. I., Vetiska, S., Bonilla, X., Boudreau, E., Jauhainen, S., Rezai Jahromi, B., Khyzha, N., DiStefano, P. V., Suutarinen, S., Kiehl, T. R., Mendes Pereira, V., Herman, A. M., Krings, T., Andrade-Barazarte, H., Tung, T., Valiante, T., Zadeh, G., Tymianski, M., Rauramaa, T., Yla-Herttuala, S., Wythe, J. D., Antonarakis, S. E., Frosen, J., Fish, J. E., & Radovanovic, I. (2018). Somatic Activating KRAS Mutations in Arteriovenous Malformations of the Brain. *N Engl J Med*, 378(3), 250–261.
URL <https://www.ncbi.nlm.nih.gov/pubmed/29298116>
- North, P. E., Waner, M., Mizeracki, A., & Mihm, J., M. C. (2000). GLUT1: a newly discovered immunohistochemical marker for juvenile hemangiomas. *Hum Pathol*, 31(1), 11–22.
URL <https://www.ncbi.nlm.nih.gov/pubmed/10665907>
- North, P. E., Waner, M., Mizeracki, A., Mrak, R. E., Nicholas, R., Kincannon, J., Suen, J. Y., & Mihm, J., M. C. (2001). A unique microvascular phenotype shared by juvenile hemangiomas and human placenta. *Arch Dermatol*, 137(5), 559–70.
URL <https://www.ncbi.nlm.nih.gov/pubmed/11346333>
- Ola, R., Kunzel, S. H., Zhang, F., Genet, G., Chakraborty, R., Pibouin-Fragner, L., Martin, K., Sessa, W., Dubrac, A., & Eichmann, A. (2018). SMAD4 Prevents Flow Induced Arteriovenous Malformations by Inhibiting Casein Kinase 2. *Circulation*, 138(21), 2379–2394.
URL <https://www.ncbi.nlm.nih.gov/pubmed/29976569>
- Olivieri, C., Pagella, F., Semino, L., Lanzarini, L., Valacca, C., Pilotto, A., Corno, S., Scappaticci, S., Manfredi, G., Buscarini, E., & Danesino, C. (2007). Analysis of ENG and ACVRL1 genes in 137 HHT Italian families identifies 76 different mutations (24 novel). Comparison with other European studies. *J Hum Genet*, 52(10), 820–9.
URL <https://www.ncbi.nlm.nih.gov/pubmed/17786384>
- Pece, N., Vera, S., Cymerman, U., White, J., R. I., Wrana, J. L., & Letarte, M. (1997). Mutant endoglin in hereditary hemorrhagic telangiectasia type 1 is transiently expressed intracellularly and is not a dominant negative. *J Clin Invest*, 100(10), 2568–79.
URL <https://www.ncbi.nlm.nih.gov/pubmed/9366572>
- Pece-Barbara, N., Cymerman, U., Vera, S., Marchuk, D. A., & Letarte, M. (1999). Expression analysis of four endoglin missense mutations suggests that haploinsufficiency is the predominant mechanism for hereditary hemorrhagic telangiectasia type 1. *Hum Mol Genet*, 8(12), 2171–81.
URL <https://www.ncbi.nlm.nih.gov/pubmed/10545596>
- Pittman, K. M., Losken, H. W., Kleinman, M. E., Marcus, J. R., Blei, F., Gurtner, G. C., & Marchuk, D. A. (2006). No evidence for maternal-fetal microchimerism

- in infantile hemangioma: a molecular genetic investigation. *J Invest Dermatol*, *126*(11), 2533–8.
URL <https://www.ncbi.nlm.nih.gov/pubmed/16902414>
- Plauchu, H., de Chadarevian, J. P., Bideau, A., & Robert, J. M. (1989). Age-related clinical profile of hereditary hemorrhagic telangiectasia in an epidemiologically recruited population. *Am J Med Genet*, *32*(3), 291–7.
URL <https://www.ncbi.nlm.nih.gov/pubmed/2729347>
- Plummer, N. W., Zawistowski, J. S., & Marchuk, D. A. (2005). Genetics of cerebral cavernous malformations. *Curr Neurol Neurosci Rep*, *5*(5), 391–6.
URL <https://www.ncbi.nlm.nih.gov/pubmed/16131422>
- Polster, S. P., Cao, Y., Carroll, T., Flemming, K., Girard, R., Hanley, D., Hobson, N., Kim, H., Koenig, J., Koskimaki, J., Lane, K., Majersik, J. J., McBee, N., Morrison, L., Shenkar, R., Stadnik, A., Thompson, R. E., Zabramski, J., Zeineddine, H. A., & Awad, I. A. (2019). Trial Readiness in Cavernous Angiomas With Symptomatic Hemorrhage (CASH). *Neurosurgery*, *84*(4), 954–964.
URL <https://www.ncbi.nlm.nih.gov/pubmed/29660039>
- Polster, S. P., Sharma, A., Tanes, C., Tang, A. T., Mericko, P., Cao, Y., Carrion-Penagos, J., Girard, R., Koskimaki, J., Zhang, D., Stadnik, A., Romanos, S. G., Lyne, S. B., Shenkar, R., Yan, K., Lee, C., Akers, A., Morrison, L., Robinson, M., Zafar, A., Bittinger, K., Kim, H., Gilbert, J. A., Kahn, M. L., Shen, L., & Awad, I. A. (2020). Permissive microbiome characterizes human subjects with a neurovascular disease cavernous angioma. *Nat Commun*, *11*(1), 2659.
URL <https://www.ncbi.nlm.nih.gov/pubmed/32461638>
- Porter, P. J., Willinsky, R. A., Harper, W., & Wallace, M. C. (1997). Cerebral cavernous malformations: natural history and prognosis after clinical deterioration with or without hemorrhage. *J Neurosurg*, *87*(2), 190–7.
URL <https://www.ncbi.nlm.nih.gov/pubmed/9254081>
- Porter, R. W., Detwiler, P. W., Spetzler, R. F., Lawton, M. T., Baskin, J. J., Derk森, P. T., & Zabramski, J. M. (1999). Cavernous malformations of the brainstem: experience with 100 patients. *J Neurosurg*, *90*(1), 50–8.
URL <https://www.ncbi.nlm.nih.gov/pubmed/10413155>
- Queisser, A., Boon, L. M., & Vikkula, M. (2018). Etiology and Genetics of Congenital Vascular Lesions. *Otolaryngol Clin North Am*, *51*(1), 41–53.
URL <https://www.ncbi.nlm.nih.gov/pubmed/29217067>
- Rasalkar, D. D., & Paunipagar, B. K. (2010). Developmental venous anomaly associated with cortical dysplasia. *Pediatr Radiol*, *40 Suppl 1*, S165.
URL <https://www.ncbi.nlm.nih.gov/pubmed/20429001>

- Ren, A. A., Snellings, D. A., Su, Y. S., Hong, C. C., Castro, M., Tang, A. T., Detter, M. R., Hobson, N., Girard, R., Romanos, S., Lightle, R., Moore, T., Shenkar, R., Benavides, C., Beaman, M. M., Mueller-Fielitz, H., Chen, M., Mericko, P., Yang, J., Sung, D. C., Lawton, M. T., Ruppert, M., Schwaninger, M., Korbelin, J., Potente, M., Awad, I. A., Marchuk, D. A., & Kahn, M. L. (2021). *PIK3CA* and CCM mutations fuel cavernomas through a cancer-like mechanism. *Nature*. URL <https://www.ncbi.nlm.nih.gov/pubmed/33910229>
- Reuss, D. E., Piro, R. M., Jones, D. T., Simon, M., Ketter, R., Kool, M., Becker, A., Sahm, F., Pusch, S., Meyer, J., Hagenlocher, C., Schweizer, L., Capper, D., Kickingereder, P., Mucha, J., Koelsche, C., Jager, N., Santarius, T., Tarpey, P. S., Stephens, P. J., Andrew Futreal, P., Wellenreuther, R., Kraus, J., Lenartz, D., Herold-Mende, C., Hartmann, C., Mawrin, C., Giese, N., Eils, R., Collins, V. P., Konig, R., Wiestler, O. D., Pfister, S. M., & von Deimling, A. (2013). Secretory meningiomas are defined by combined *KLF4* K409Q and *TRAF7* mutations. *Acta Neuropathol*, 125(3), 351–8. URL <https://www.ncbi.nlm.nih.gov/pubmed/23404370>
- Riant, F., Bergametti, F., Fournier, H. D., Chapon, F., Michalak-Provost, S., Cecillon, M., Lejeune, P., Hosseini, H., Choe, C., Orth, M., Bernreuther, C., Boulday, G., Denier, C., Labauge, P., & Tournier-Lasserve, E. (2013). CCM3 Mutations Are Associated with Early-Onset Cerebral Hemorrhage and Multiple Meningiomas. *Mol Syndromol*, 4(4), 165–72. URL <https://www.ncbi.nlm.nih.gov/pubmed/23801932>
- Ricard, N., Bidart, M., Mallet, C., Lesca, G., Giraud, S., Prudent, R., Feige, J. J., & Bailly, S. (2010). Functional analysis of the BMP9 response of ALK1 mutants from HHT2 patients: a diagnostic tool for novel ACVRL1 mutations. *Blood*, 116(9), 1604–12. URL <https://www.ncbi.nlm.nih.gov/pubmed/20501893>
- Richards, S., Aziz, N., Bale, S., Bick, D., Das, S., Gastier-Foster, J., Grody, W. W., Hegde, M., Lyon, E., Spector, E., Voelkerding, K., Rehm, H. L., & Committee, A. L. Q. A. (2015). Standards and guidelines for the interpretation of sequence variants: a joint consensus recommendation of the American College of Medical Genetics and Genomics and the Association for Molecular Pathology. *Genet Med*, 17(5), 405–24. URL <https://www.ncbi.nlm.nih.gov/pubmed/25741868>
- Rodin, R. E., Dou, Y., Kwon, M., Sherman, M. A., D'Gama, A. M., Doan, R. N., Rento, L. M., Girsakis, K. M., Bohrson, C. L., Kim, S. N., Nadig, A., Luquette, L. J., Gulhan, D. C., Brain Somatic Mosaicism, N., Park, P. J., & Walsh, C. A. (2021). The landscape of somatic mutation in cerebral cortex of autistic and neurotypical individuals revealed by ultra-deep whole-genome sequencing. *Nat*

Neurosci, 24(2), 176–185.

URL <https://www.ncbi.nlm.nih.gov/pubmed/33432195>

Rodriguez-Laguna, L., Agra, N., Ibanez, K., Oliva-Molina, G., Gordo, G., Khurana, N., Hominick, D., Beato, M., Colmenero, I., Herranz, G., Torres Canizalez, J. M., Rodriguez Pena, R., Vallespin, E., Martin-Arenas, R., Del Pozo, A., Villaverde, C., Bustamante, A., Ayuso, C., Lapunzina, P., Lopez-Gutierrez, J. C., Dellinger, M. T., & Martinez-Glez, V. (2019). Somatic activating mutations in PIK3CA cause generalized lymphatic anomaly. *J Exp Med*, 216(2), 407–418.

URL <https://www.ncbi.nlm.nih.gov/pubmed/30591517>

Roux, A., Boddaert, N., Grill, J., Castel, D., Zanello, M., Zah-Bi, G., Chretien, F., Lefevre, E., Ros, V. D., Zerah, M., Puget, S., Pallud, J., & Varlet, P. (2020). High Prevalence of Developmental Venous Anomaly in Diffuse Intrinsic Pontine Gliomas: A Pediatric Control Study. *Neurosurgery*, 86(4), 517–523.

URL <https://www.ncbi.nlm.nih.gov/pubmed/31342064>

Rueda, A., Barturen, G., Lebron, R., Gomez-Martin, C., Alganza, A., Oliver, J. L., & Hackenberg, M. (2015). sRNAtoolbox: an integrated collection of small RNA research tools. *Nucleic Acids Res*, 43(W1), W467–73.

URL <https://www.ncbi.nlm.nih.gov/pubmed/26019179>

Ruiz-Llorente, L., Gallardo-Vara, E., Rossi, E., Smadja, D. M., Botella, L. M., & Bernabeu, C. (2017). Endoglin and alk1 as therapeutic targets for hereditary hemorrhagic telangiectasia. *Expert Opin Ther Targets*, 21(10), 933–947.

URL <https://www.ncbi.nlm.nih.gov/pubmed/28796572>

Sahoo, T., Johnson, E. W., Thomas, J. W., Kuehl, P. M., Jones, T. L., Dokken, C. G., Touchman, J. W., Gallione, C. J., Lee-Lin, S. Q., Kosofsky, B., Kurth, J. H., Louis, D. N., Mettler, G., Morrison, L., Gil-Nagel, A., Rich, S. S., Zabramski, J. M., Boguski, M. S., Green, E. D., & Marchuk, D. A. (1999). Mutations in the gene encoding KRIT1, a Krev-1/rap1a binding protein, cause cerebral cavernous malformations (CCM1). *Hum Mol Genet*, 8(12), 2325–33.

URL <https://www.ncbi.nlm.nih.gov/pubmed/10545614>

Samuels, Y., Diaz, J., L. A., Schmidt-Kittler, O., Cummins, J. M., Delong, L., Cheong, I., Rago, C., Huso, D. L., Lengauer, C., Kinzler, K. W., Vogelstein, B., & Velculescu, V. E. (2005). Mutant PIK3CA promotes cell growth and invasion of human cancer cells. *Cancer Cell*, 7(6), 561–73.

URL <https://www.ncbi.nlm.nih.gov/pubmed/15950905>

Santucci, G. M., Leach, J. L., Ying, J., Leach, S. D., & Tomsick, T. A. (2008). Brain parenchymal signal abnormalities associated with developmental venous anomalies: detailed MR imaging assessment. *AJNR Am J Neuroradiol*, 29(7), 1317–23.

URL <https://www.ncbi.nlm.nih.gov/pubmed/18417603>

- Satas, G., & Raphael, B. J. (2018). Haplotype phasing in single-cell DNA-sequencing data. *Bioinformatics*, 34(13), i211–i217.
URL <https://www.ncbi.nlm.nih.gov/pubmed/29950014>
- Schuetz, A., Nana, D., Rose, C., Zocher, G., Milanovic, M., Koenigsmann, J., Blasig, R., Heinemann, U., & Carstanjen, D. (2011). The structure of the Klf4 DNA-binding domain links to self-renewal and macrophage differentiation. *Cell Mol Life Sci*, 68(18), 3121–31.
URL <https://www.ncbi.nlm.nih.gov/pubmed/21290164>
- Seki, T., Yun, J., & Oh, S. P. (2003). Arterial endothelium-specific activin receptor-like kinase 1 expression suggests its role in arterialization and vascular remodeling. *Circ Res*, 93(7), 682–9.
URL <https://www.ncbi.nlm.nih.gov/pubmed/12970115>
- Sender, R., Fuchs, S., & Milo, R. (2016). Revised Estimates for the Number of Human and Bacteria Cells in the Body. *PLoS Biol*, 14(8), e1002533.
URL <https://www.ncbi.nlm.nih.gov/pubmed/27541692>
- Shirley, M. D., Tang, H., Gallione, C. J., Baugher, J. D., Frelin, L. P., Cohen, B., North, P. E., Marchuk, D. A., Comi, A. M., & Pevsner, J. (2013). Sturge-Weber syndrome and port-wine stains caused by somatic mutation in GNAQ. *N Engl J Med*, 368(21), 1971–9.
URL <https://www.ncbi.nlm.nih.gov/pubmed/23656586>
- Shovlin, C. L., Guttmacher, A. E., Buscarini, E., Faughnan, M. E., Hyland, R. H., Westermann, C. J., Kjeldsen, A. D., & Plauchu, H. (2000). Diagnostic criteria for hereditary hemorrhagic telangiectasia (Rendu-Osler-Weber syndrome). *Am J Med Genet*, 91(1), 66–7.
URL <https://www.ncbi.nlm.nih.gov/pubmed/10751092>
- Shovlin, C. L., Hughes, J. M., Scott, J., Seidman, C. E., & Seidman, J. G. (1997). Characterization of endoglin and identification of novel mutations in hereditary hemorrhagic telangiectasia. *Am J Hum Genet*, 61(1), 68–79.
URL <https://www.ncbi.nlm.nih.gov/pubmed/9245986>
- Snellings, D. A., Gallione, C. J., Clark, D. S., Vozoris, N. T., Faughnan, M. E., & Marchuk, D. A. (2019). Somatic Mutations in Vascular Malformations of Hereditary Hemorrhagic Telangiectasia Result in Bi-allelic Loss of ENG or ACVRL1. *Am J Hum Genet*, 105(5), 894–906.
URL <https://www.ncbi.nlm.nih.gov/pubmed/31630786>
- Snellings*, D. A., Hong*, C. C., Ren*, A. A., Lopez-Ramirez*, M. A., Girard*, R., Srinath*, A., Marchuk, D. A., Ginsberg, M. H., Awad, I. A., & Kahn, M. L. (2021). Cerebral Cavernous Malformation: From Mechanism to Therapy. *Circ*

Res, 129(1), 195–215.

URL <https://www.ncbi.nlm.nih.gov/pubmed/34166073>

Soblet, J., Kangas, J., Natynki, M., Mendola, A., Helaers, R., Uebelhoer, M., Kaakinen, M., Cordisco, M., Dompmartin, A., Enjolras, O., Holden, S., Irvine, A. D., Kangesu, L., Leaute-Labreze, C., Lanoel, A., Lokmic, Z., Maas, S., McAleer, M. A., Penington, A., Rieu, P., Syed, S., van der Vleuten, C., Watson, R., Fishman, S. J., Mulliken, J. B., Eklund, L., Limaye, N., Boon, L. M., & Vikkula, M. (2017). Blue Rubber Bleb Nevus (BRBN) Syndrome Is Caused by Somatic TEK (TIE2) Mutations. *J Invest Dermatol*, 137(1), 207–216.

URL <https://www.ncbi.nlm.nih.gov/pubmed/27519652>

Srinivasan, S., Hanes, M. A., Dickens, T., Porteous, M. E., Oh, S. P., Hale, L. P., & Marchuk, D. A. (2003). A mouse model for hereditary hemorrhagic telangiectasia (HHT) type 2. *Hum Mol Genet*, 12(5), 473–82.

URL <https://www.ncbi.nlm.nih.gov/pubmed/12588795>

Sticht, C., De La Torre, C., Parveen, A., & Gretz, N. (2018). miRWALK: An online resource for prediction of microRNA binding sites. *PLoS One*, 13(10), e0206239.

URL <https://www.ncbi.nlm.nih.gov/pubmed/30335862>

Szulwach, K. E., Chen, P., Wang, X., Wang, J., Weaver, L. S., Gonzales, M. L., Sun, G., Unger, M. A., & Ramakrishnan, R. (2015). Single-Cell Genetic Analysis Using Automated Microfluidics to Resolve Somatic Mosaicism. *PLoS One*, 10(8), e0135007.

URL <https://www.ncbi.nlm.nih.gov/pubmed/26302375>

Tan, W. H., Baris, H. N., Burrows, P. E., Robson, C. D., Alomari, A. I., Mulliken, J. B., Fishman, S. J., & Irons, M. B. (2007). The spectrum of vascular anomalies in patients with PTEN mutations: implications for diagnosis and management. *J Med Genet*, 44(9), 594–602.

URL <https://www.ncbi.nlm.nih.gov/pubmed/17526801>

Tang, A. T., Choi, J. P., Kotzin, J. J., Yang, Y., Hong, C. C., Hobson, N., Girard, R., Zeineddine, H. A., Lightle, R., Moore, T., Cao, Y., Shenkar, R., Chen, M., Mericko, P., Yang, J., Li, L., Tanes, C., Kobuley, D., Vosa, U., Whitehead, K. J., Li, D. Y., Franke, L., Hart, B., Schwaninger, M., Henao-Mejia, J., Morrison, L., Kim, H., Awad, I. A., Zheng, X., & Kahn, M. L. (2017). Endothelial TLR4 and the microbiome drive cerebral cavernous malformations. *Nature*, 545(7654), 305–310.

URL <https://www.ncbi.nlm.nih.gov/pubmed/28489816>

Tang, A. T., Sullivan, K. R., Hong, C. C., Goddard, L. M., Mahadevan, A., Ren, A., Pardo, H., Peiper, A., Griffin, E., Tanes, C., Mattei, L. M., Yang, J., Li, L., Mericko-Ishizuka, P., Shen, L., Hobson, N., Girard, R., Lightle, R., Moore, T., Shenkar, R., Polster, S. P., Roedel, C. J., Li, N., Zhu, Q., Whitehead, K. J., Zheng,

- X., Akers, A., Morrison, L., Kim, H., Bittinger, K., Lengner, C. J., Schwaninger, M., Velcich, A., Augenlicht, L., Abdelilah-Seyfried, S., Min, W., Marchuk, D. A., Awad, I. A., & Kahn, M. L. (2019). Distinct cellular roles for PDCD10 define a gut-brain axis in cerebral cavernous malformation. *Sci Transl Med*, 11(520).
URL <https://www.ncbi.nlm.nih.gov/pubmed/31776290>
- Ten Broek, R. W., Eijkelenboom, A., van der Vleuten, C. J. M., Kamping, E. J., Kets, M., Verhoeven, B. H., Grunberg, K., Schultze Kool, L. J., Tops, B. B. J., Ligtenberg, M. J. L., & Flucke, U. (2019). Comprehensive molecular and clinicopathological analysis of vascular malformations: A study of 319 cases. *Genes Chromosomes Cancer*, 58(8), 541–550.
URL <https://www.ncbi.nlm.nih.gov/pubmed/30677207>
- Tual-Chalot, S., Oh, S. P., & Arthur, H. M. (2015). Mouse models of hereditary hemorrhagic telangiectasia: recent advances and future challenges. *Front Genet*, 6, 25.
URL <https://www.ncbi.nlm.nih.gov/pubmed/25741358>
- Ucler, N. (2019). An intracranial developmental venous anomaly presenting with seizure. *Neurol India*, 67(2), 604–605.
URL <https://www.ncbi.nlm.nih.gov/pubmed/31085894>
- von Spreckelsen, N., Waldt, N., Poetschke, R., Kesseler, C., Dohmen, H., Jiao, H. K., Nemeth, A., Schob, S., Scherlach, C., Sandalcioglu, I. E., Deckert, M., Angenstein, F., Krischek, B., Stavrinou, P., Timmer, M., Remke, M., Kirches, E., Goldbrunner, R., Chiocca, E. A., Huettelmaier, S., Acker, T., & Mawrin, C. (2020). KLF4(K409Q)-mutated meningiomas show enhanced hypoxia signaling and respond to mTORC1 inhibitor treatment. *Acta Neuropathol Commun*, 8(1), 41.
URL <https://www.ncbi.nlm.nih.gov/pubmed/32245394>
- Wang, C., Schultzhaus, J. N., Taitt, C. R., Leary, D. H., Shriver-Lake, L. C., Snellings, D., Sturiale, S., North, S. H., Orihuela, B., Rittschof, D., Wahl, K. J., & Spillmann, C. M. (2018). Characterization of longitudinal canal tissue in the acorn barnacle *Amphibalanus amphitrite*. *PLoS One*, 13(12), e0208352.
URL <https://www.ncbi.nlm.nih.gov/pubmed/30532169>
- Weng, J., Yang, Y., Song, D., Huo, R., Li, H., Chen, Y., Nam, Y., Zhou, Q., Jiao, Y., Fu, W., Yan, Z., Wang, J., Xu, H., Di, L., Li, J., Wang, S., Zhao, J., Wang, J., & Cao, Y. (2021). Somatic MAP3K3 mutation defines a subclass of cerebral cavernous malformation. *Am J Hum Genet*, 108(5), 942–950.
URL <https://www.ncbi.nlm.nih.gov/pubmed/33891857>
- Wetzel-Strong, S. E., Detter, M. R., & Marchuk, D. A. (2017). The pathobiology of vascular malformations: insights from human and model organism genetics. *J*

Pathol, 241(2), 281–293.

URL <https://www.ncbi.nlm.nih.gov/pubmed/27859310>

Wurm, G., Schnizer, M., & Fellner, F. A. (2005). Cerebral cavernous malformations associated with venous anomalies: surgical considerations. *Neurosurgery*, 57(1 Suppl), 42–58; discussion 42–58.

URL <https://www.ncbi.nlm.nih.gov/pubmed/15987569>

Xu, L., Durruthy-Durruthy, R., Eastburn, D. J., Pellegrino, M., Shah, O., Meyer, E., & Zehnder, J. (2019). Clonal Evolution and Changes in Two AML Patients Detected with A Novel Single-Cell DNA Sequencing Platform. *Sci Rep*, 9(1), 11119.

URL <https://www.ncbi.nlm.nih.gov/pubmed/31366893>

Zhou, Z., Rawnsley, D. R., Goddard, L. M., Pan, W., Cao, X. J., Jakus, Z., Zheng, H., Yang, J., Arthur, J. S., Whitehead, K. J., Li, D., Zhou, B., Garcia, B. A., Zheng, X., & Kahn, M. L. (2015). The cerebral cavernous malformation pathway controls cardiac development via regulation of endocardial MEKK3 signaling and KLF expression. *Dev Cell*, 32(2), 168–80.

URL <https://www.ncbi.nlm.nih.gov/pubmed/25625206>

Zhou, Z., Tang, A. T., Wong, W. Y., Bamezai, S., Goddard, L. M., Shenkar, R., Zhou, S., Yang, J., Wright, A. C., Foley, M., Arthur, J. S., Whitehead, K. J., Awad, I. A., Li, D. Y., Zheng, X., & Kahn, M. L. (2016). Cerebral cavernous malformations arise from endothelial gain of MEKK3-KLF2/4 signalling. *Nature*, 532(7597), 122–6.

URL <https://www.ncbi.nlm.nih.gov/pubmed/27027284>

Biography

Daniel Aaron Snellings was born in La Plata, Maryland on the 23rd of October, 1995. He graduated from the Pennsylvania State University in 2017 with a Bachelor of Science in Biochemistry and Molecular Biology. Daniel entered Duke in 2017 through the Cell and Molecular Biology graduate program and joined the lab of Douglas A. Marchuk in 2018. Daniel was awarded a Ruth L. Kirschstein predoctoral fellowship from the NHLBI in 2020. In 2021, Daniel was selected as a featured plenary speaker for the annual meeting of the American Society of Human Genetics and there was selected as a semifinalist for the Charles J. Epstein award. Daniel received a Ph.D. in Molecular Genetics and Microbiology from Duke University in 2022. In April 2022, Daniel began a postdoctoral fellowship in the lab of Christopher A. Walsh at Boston Children's Hospital.

Publications

- D. A. Snellings**, et al. (2021) *bioRxiv*
- D. A. Snellings**, et al. (2021) *Circ Res*
- A. A. Ren & **D. A. Snellings**, et al. (2021) *Nature*
- D. A. Snellings**, et al. (2019) *Am J Hum Genet*
- J. Koskimaki, et al. (2019) *Acta Neuropathol Commun*
- M. R. Detter, **D. A. Snellings**, D. A. Marchuk. (2018) *Circ Res*
- C. Wang, et al. (2018) *PLoS One*